The Dissertation Committee for Dana Diane Wise certifies that this is the approved version of the following dissertation:

Tracking Neuronal Content Using Capillary Electrophoresis with Multiphoton Excitation of Fluorescence

Committee:

Jason B. Shear, Supervisor

Dean R. Appling

Yvon Delville

Rueben A. Gonzales

Mehdi Moini

Tracking Neuronal Content Using Capillary Electrophoresis with Multiphoton Excitation of Fluorescence

by

Dana Diane Wise, B.S.

Dissertation

Presented to the Faculty of the Graduate School of

The University of Texas at Austin

in Partial Fulfillment

of the Requirements

for the Degree of

Doctor of Philosophy

The University of Texas at Austin

May, 2005

Dedication

To Michelle Cross, who changed my life.

Acknowledgements

Much gratitude to Jason Shear, who gave me the perfect combination of freedom and support; independence when I wanted it, and guidance when I needed it. He's also been patient and forgiving with me when I was headstrong. I've been lucky.

My coworkers are amazing; such a brilliant collection of musical, scientific, and amusing minds has almost certainly never been assembled. In particular, I'm grateful to Matt Plenert for fixing everything I broke, for generously and patiently sharing an instrument, and for being a friend. Richard Allen was always my resource for biological questions, and has such a breadth of knowledge and a genius, whipcrack wit; my utmost respect and gratitude. Ryan Hill and Bryan Kaehr were my brothers-in-arms; their understanding and sharing meant more than they know. The upcoming generation of Shear Labbers—Rex Nielson and Eric Ritschdorff—show every potential to be what I've come to expect from this group. I am exceedingly sorry to leave.

Professionally, I owe thanks to Drs D.J. Earnest, S.R. Whittemore, J.C. Shih, and J.H. Son for sharing cells, and to R. Gonzales and T.K. Starn for sharing LabView programs. Financial support from P.E.O. International, the Welch Foundation, and the Dorothy Banks Foundation made this work possible.

Tracking Neuronal Content Using Capillary Electrophoresis with Multiphoton Excitation of Fluorescence

Publication No._____

Dana Diane Wise, Ph.D.

The University of Texas at Austin, 2005

Supervisor: Jason B. Shear

Capillary electrophoresis with multiphoton-excited fluorescence detection (CE-MPE) allows low-background analysis of many spectrally distinct biological fluorophores using a single long-wavelength laser. This work demonstrates the methodical transformation of CE-MPE from a proof-of-concept instrument to a reliable and powerful workhorse for complex cellular samples. Preparation of cell extracts and their long-term storage prior to CE-MPE analysis have also been exhaustively characterized (Chapter 4). The process is suitable for extractions at 2 to 3 hour intervals over a day or more, or as frequently as every hour for shorter durations. With these methods, answers were obtained for hypothesis-driven research—answers not readily available from other techniques.

For example, evidence suggested intracellular levels of vitamin B_3 (nicotinamide) derivatives might exhibit a circadian rhythm in suprachiasmatic nuclei neurons. Therefore, Chapter 4 presents the tracking of these cofactors over 24 – 48 h periods in extracts prepared from an immortalized biological clock cell line. Chapter 5 extends this

single-fluorophore work to investigate hypothesized intracellular changes in both indole and nicotinamide derivatives during depolarization-induced upregulation of serotonergic phenotype, using cells immortalized from the raphe nuclei of the brain. Chapter 5 also demonstrates detection of riboflavin (vitamin B_2) derivatives in cell extracts, and proposes several relevant continuation experiments. Finally, Chapter 6 broadens the capabilities of CE-MPE to neutral analytes, such as melatonin, for the circadian investigation of multiple analytes in cells immortalized from the pineal gland, another clock-like area of the brain.

Table of Contents

List of Tables

List of Figures

Chapter 1: Nicotinamide Adenine Dinucleotides in Neural Cells

1.1 INTRODUCTION

The nicotinamide dinucleotides, which are vitamin B_3 derivatives, serve a multitude of biological functions. The reduced form of nicotinamide adenine dinucleotide (NADH, Figure 1.1A), transports reducing equivalents from one biological reaction to another, and is primarily used in the generation of adenosine triphospate (ATP), another energy transport molecule **[1]**. Reduced nicotinamide adenine dinucleotide phosphate (NADPH, Figure 1.1B) similarly transports reducing equivalents, but is primarily used for biosynthetic reactions, such as the synthesis of cholesterol, fatty acids, and hormones **[1]**. NADPH is also used in antioxidant salvage pathways, to regenerate glutathione and ascorbate (vitamin C) **[1, 2]**. These two cofactors, collectively called NAD(P)H, are formed by reduction of their oxidized counterparts, NAD and NADP (NAD(P), Figure 1.1C and 1.1D).

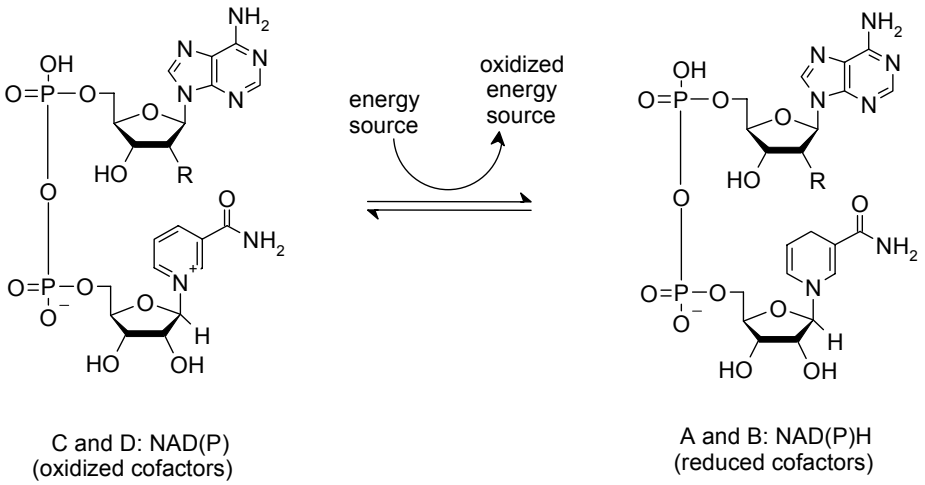

Figure 1.1: The nicotinamide adenine dinucleotides. A. NADH (R = OH). B. NADPH (R = phosphate). C. NAD (R = OH). D. NADP (R = phosphate). Structures are shown in their approximate charge state at pH 7; the resonance structure of the pyrophosphate linkage is arbitrarily chosen. Approximate pK_as of pyrophosphate are 9.4 and 6.7, while pK_as of phosphate are ~12.2 and ~7.2 **[3]**. The naturally-occurring β-anomers are shown, in which the nicotinamide moiety is above the plane of the sugar ring.

One glucose molecule, or other energy source, can yield multiple molecules of NAD(P)H from as many NAD(P), depending on metabolic pathways (glycolysis, pentose phosphate shunt, Krebs cycle, etc.) **[1]**. The classic pathway for NADH production is shown in Figure 1.2.

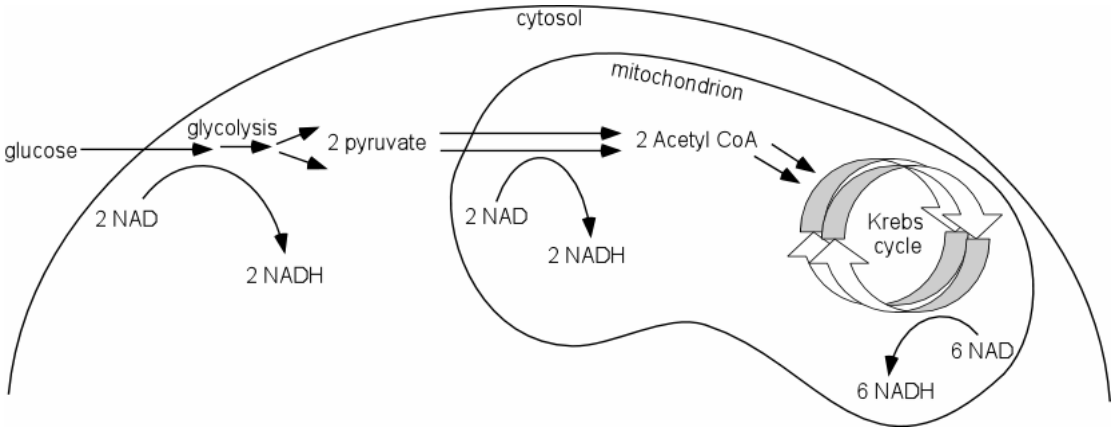

Figure 1.2: Glycolysis and the Krebs cycle. In this pathway, ten NADH molecules are produced from the metabolism of one glucose molecule.

There are a number of biosynthetic pathways to provide a cell with the four cofactors (collectively abbreviated NAD(P)(H)), and all start with synthesis of NAD, the base molecule. Rat brain contains none of the enzymes required to synthesize NAD from tryptophan, and only traces of the enzymes needed to synthesize NAD from nicotinate, but significant amounts of the enzymes for synthesis of nicotinamide **[4]**; therefore, the major biosynthetic pathway in brain cells is as given in Figure 1.3. Nicotinamide phosphoribosyltransferase is cytosolic **[5]**, while nicotinamide mononucleotide adenylyltransferase is found in the nucleus, cytosol and mitochondria **[6]**, though historically this second step was thought to be exclusively nuclear **[5, 6]**. Finally, NAD can be phosphorylated by NAD kinase to form NADP: in rat brain, the activity of NAD kinase is highest in the cytoplasm, though activity also exists in the mitochondrial/nuclear fraction **[7]**.

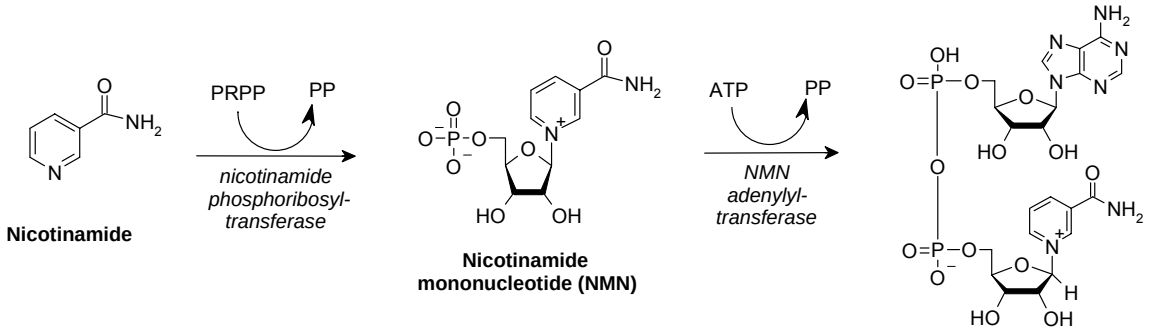

Figure 1.3: Biosynthesis of NAD **[8]**. PRPP = 5-phosphoribosyl-1-pyrophosphate, a product of ATP and ribose. PP = pyrophosphate.

Though synthesis is somewhat compartmentalized within the cell, NAD(P) are apparently able to pass through mitochondrial and nuclear membranes **[5, 9]**. Conversely, the mitochondrial membrane is impermeable to the reduced forms, making compartmentalization quite pronounced. For example, in liver cells, the total concentration ratio NADH/NAD(H) is threefold greater in mitochondria than cytosol, and NADPH/NADP(H) is about 1.3-fold greater **[10]**. Compartmentalization is further exaggerated by tight protein binding of the reduced cofactors, which is greater in cytosol than mitochondria: in liver cells, the mitochondrial unbound NADH/NAD(H) concentration ratio is 100-fold greater than cytosolic **[10]**.

Since NAD(P)H cannot cross mitochondrial membranes, reducing equivalents are moved via molecular shuttles to help balance the concentration ratios between mitochondrial and cytosolic pools. For example, in brain, the malate/aspartate shuttle allows transfer of NADH equivalents from cytosol to mitochondria **[5, 11]**. This transfer is nearly so rapid as the production of NADH itself: when pancreatic islet cells were given a glucose bolus, the cytoplasmic increase in NAD(P)H preceded the mitochondrial increase by only about 20 seconds, and both reached their maximal levels within ~40 seconds of the bolus **[12]**. Molecular shuttles apparently coupled the initial glycolytic

NADH increase into mitochondria, thus producing a measurable increase in mitochondrial membrane potential, which stimulated uptake of pyruvate and its metabolism through the Krebs cycle **[12]**. In contrast to this influx to mitochondria, there is practically no backflow of NADH from mitochondria to cytosol **[5]**, but the isocitrate/α-ketoglutarate shuttle allows significant flow of NADPH reducing equivalents from mitochondrial matrix to cytosol **[5, 13]**. The malate/aspartate and isocitrate/α-ketoglutarate shuttles are summarized in Figure 1.4.

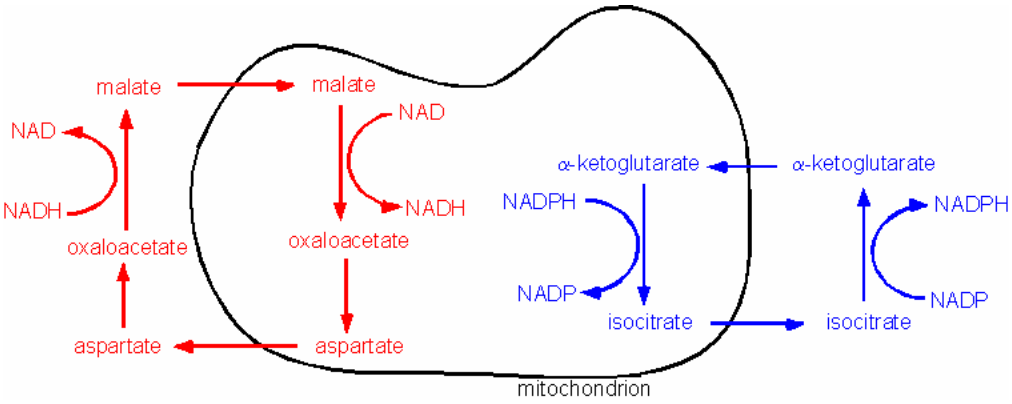

Figure 1.4: Some key components of the malate/aspartate (red) and isocitrate/α-ketoglutarate (blue) shuttles. Antiporters (not shown) allow shuttle molecules to cross the mitochondrial membrane.

Communication does exist between NAD(H) and NADP(H) systems: some enzymes can use either type of cofactor, and an energy-requiring nicotinamide nucleotide transhydrogenase even allows formation of one type from the other. However, the two systems are largely independent. Not only are they used for different purposes, as previously mentioned, but they are also differently compartmentalized: in brain, 18% of NAD(H) is mitochondrial, while 35% of NADP(H) is mitochondrial **[5]**. Moreover, these two systems are maintained at different levels of reduction: in general, the bulk of NAD(H) is present as NAD, while most NADP(H) is present as NADPH **[5]**. These levels of reduction, called the redox state, vary among different tissues. In rat midbrain,

for example, the NADH/NAD(H) ratio is 0.3 ± 0.1, while NADPH/NADP(H) ratio is 0.6 ± 0.1 **[14]**. Absolute levels of cofactors also vary: NADPH levels in rat striatum are about twofold greater than in cortex, and NADH levels were found to be at least double NADPH in both regions **[14]**.

1.2 NAD(P)(H) AND CLOCK-LIKE PROTEINS

Mammalian physiology and behavior are subject to daily cycles driven by the master biological clock of the brain, the paired suprachiasmatic nuclei (SCN) of the hypothalamus. The SCN generate endogenous ~24-hour rhythms in peptide content, firing rate, metabolism, and other variables, even when excised from the brain and cultured *in vitro* **[15]**. In the brain, the SCN receives input from the eyes, which allows it to correlate its timing with the external world. In fact, the name of the SCN is derived from its proximity to the eyes, because it is above the optic nerve crossing (or chiasm), as shown in Figure 1.5.

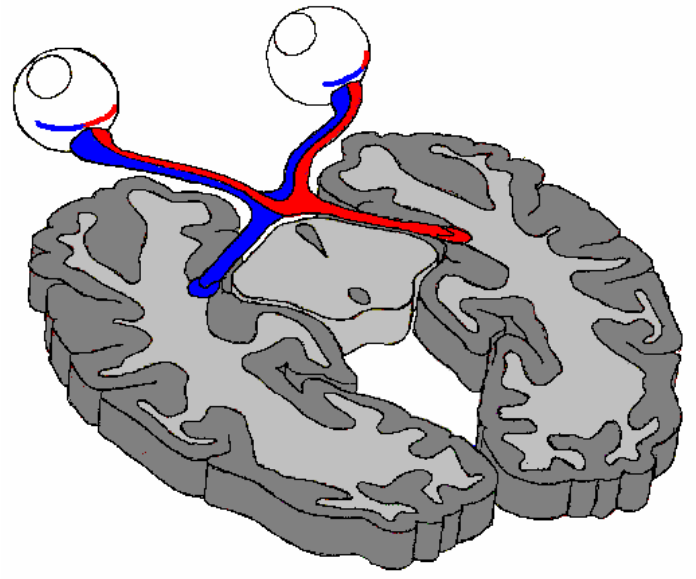

Figure 1.5: Horizontal section of the human brain, showing the optic nerves crossing on their path to the hypothalamus. The SCN are located dorsal to this chiasm.

The SCN receive glutamatergic input from about 1% of retinal axons, arising from retinal ganglion cells containing a specialized photopigment and dedicated to measuring ambient light levels rather than image processing **[16]**.

The timing information generated by the SCN and synchronized to the outside world via the eyes must then be conveyed to the rest of the brain and body. Two of the SCN's most important output pathways—to the pineal and pituitary glands—drive rhythmic secretion of melatonin and adrenocorticotrophic hormone, respectively **[17]**. Blood levels of melatonin, a hormone commonly thought of as a sleep-promoting in humans, are highest at night **[15, 17]**. Plasma adrenocorticotrophic hormone levels, conversely, peak just before dawn **[15]**; this hormone stimulates release of cortisol from the adrenal cortex, to mobilize blood sugar and provide energy upon waking. These inputs and outputs of the SCN are shown in Figure 1.6.

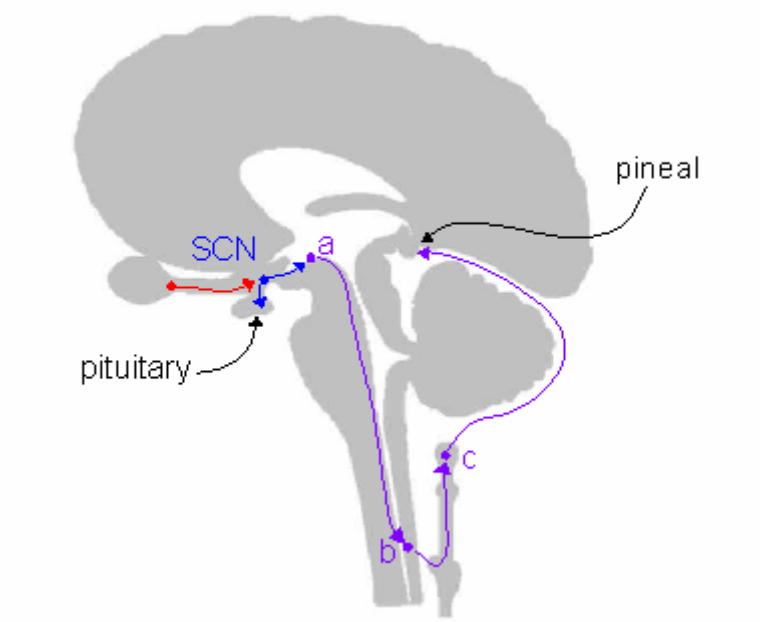

Figure 1.6: Sagittal plane human neuroanatomy relevant to the SCN. The SCN and its outputs are shown in blue, input from the eye in red, and violet designates the multisynaptic pathway to the pineal gland (via such structures as: a. the periventricular nucleus, b. spinal cord, and c. superior cervical ganglion).

Though the pineal gland is thus somewhat a 'slave' of the master clock, it also has interesting clocklike properties of its own. Both the SCN and the pineal gland intensely express the transcription factors CLOCK and BMAL1, which play a critical role in the generation of circadian rhythms **[18]**. Both the pineal gland and the SCN express CLOCK in a cycle antiphase to the BMAL cycle **[18]**, but the two brain structures are also antiphase to each other in these cycles, as shown in Figure 1.7.

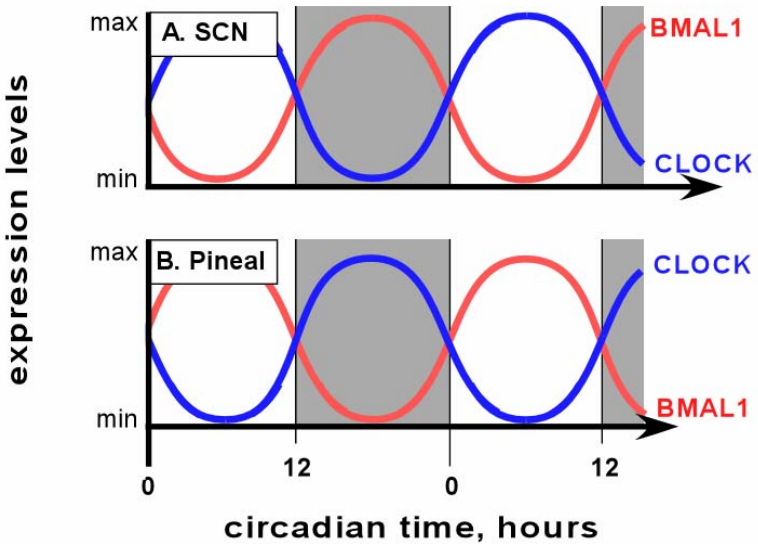

Figure 1.7: Cyclic expression of clock-like transcription factors in the pineal gland and SCN. Shading represents subjective night.

The clock-like genes that generate endogenous rhythms are not confined to the SCN and pineal gland; similar or identical genes are extensively expressed throughout the brain and body in mammals, as well as across the phyla. Recently, the heterodimeric CLOCK:BMAL1 complex, and its forebrain analogue NPAS2:BMAL1, were found to be regulated *in vitro* by the nicotinamide adenine dinucleotides **[19-21]**. The reduced forms strongly enhance DNA binding of the transcription factors, with NADPH approximately threefold more efficient than NADH. Furthermore, the oxidized forms of the cofactors

inhibit DNA binding of the transcription factors. It was hypothesized that this interaction between NAD(P)(H) and the transcription factors is closed into a characteristic clock-like feedback loop by lactate dehydrogenase, which is expressed in response to the transcription factors and is a catalyst for consumption of NADH. This loop is summarized in Figure 1.8.

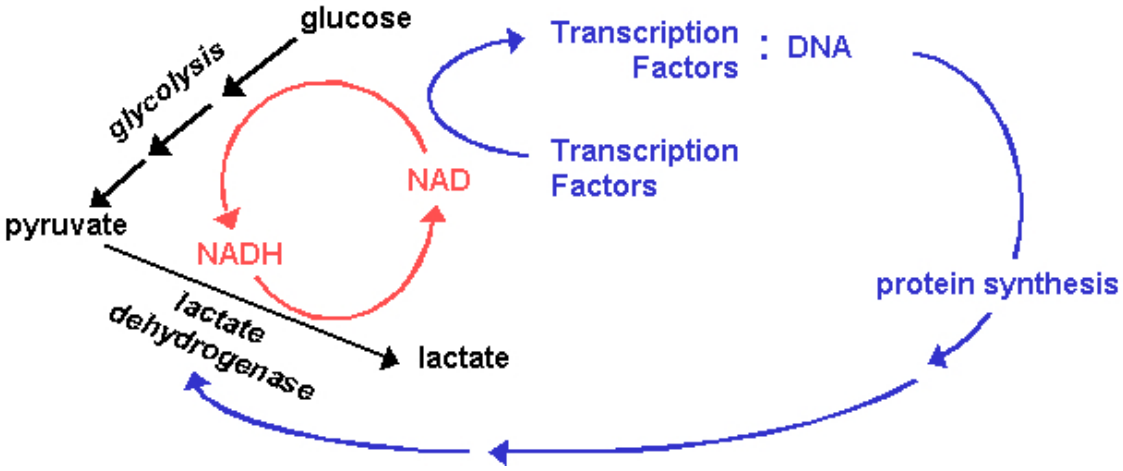

Figure 1.8: The hypothesized interaction of NADH, lactate dehydrogenase, and clock-like transcription factors.

Taken together, this evidence suggests that nicotinamide cofactors might be expected to influence, exhibit, and/or reflect biological rhythms. Total nicotinamide cofactor concentrations—i.e., NADP(H) or NAD(H)—are not thought to vary with the light-dark cycle, food ingestion, or neuronal activity **[19]**, since such a change requires synthesis or degradation of cofactors. In contrast, changes in reduced cofactor levels require only a change in cellular energetics, as previously discussed. Because glucose uptake and use increase with cellular activity, and SCN cells exhibit cyclic daily glucose consumption, a circadian rhythm in the ratio of reduced NAD(P)H to their oxidized counterparts might be expected. Furthermore, SCN cells exhibit circadian rhythms in firing rate **[15]**, and neuronal action potentials can generate a stimulus-dependent increase

in mitochondrial NAD(P)H fluorescence **[22]**. Although this increase in NAD(P)H fluorescence decays within about one minute after firing, a buildup of NAD(P)H might be experienced with prolonged elevation of activity, leading to a circadian rhythm in NAD(P)H that tracks with the neuronal firing rhythm. An analogous NADPH-to-NADP circadian rhythm has already been observed in plants **[23]**, but apparently has not yet been reported in brain tissues.

Beyond rhythmic behavior, the absolute concentrations of all four NAD(P)(H) species are also of interest; it is not clear whether the concentrations required for half-maximal DNA binding (EC_{50}) of NPAS2:BMAL1 *in vitro* are biologically possible. For example, two-photon microscopy suggests the concentration of free NAD(P)H in the nucleus of a Cos7 cell is < 1 mM **[24]**, but the EC_{50} for NADH and NADPH are 6.3 and 2.3 mM, respectively **[19]**. Moreover, when a more physiologically relevant *in vitro* experiment was performed, in which the total NADP(H) or NAD(H) concentration was held constant and the ratio of reduced and oxidized cofactors was varied, the EC_{50} increased to 9.0 mM NADH and 4.1 mM NADPH **[19]**. The microscopy and *in vitro* experiments may not be directly comparable; microscopic analyses used non-neuronal cells and required a number of assumptions concerning both the cofactor fluorescence when bound to proteins and the concentration ratios of NADPH/NADH and NAD/NADH **[24]**. The true values of these ratios are crucial: a small increase in the NADPH/NADP(H) concentration ratio (from 0.6 to 0.8) induces a tenfold increase in DNA-binding of NPAS2:BMAL1 **[19]**.

1.3 POLY-ADP-RIBOSE IN THE BRAIN

Though NAD(P) serve primarily as electron acceptors in the metabolic processes described in Section 1.1, they are also molecules of interest in their own right. The adenosine-diphosphate-ribose (ADP-ribose) moiety of NAD is sometimes used to

covalently modify a protein, thereby dramatically changing the biological activity of the acceptor **[25]**. That ADP-ribosylation can also be built upon, using up to 200 NAD molecules to form a polymer **[26]**. Poly-ADP-ribose is synthesized by a family of polymerases, of which poly-ADP-ribose polymerase-1 (PARP-1) is the most abundant **[26, 27]**. The PARP-1 reaction is shown in Figure 1.9.

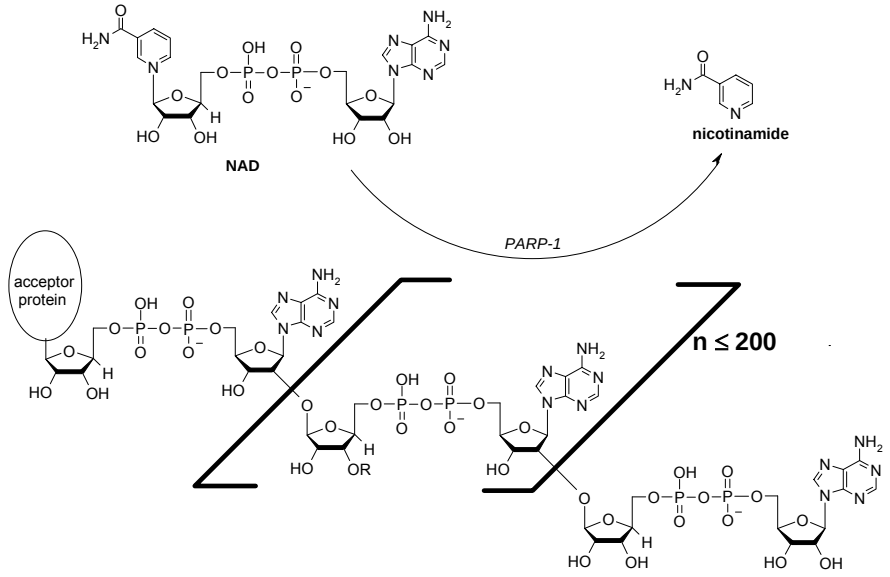

Figure 1.9: Poly-ADP-ribosylation of a protein by PARP-1. The acceptor protein may be modified at arginine, glutamate, or other residues **[26]**. Within the repeating brackets, branch points for another polymer of poly-ADP-ribose may occur at the R group; there are ~ 6 branches per polymer **[26]** or about one branch point every 25 monomer units **[25]**. For linear stretches of polymer, R = H.

PARP-1 is a well-studied nuclear enzyme that is rapidly activated by small amounts of DNA damage. It is an abundant enzyme (up to one million molecules per cell) with a long half-life, though the half-life of poly-ADP-ribose is only about a minute **[26]**. Poly-ADP-ribosylation of nuclear proteins, such as histones, facilitates DNA repair: poly-ADP-ribosylated histones decondense, perhaps simply by repulsion of the negatively

charged ADP-ribose polymers against the negative charges of the DNA backbone **[26]**. This relaxation of chromatin is thought to facilitate the repair of DNA at sites of damage.

With excessive DNA damage, PARP-1 depletes cellular NAD; in efforts to resynthesize NAD, levels of ATP also fall. For example, when cultured cells were treated with high concentrations of a DNA-damaging agent, cellular levels of NAD fell 90% within half an hour, while ATP levels dropped 60% **[28]**. NADP levels did not change in this time period, likely because PARP-1 cannot use NADP as a substrate. However, NADP levels did eventually decrease (a 75% drop after 3 hours), likely a reflection of the inability of the cells to synthesize new NADP without sufficient ATP and NAD as reactants **[28]**. This overall metabolic depletion leads to cell death, though it can be prevented by PARP-1 inhibitors **[26, 28]**. Alternatively, lower amounts of DNA damage lead to less dramatic metabolic depletion, and both cellular levels and cell viability may recover. When the aforementioned experiment was repeated at one-tenth the concentration of DNA-damaging agent, NAD levels fell only 60% in the first 30 min, while ATP levels did not change at all; moreover, NAD levels began to recover within 6 hours **[28]**. An important part of recovery is the degradation of poly-ADP-ribose polymers by poly-ADP-ribose glycohydrolase. This enzyme, though it is about 30-fold less abundant than PARP-1, has a much higher specific catalytic activity (~ 60-fold); thus, there are no kinetic constraints in its ability to degrade large amounts of poly-ADP-ribose formed by PARP-1 **[26]**.

Though PARP-1 in the brain has long been associated with DNA repair after toxic events such as ischemic injury (stroke) and excitotoxicity mediated by glutamate and/or nitric oxide **[26]**, PARP-1 is also associated with other DNA-related activities, such as transcription, replication, and recombination **[27]**, particularly during cell proliferation and differentiation **[29]**. New findings even implicate PARP-1 in neural events that are

non-traumatic and require no DNA damage, such as long-term memory formation **[30]** and intracellular signaling from cell membrane to nucleus **[31]**. Membrane depolarization enhances neuronal differentiation and prevents neuronal apoptosis in cultures deprived of growth factors, suggesting that neuronal activity is necessary to preserve cell viability; since PARP-1 is a downstream target of membrane depolarization, it may be an integral part of this process **[31]**. Of particular interest to this lab is depolarization-induced upregulation of serotonergic phenotype **[32, 33]**; we have a longstanding interest in serotonergic neurons, but it is not known whether PARP-1, and fluctuations in NAD levels, are involved in the differentiation of these cells.

1.4 CONCLUSIONS

The nicotinamide adenine dinucleotides are complexly regulated molecules which give insight into the metabolic state of neurons, and have recently been implicated in at least two processes which may involve changing levels of NAD(P)(H) over hours to days. These changes may occur concomitantly with changing levels of indole-derived molecules, such as serotonin or melatonin.

Chapter 2: Cultured Cells as Neural Models

2.1 INTRODUCTION

2.1.1 Establishment of Cell Lines

Cultured cell lines can be extremely useful and convenient models of neural behavior. Not only do cell lines circumvent technically and legally complicated animal handling and surgery (relevant anatomy in Figure 2.1), but they also provide more cells than can practically be obtained from animals. The rat pineal gland, the largest of the brain structures of interest to this work, has a maximum volume of only 4 mm^3 **[34]**. Similarly, the dorsal raphe nucleus—which contains the largest collection of serotonergic neurons in the rat brain—has a volume of only ~ 2 mm^3 **[35]**. The SCN, which are the smallest of the rat brain structures under investigation here, have a volume of 0.14 mm^3 and contain only ~ 32,000 cells **[36]**.

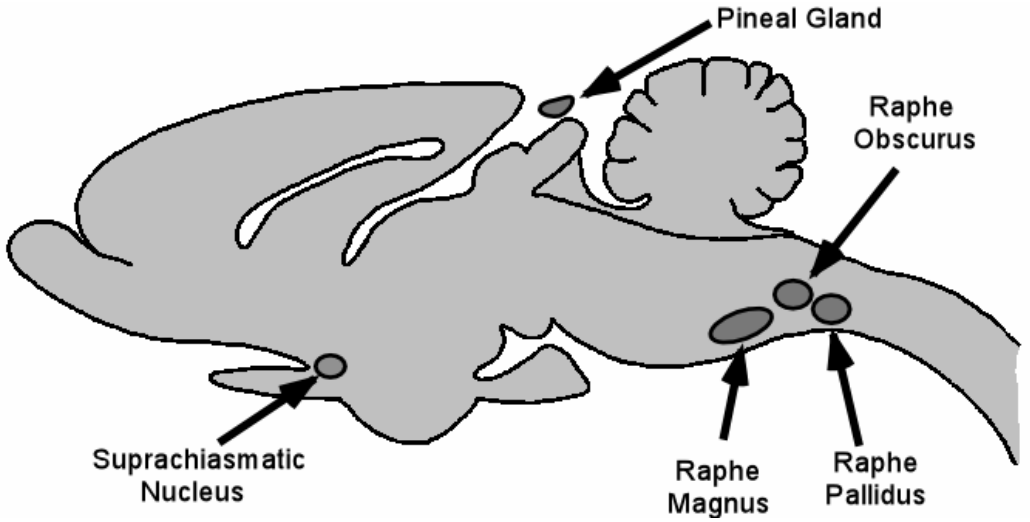

Figure 2.1: Sagittal plane of rat brain, highlighting structures immortalized into cell lines for use in this work. Only the three relevant (of nine total) raphe nuclei are shown.

By contrast, one 8 cm^2 Petri dish of immortalized SCN2.2 cells contains approximately seven million cells, the equivalent of more than two hundred rats. Furthermore, cultured cells multiply much faster than animals gestate: doubling times for all cell lines used in this work are 1 – 2 days. Cultured cells also allow immediate and direct access for manipulation and sampling, which provides greater control of variables than *in vivo* and minimizes sampling time. The duration of the sampling process is crucial, as shall be discussed in Chapter 4, since sampling can cause cellular metabolic changes within seconds.

The first neuronal cell lines were derived from spontaneously arising or exogenously induced tumors, which allowed only arbitrary access to cell types. Since then, neuronal cell lines have been established from four other sources: transgenic animals, stem cells, neurons fused with immortal cells, and viral transduction of neuroepithelial precursor cells **[37]**. The latter method was used to establish all cell lines investigated in this work, except pinealocytes. The first step required dissection of the desired nuclei from rat brain (embryonic day 12.5 for medullary raphe cells **[38]**, and embryonic day 15 – 16 for SCN cells **[39]**). Cells then were cultured and infected by inactivated viruses: SCN cells were incubated with adenovirus **[39]**, which commonly causes respiratory infections in humans, and raphe cells were incubated with simian virus 40 **[40]**, which infects monkeys without causing any apparent symptoms or disease. Both virus types can be tumorigenic in rodents. In contrast to the other cell lines, the pineal cell line PGT811 was immortalized from transgenic animals. Mouse zygotes were microinjected with a DNA plasmid containing the tryptophan hydroxylase promoter fused to a simian virus 40 gene **[41]**. The animals developed pineal tumors, which were harvested when the animals reached 8 – 12 weeks of age **[41]**.

The relevant oncogenes carried by the viruses are the adenoviral early-region 1A 12S, and the large T antigen in the simian virus. Large T antigen promiscuously activates promoter regions containing both a TATA box and at least one upstream transcription factor-binding site **[42]**. In contrast, early-region 1A adenoviral gene products interact with transcriptional modulators, including histone and chromatin remodeling factors **[43]**. Besides these oncogenes, the vectors used to immortalize the raphe and SCN cell lines also contained the neomycin phosphotransferase gene, which allows selection of infected cells by addition of G418 antibiotic or gentamycin to the medium **[39, 40]**.

2.1.2 Characterization of Cell Lines

The SCN2.2 cell line has been extensively characterized **[39, 44-47]**. SCN2.2 cultures are known to achieve maximum neuronal character (up to 80% of cells) by differentiation in N2-containing medium or on laminin **[39]**, a protein which (*in vivo*) is secreted by astrocytes and incorporated into the extracellular matrix. Differentiated cells express neuronal markers, genes, and neuropeptides found within SCN neurons *in vivo* **[39, 46]**. More importantly for this study, SCN2.2 cells express Clock and BMAL1 **[46]** and exhibit cycles in both uptake of 2-deoxyglucose and in its conversion to 2-deoxyglucose-6-phosphate **[47]**. In the rat SCN, the maxima of these cycles correspond to circadian time 6, or subjective midday **[48]**. The magnitude of the cycles in rat brain slices and SCN2.2 cells is similar (approximately a twofold change in both cases). These comparisons between the SCN2.2 line and rat brain have made it possible to induce a definable and reproducible circadian time in SCN2.2 cells by following a careful culture-medium protocol which culminates in a serum shock **[46]**. Such a stimulus has even been shown to induce a robust, precise, and sustained circadian rhythm of some gene products in rat fibroblasts that had been kept in culture for more than 25 years **[49]**. However,

even serum-shocked fibroblasts do not achieve the rhythmic metabolic activity that SCN2.2 cells can display by virtue of plating alone **[44]**.

Similarly, the raphe cell lines RN46A and RN33B have been well characterized with comparisons to the *in vivo* medullary raphe nuclei. After differentiation, these cell lines are highly neuronal, and under no conditions were oligodendrocytic, astrocytic, or microglial markers detected **[37]**. The cell lines differ in that RN33B cells—like SCN2.2 cells—are contact-inhibited, while RN46A cells are not. Furthermore, RN33B cells are glutamatergic, while RN46A cells are serotonergic; this is not unexpected, as both types of neurons are found in the medullary raphe **[37]**. While glutamate expression in differentiated RN33B cells is constitutive, the potentiation of the serotonergic phenotype in RN46A cells is more complex, as shown in Figure 2.2.

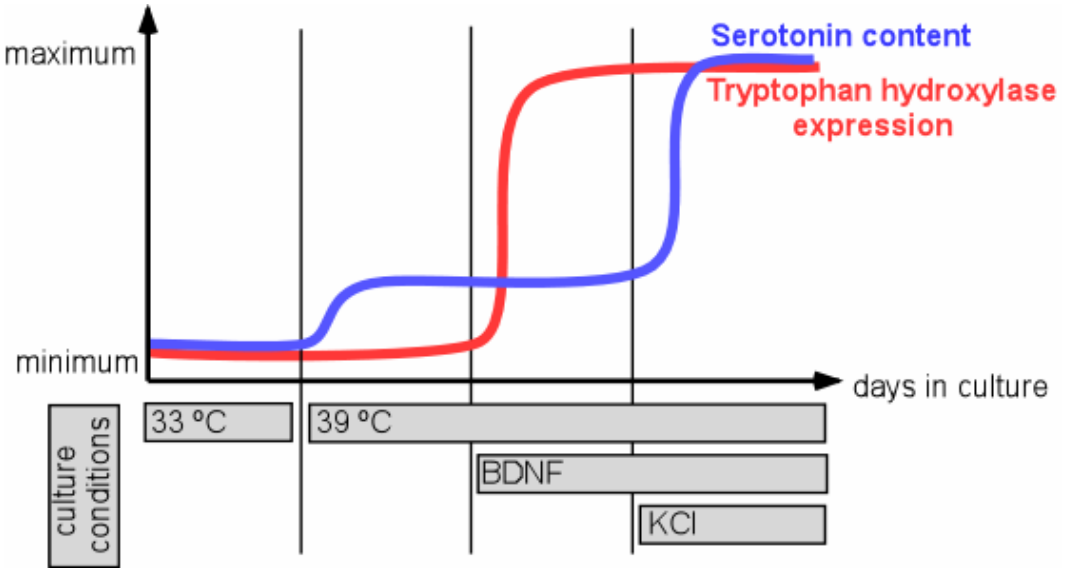

Figure 2.2: Culture conditions that produce serotonergic phenotype in immortalized raphe cells **[37]**. BDNF = brain-derived neurotrophic factor.

The complexity of this system potentially offers a relevant model for tracking interesting changes in indole levels, as well as possible concomitant changes in NAD(H) levels.

Differentiated RN46A cells express both tryptophan hydroxylase and aromatic amino acid decarboxylase **[32]**, the two enzymes required to synthesize serotonin from tryptophan. However, under basal differentiating conditions, RN46A cells synthesize low quantities of serotonin. Robust increases (threefold) in serotonin levels were seen only when cells were differentiated in the presence of BDNF for days 0 – 8 with 40 mM KCl on days 4 – 8 **[32]**. Because BDNF was essential to the serotonergic phenotype of RN46A cells, and because it also promotes survival of these cells during differentiation, a subclone of RN46A cells was developed to constitutively expresses BDNF **[50]**. This subclone, the RN46A-B14 cell line, was transfected liposomally with a vector containing the rat BDNF construct and a hygromycin resistance gene, which allows selection of plasmid-expressing cells **[50]**.

Of cell lines studied in this work, least is known about PGT811 cells. These cells express functionally active tryptophan hydroxylase and N-acetyl-transferase, which are enzymes required for melatonin synthesis; tryptophan hydroxylase has a specific activity one-tenth that of the rat pineal daytime activity, and the activity of N-acetyl-transferase is 3- to 4-fold higher than *in vivo* **[41]**. The mRNA levels for the genes encoding these enzymes have diurnal changes, with nighttime tryptophan hydroxylase and N-acetyl-transferase 6-fold and 4-fold higher, respectively, than their daytime values **[51]**. The value for tryptophan hydroxylase (TPH) matches *in vivo* pineal gland findings, in which TPH mRNA exhibits a 4-fold nocturnal increase in expression **[52]**. *In vivo* rhythms of N-acetyl-transferase (NAT) are more complex; in the intact rat, pineal NAT mRNA levels increase 150-fold at night **[53]**. However, removing the superior cervical ganglion (which normally relays SCN input to the pineal gland) abolishes this rhythm; mimicking the ganglion's input by applying noradrenaline—or other chemicals with similar modes

of action—almost fully restores the rhythm **[53]**. Therefore, one might expect the PGT811 rhythms of NAT mRNA to be similarly manipulable.

In a sister cell line (PGTβ, isolated by serial dilution from the same rat pineal gland tumor), the effects of adrenergic compounds have been characterized **[41, 54]**. Adrenaline and noradrenaline had maximal effects on cyclic-AMP production in these cells at concentrations of 1 and 300 μM, respectively **[54]**. This finding, coupled with other pharmacological data, implies PGTβ cells express β_2-adrenoceptors, which have a higher affinity for adrenaline than for noradrenaline **[54]**. Furthermore, while forskolin also induced accumulation of cyclic-AMP in a concentration-dependent manner, co-treatment with 1 μM adrenaline synergistically enhanced its effect; 10 μM forskolin plus 1 μM adrenaline produced a 20-fold increase over the effect of forskolin alone **[54]**.

2.2 EXPERIMENTAL METHODS

Unless otherwise noted, all chemicals and supplies were obtained from Fisher Scientific (Pittsburgh, PA), Sigma Chemical (St. Louis, MO), or Invitrogen (Carlsbad, CA) and were used as received. See Supplemental Information Section 2.4 for a detailed list of components in various media formulations.

2.2.1 Passages

Cells were rinsed in calcium/magnesium free phosphate-buffered saline containing 20 mM glucose and incubated for 1 – 2 min in 0.05% trypsin and 0.53 mM ethylene diamine tetraacetic acid (EDTA) in Hank's balanced salt solution. When cells were loosened from the culture dish, fetal bovine serum (FBS) was added at a 1:10 volume ratio to quench proteolysis. Cells were pelleted ($250 - 500$ g, 1 – 2 min), supernatant was removed, and cells were resuspended in the desired volume of growth medium for re-plating.

2.2.2 Cell Counting

Once per day for each experiment, one plate of cells was rinsed in calcium/magnesium free phosphate-buffered saline containing 20 mM glucose, then incubated for 4 min at 37 °C in 3 ml Hank's Balanced Salt Solution containing 2.5 g/l trypsin and 1 g/l EDTA. Trypsinization was quenched by trituration with 0.5 ml FBS and cells were transferred with rinsing to a 15 ml centrifuge tube. After pelleting cells at 500 *g* for 3 min, supernatant was removed and cells were resuspended in 4 ml growth medium for hemacytometer counting. For serotonergic and pinealocyte experiments, in which plates were counted once per day, pelleting and resuspension were skipped. Cells were loosened in 1 – 1.5 ml trypsin mixture, quenched with 0.5 ml FBS, and diluted with 0.5 - 2 ml Dulbecco's minimum essential medium (DMEM): the volume of this suspension was measured via the same serological pipette used for final trituration. These cell counts then were used in conjunction with extract concentrations (corrected for dilution by acid or addition of enzymatic reagents) to calculate moles of analyte per cell.

2.2.3 SCN2.2 Cells

SCN2.2 cells, received as passage 17 from Professor David J. Earnest (Texas A&M University Health Science Center), were raised on tissue-culture treated flasks (incubated 37 ºC, 5% CO_2) in a growth medium of minimum essential medium (MEM), 10% FBS, 2 mM L-glutamine, and 50 µg/ml gentamycin. At passage 23, cell stocks were frozen (slowly to – 80 ºC over a period of 8 h, and then to liquid nitrogen) in growth medium containing 10% dimethyl sulfoxide. One vial of ~ 10^6 cells was raised for each experiment, and cells never experienced more than 25 total passages before sampling. Cells were expanded at ~ 1:3 splits on tissue-culture treated plastic flasks until final passage onto an appropriate number of 8 cm^2 Petri dishes; laminin-coated plastic also was used for one experiment. Following the general culture procedures given by Hurst *et*

al. (2002b), differentiation was promoted after 24 – 48 hours at confluence by replacing growth medium with neuronal medium (50% DMEM, 50% Ham's F12, N2 supplement, 50 μg/ml gentamycin) for 48 – 72 h. Cultures then were exposed to a 2-h serum shock (50% FBS, 50% DMEM:F12), rinsed in DMEM:F12, and returned to neuronal medium. All media changes and passages were at the same time of day (± 2 h). Although plating is sufficient for synchronization of parallel cultures, at least over a several-day period **[47]**, this protocol has been shown to reinforce/reset synchronization; more importantly, this protocol sets SCN2.2 cells to a state consistent with the day/night transition, circadian time 12 **[46]**. Control cultures were treated identically, except that neuronal medium was used instead of the serum pulse. Usual ratios of media to growth surface were ~ 1:4 (ml/cm^2), but for final plating (when sampling made media changes undesirable), medium volume was doubled to sustain cells through several days. For experiments that continued longer than 80 h post pulse, fungizone was added to neuronal medium at 0.8 μg/ml.

2.2.4 Raphe Cells

RN33B cells (passage 43), RN46A cells (passage 27), and RN46A-B14 cells (passage 27), received from Professor Scott R. Whittemore (University of Louisville, KY, Department of Neurological Surgery), were raised on tissue-culture treated flasks (incubated 33–35 ºC, 5% CO_2) in a raphe growth medium of 50:50 DMEM:F12, 10% FBS, 250 μg/ml gentamycin, 100 U/ml penicillin, 100 μg/ml streptomycin, and in the case of RN46A-B14 cells only, 100 μg/ml hygromycin. At passage 44 (RN33B cells), passages 29-30 (RN46A cells), and passages 29-30 (RN46A-B14 cells), cell stocks were frozen (slowly to -80 ºC over a period of 8 h, and then to liquid nitrogen) in growth medium containing 10% dimethyl sulfoxide.

For comparison to SCN cells, RN33B cells were expanded at ~ 1:3 splits on tissue-culture treated plastic flasks until final passage (no greater than passage 50) onto an appropriate number of 8 cm^2 Petri dishes. After 24 – 48 at confluence, cultures were exposed for 30 min to a 15 μM forskolin pulse. Forskolin is a protein kinase A stimulator, which elevates intracellular cyclic-AMP levels and synchronizes cells in a manner similar to a serum shock **[55]**. Cells then were returned to raphe growth medium and sampled 3 – 17 h later. These cells were incubated at 35 ºC throughout all phases of growth and sampling.

The raphe cell lines have a temperature-sensitive mutant of large T-antigen, designated tsA58. This allows the cells to be shifted from growth phase (33 ºC), during which large T antigen drives proliferation, to a differentiation phase (39 ºC) during which large T antigen is not expressed. Unfortunately, this shift is also somewhat cytotoxic; for raphe cells, experimenters report as much as 25% cell death in the first three days of differentiation **[56]**, and other cell lines immortalized with tsA58 undergo "massive induction of apoptosis" upon shift to nonpermissive temperature **[57]**. Therefore, some researchers suggest an intermediate temperature; at 37 ºC, tsA58 is present in amounts that preserve cell growth, allowing cells to transform into a more differentiated phenotype before developing features of apoptosis **[58]**. Other cell culture conditions can also affect survival: if serum is not excluded from the medium, the temperature shift neither fully differentiates nor kills raphe cell lines **[38]**. Excitatory amino acids in medium can be toxic, while a collagen substrate can significantly prolong survival **[37]**. All of these cell culture variables were manipulated in this work in attempts to preserve cell viability.

Two types of differentiation media were used for RN46A and RN46A-B14 cells. One is a modified B16 base medium **[56, 59]**, which is essentially a 3:1 mix of

DMEM:F12 supplemented with transferrin, insulin, bovine albumin, progesterone, and putrescine (see Section 2.4). The second type of differentiation medium was Neurobasal™, which contains no excitatory amino acids, supplemented with glutamine (2.5 mM, final) and B27. Both differentiation media contained gentamycin (250 μg/ml), and when used with RN46A-B14 cells, also hygromycin (100 μg/ml).

2.2.5 Pineal Cells

PGT811 cells were received as passage 15 from Professor Jean C. Shih (University of Southern California) with permission from Professor H. Jin Son (Cornell University Medical College, NY). Cells were raised on tissue-culture treated flasks (incubated 37 ºC, 5% CO_2) in a growth medium of DMEM, 10% FBS, 50 U/ml penicillin, and 50 μg/ml streptomycin. At passage 18, cell stocks were frozen (slowly to – 80 ºC over a period of 8 h, and then to liquid nitrogen) in growth medium containing 10% v/v dimethyl sulfoxide. When being propagated for a circadian experiment, all media changes and passages were made at the same time of day (± 2 h).

A synchronization procedure was adapted from experience with SCN2.2 cells and a published method for PGTβ cells **[54]**; cells were expanded at ~ 1:3 splits on tissue-culture treated plastic flasks until final passage onto an appropriate number of 8 cm^2 Petri dishes. After 48 h at confluence, differentiation was promoted by replacing growth medium with serumless DMEM (plus antibiotics) for 48 h and then B27-supplemented DMEM (plus antibiotics) for 24 h. The final medium change was made to a minimum amount of medium in order to minimize loss of analytes by diffusion; cultures were given either a control medium change (to 1 ml medium per 8 cm^2 Petri dish) or stimulated with 1 ml of matched medium supplemented with 1 μM adrenaline and 10 μM forskolin. In PGTβ cells, this combination of stimulants was shown to optimally increase activity of N-acetyl-transferase **[54]**, the enzyme that synthesizes melatonin. Activity rose 3-fold

after 6 h, then slowly declined to basal levels within 24 h; while significant, this increase is much less than the noradrenaline-induced 100-fold increase in NAT activity observed in isolated rat pineal glands *in vitro* **[54]**. The weakness of the NAT response was ascribed to the cell line's origin in transgenic mice that were hybridized with a circadian clock-deficient strain; it had been demonstrated that most mice had no pineal melatonin because of a genetic defect in NAT activity **[54]**. For the purposes of the current work, however, it was hoped that a 3-fold increase would be sufficient to observe changes in indole levels. Moreover, it was anticipated that other indoles would be more readily detectable in pinealocytes than in raphe cells, since the *in vivo* level of pinealocyte tryptophan hydroxylase transcript is 100- to 150-fold higher than in raphe cells, though the enzyme is 3- to 5-fold more active (per mg protein) in raphe neurons **[41]**.

2.3 RESULTS

Petri dishes (8 cm^2, N = 3; one from each circadian experiment) contained an average of 6.9 ± 0.2 million SCN2.2 cells. Petri dishes of RN33B cells (N = 3) contained an average of 3.8 ± 0.8 million cells. The number of proliferative-type cells (PGT811, RN46A, or RN46A-B14) in a Petri dish varied; values are given where relevant throughout this manuscript. Some example images of cultured cells used in this work are given in Figures 2.3 and 2.4.

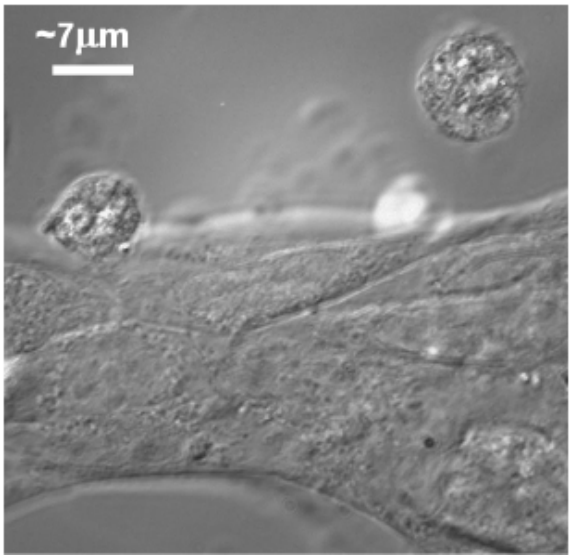

Figure 2.3: Differential interference contrast micrograph of SCN2.2 cells. Cells were not allowed to grow to confluence so that cell edges could be seen more clearly. Image was taken using a 100x oil-immersion objective. Comparison to literature descriptions **[39]** suggests the large, tightly-packed network of cells are glia and small round cells are neurons.

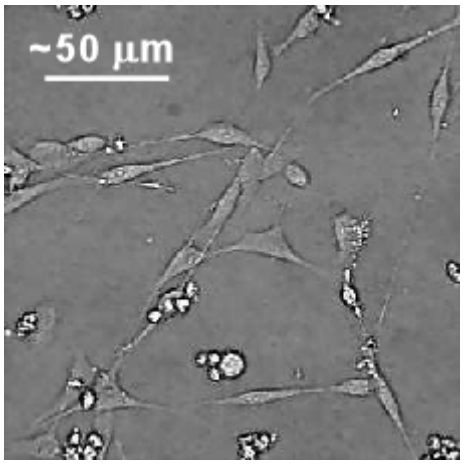

Figure 2.4: Differential interference contrast micrograph of RN46A-B14 cells. Image was taken using a 10x objective. Cells were differentiated four days in Neurobasal™ medium at 37 ºC followed by four days of 60 mM KCl supplementation, as described in Experimental Methods.

2.4 SUPPLEMENTAL INFORMATION: CELL CULTURE FORMULATIONS

From product information sheets and literature references **[56, 59, 60]**.

Table 2.1: Media supplements.

N2 (Defined)	B27 (Defined)	Fetal Bovine Serum[a]	In B16 Base (final)
Insulin, 2.5 g/l[b]	Insulin, 2.5 g/l[b]	Insulin, 0.2 mg/l	4 mg/l
Transferrin	Transferrin		Transferrin, 5 mg/l
Progesterone	Progesterone	Progesterone	Progesterone, 6.3 µg/l
Bovine albumin	Bovine albumin	Bovine albumin	Bovine albumin, 2.5 g/l
Linoleic acid	Linoleic acid		
Linolenic acid	Linolenic acid		
Putrescine	Putrescine		
Selenium	Selenium	Selenium	
	Retinyl acetate	Vitamin A	
	Biotin	Biotin	
	Vitamin E	Vitamin E	
	Vitamin E acetate	Phospholipids	
	Glutathione	Creatinine	
	L-carnitine	Triglycerides	
	T3 (triiodo-1-thyronine)	Niacin	
	Corticosterone	Magnesium	
	Ethanolamine	Glucose	
	Catalase	Parathyroid Hormone	
	Superoxide dismutase	Cholesterol	
	D-galactose	Globulins	

[a]FBS contains a multitude of vitamins, inorganic ions, proteins, and other components, not all of which are known or defined. A selection of known components is included here for comparison to B27 and N2 supplements.

[b]While suppliers provide concentrations of N2 components, the formulation of B27 is proprietary. However, B27 is described as a supplemented N2, so insulin levels in B27 should be at least as high as in N2. Since N2 is a 100x stock, N2- (or B27-) supplemented medium has 25 mg/l insulin, while 50% serum in DMEM:F12 has 0.1 mg/l insulin.

Table 2.2: Media formulations.

	MEM	DMEM	DMEM:F12	B16 Base	Neurobasal™
Amino Acids, µM					
L-Alanine			50	25	20
L-Arginine	600	400	700	700	400
L-Asparagine			50	38	5
L-Aspartic Acid			50	28	
L-Cystine	100	150	100	130	10
Glycine		400	250	33	400
L-Glutamic Acid			50	28	
L-Glutamine	2000	4000	2500	1775	500
L-Histidine	200	200	150	175	200
L-Isoleucine	400	800	400	308	800
L-Leucine	400	800	450	325	800
L-Lysine	400	800	500	350	5
L-Methionine	100	200	100	83	200
L-Phenylalanine	200	400	200	158	400
L-Proline			150	75	70
L-Serine		400	250	25	400
L-Threonine	400	800	450	325	800
L-Tryptophan	50	80	40	40	80
L-Tyrosine	200	400	200	158	400
L-Valine	400	800	450	325	800
VITAMINS, µM					
Choline Chloride	7	30	60	30	30
D-Biotin			0.01	0.01	
Folic Acid	2	9	6	2	8
Inositol	10	40	70	33	40
Niacinamide	8	30	17	7	30
D-Pantothenic Acid	2	8	5	2	8
Pyridoxal/Pyridoxine	5	20	10	4	210
Riboflavin	0.3	1	0.6	0.3	1
Thiamine	3	10	6	3	10
Vitamin B_{12}			0.5	0.3	0.2
INORGANICS (inactive counterions excluded), µM					
$CaCl_2$	1800	1800	1000	1400	1800
Cu			0.005		
Fe		0.2	1.6	0.8	0.2
Mg	800	800	700	750	800
KCl	5300	5300	4000	4650	5400
NaCl	117000	110000	120000	120000	51000
Phosphate	1000	900	950	1000	900
Zn			1.5	0.8	
Bicarbonate	26000	44000	14000	23000	26000
OTHER, µM					
D-glucose	25000	25000	17500	21250	25000
HEPES[a]			15000	15000	10000
Hypoxanthine			15	8	
Linoleic Acid			0.15	0.1	
Lipoic Acid			0.5	0.3	
Phenol Red	30	40	20	24	23
Putrescine			0.5	180	
Pyruvic Acid		1000	500	200	230
Thymidine			1.5	0.8	

[a] N-(2-Hydroxyethyl)piperazine-N'-(2-ethanesulfonic acid)

Chapter 3: Capillary Electrophoresis with Multiphoton Excitation of Fluorescence

3.1 INTRODUCTION

3.1.1 Capillary Electrophoresis

3.1.1.1 Separations

Cell extracts potentially contain millions of components that may interfere with analyte detection and quantitation. Capillary electrophoresis (CE) is ideally suited for separation of these complex mixtures, since 10^5 theoretical plates can easily be achieved **[61]**; this efficiency can be orders of magnitude better than most chromatographic methods. Capillary electrophoresis also uses very little sample (on the order of pico- to nanoliters), which suits the small volumes yielded from cell extracts. Moreover, separations can be achieved in only a few minutes.

Capillaries are typically 30 – 100 cm long, 5 – 100 μm inner diameter, 150 – 350 μm outer diameter, and made of fused silica, though derivatized surfaces are also available. Above ~ pH 3, silanol groups of the capillary wall are deprotonated **[61]**, which fixes a negative charge on the inner surface. This charge attracts positive ions from the electrolyte solution, thus producing an electrical double layer. Cations in the double layer are attracted towards the cathode, which is typically placed in the outlet reservoir. Thus, as cations flow, and drag bulk solvent with them, electroosmotic flow is produced (Figures 3.1 and 3.2).

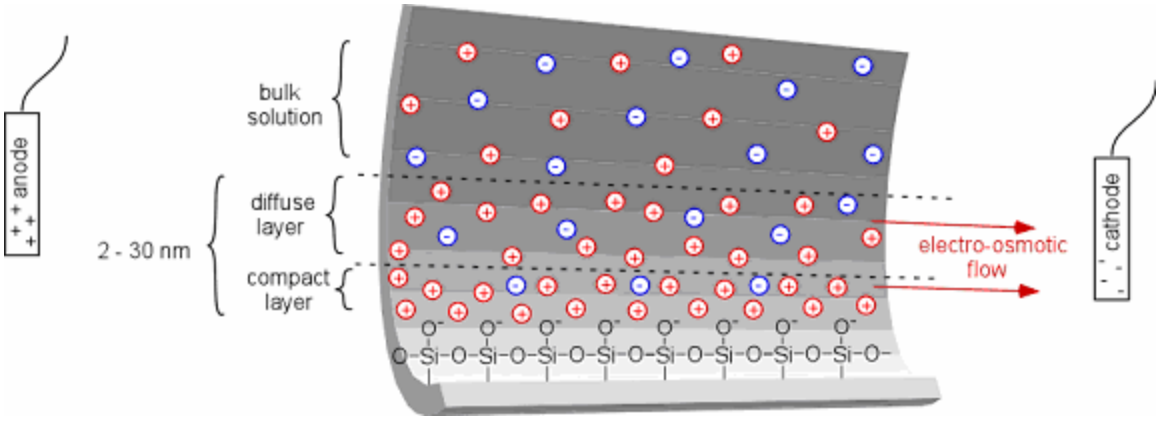

Figure 3.1: Electrical double layer in a capillary, and the electroosmotic flow it produces under applied voltage.

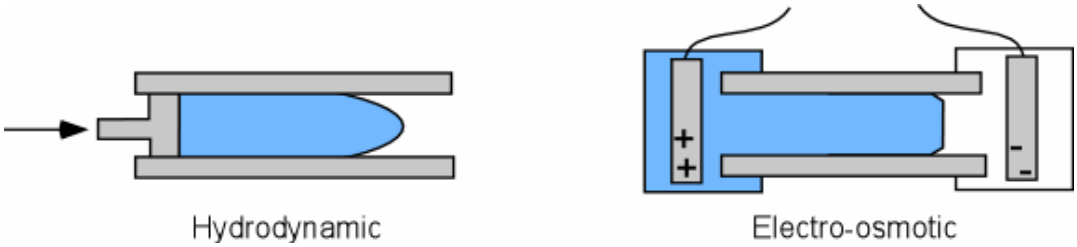

Figure 3.2: Flow profiles. The parabolic front produced by pressure-driven chromatography leads to band broadening. By contrast, the pumping action of electroosmotic flow is generated near the walls of the capillary, which yields a flat-front profile and narrower peaks.

The thickness of the double layer that drives electroosmotic flow is inversely proportional to the square root of the ionic strength of the electrolyte solution: a typical 100 mM salt solution in water produces a ~1 nm double layer, and a 1 mM solution produces a 50 – 100 nm double layer **[62]**. Since thicker layers generate greater pumping action, electroosmotic flow is suppressed by increasing the ionic strength of the solution. Besides ionic strength, factors such as pH, viscosity, and dielectric constant of the electrolyte solution also affect electroosmotic flow via their effect on the electroosmotic

mobility (μ_{EOF}) of the electrolyte ions **[62]**. The total electroosmotic velocity (v_{EOF}) is the product of this mobility and the applied electric field $\vec{E}$, in units of voltage (V)/distance:

$$v_{EOF} = \mu_{EOF} \cdot \vec{E} \qquad [3.1].$$

Besides this bulk flow, sample ions have their own electrophoretic velocities. Each analyte moves with a unique electrophoretic velocity based on its charge-to-drag ratio; highly positive, compact analytes move most rapidly towards the cathode, and negative analytes move towards the anode. Usually, electroosmotic flow is sufficient to overcome contrary negative electrophoretic mobility, and sweeps even anions toward the end of the capillary, yielding elution orders as in Figure 3.3.

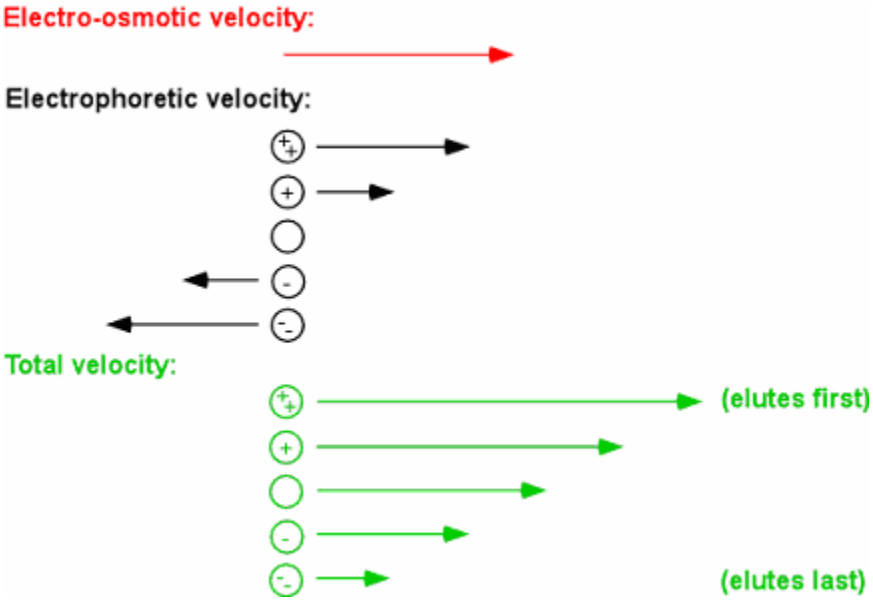

Figure 3.3. Vector-valued velocities; electroosmosis, electrophoresis, and total.

An ion's total velocity (v_{ion}) can be expressed in a manner analogous to Equation 3.1:

$$v_{ion} = (\mu_{EP} + \mu_{EOF}) \cdot \vec{E} \qquad [3.2]$$

where μ_{EP} is the electrophoretic mobility of the ion.

Equation 3.2 shows that a high electric field is desirable to achieve rapid separations; this is not only convenient, but also minimizes diffusion of analyte bands. Zone broadening of analyte bands can be described by Einstein's equation:

$$\sigma^2 = 2 \cdot D \cdot t \qquad [3.3]$$

where σ^2 is the spatial variance of the band, D is the diffusion coefficient, and t is the amount of time the band is allowed to diffuse. Spatial variance of a band—and the related quantity, peak width (w)—is a key measure of separation efficiency, which can be expressed by theoretical plate number (N_P):

$$N_P = 16 \cdot \left(\frac{t}{w} \right)^2 \qquad [3.4].$$

Separation efficiency can also be described by plate height (H), which takes into account the length of column (L) required to achieve a given theoretical plate count:

$$H = \frac{L}{N_P} = \frac{\sigma^2}{L} \qquad [3.5].$$

Equations 3.2 through 3.5 then can be combined to show that theoretical plate count in CE—unlike in traditional chromatography—is independent of capillary length:

$$N_P = \frac{(\mu_{EP} + \mu_{EOF}) \cdot V}{2 \cdot D} \qquad [3.6].$$

Equation 3.6 also shows that the highest sustainable voltages produce the most efficient separations.

Equation 3.6 also seems to suggest that efficient separations require high electroosmotic flow. While increased electroosmotic flow does produce shorter analysis times and sharper peaks, these peaks are less well resolved from each other. In fact, from a theoretical point of view, the best peak resolution is obtained when electrophoretic mobility is just balanced by electroosmotic flow **[62]**.

3.1.1.2 Injections and Stacking

The same differential migration velocities that produce CE separations also affect electrokinetic injections: positive species are overrepresented, while negatives are underrepresented. Such selective sampling is not always a drawback—to the contrary, it can be used to advantage in some situations—but nonselective injections are also possible, via pressure or gravity. The volume thereby injected can be calculated **[63]** from capillary length (L) and inner diameter (d_i), duration (t) and differential (ΔP) of the applied pressure, and solution viscosity (η):

$$\text{Volume injected} = \frac{\Delta P \cdot d_i^4 \cdot \pi \cdot t}{128 \cdot \eta \cdot L} \qquad [3.7].$$

For gravity injections, the pressure differential can be calculated **[63]** from solution density (ρ) and height difference (Δh) between inlet and outlet reservoirs:

$$\Delta P = \rho \cdot g \cdot \Delta h \qquad [3.8]$$

where g is the gravitational constant. Gravity injections are perhaps the easiest method, since they require no special equipment, but the small inner capillary diameters used in the current studies make gravity injections impractical. For instance, assuming a solution viscosity and density similar to water, a traditional capillary (75 μm inner diameter, 35 cm long) raised 5 cm injects 12 nl in 10 s. Our capillaries (15 μm inner diameter, for example) require two minutes to inject a sample the same distance into the capillary. Since pressure injection requires extra equipment, electrokinetic injections are our method of choice, especially since it is possible to automate injection time and magnitude using the same equipment used to drive the separation.

Despite the limitations on sample injection, small inner-diameter capillaries are desirable for their high surface area-to-volume ratio, which minimizes Joule heating and allows greater potentials to be applied, thereby increasing peak resolution. Alternatively,

current could be decreased by reducing ionic strength of the separation buffer; however, cell extract samples are necessarily high in ionic strength, which ideally should be matched or exceeded by the separation buffer.

Such differences in conductivity allow stacking, which is described in Figure 3.4. Stacking permits large sample plugs to be injected into the capillary without adversely affecting peak shape or resolution, thus overcoming a primary drawback of CE (the need for small sample injections to avoid overloading, and the consequently decreased detection sensitivity) **[64]**. Stacking is approximately proportional to the difference in ionic strength between the sample matrix and the separation buffer **[64]**.

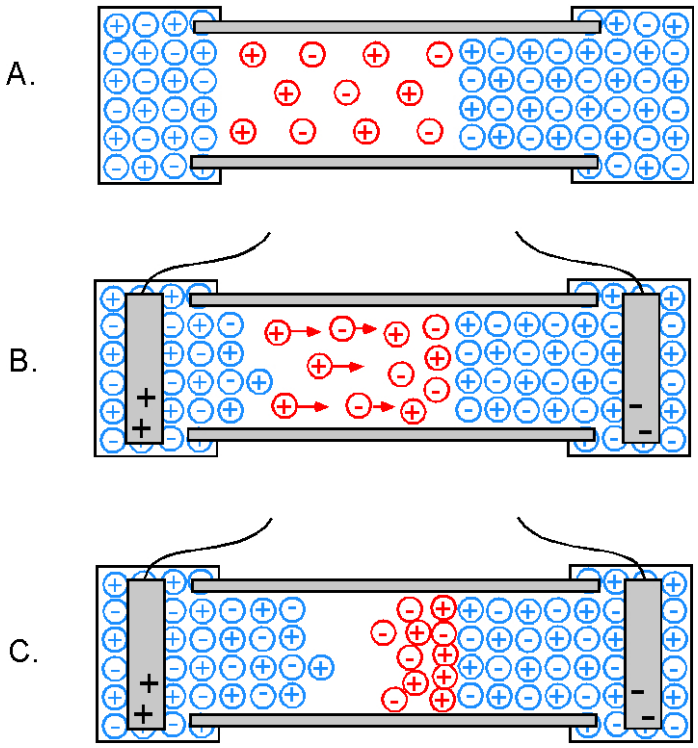

Figure 3.4: Stacking in CE **[64]**. A. A low-conductivity sample plug (red) is injected into a column filled with high-conductivity background electrolyte (blue). B. When separation voltage is applied, charged analytes experience an amplified electric field in the lower conductivity sample zone, therefore, their velocity is enhanced relative to the background electrolyte. C. Samples are stacked at the interface between the sample matrix and the separation buffer, where their velocity is decreased by the higher conductivity of the separation buffer.

3.1.1.3 CE of Neutrals

Since neutral species have no electrophoretic velocity, they can neither be stacked nor separated by conventional CE; modified strategies are required. For instance, a pseudo-stationary phase can be set up in the capillary by supplementing the mobile phase with a detergent at a concentration above its critical micellar limit. This pseudo-stationary phase does move, but if the micelles are anionic, they move more slowly than electroosmotic flow. A neutral analyte partitions in and out of micelles, which slows its

migration relative to that with electroosmosis alone. Analyte velocity is thus a function of affinity for a micelle, micelle velocity, and electroosmotic flow. This technique is called micellar capillary electrophoresis or micellar electrokinetic chromatography.

A similar technique, which uses cyclodextrins instead of detergent, can be used not only to separate neutrals, but even to separate enantiomers under some conditions. Cyclodextrins are cyclic oligosaccharides (Figure 3.5) produced from starch by a number of microorganisms **[65]**. The cyclodextrins assume a characteristic funnel shape in water, with a hydrophobic cavity into which neutrals may prefer to associate. Preliminary work in this lab has shown cyclodextrins are often preferable to detergents for our purposes, since detergents yield a high background signal and do not conveniently allow separation buffers to be deoxygenated by bubbling.

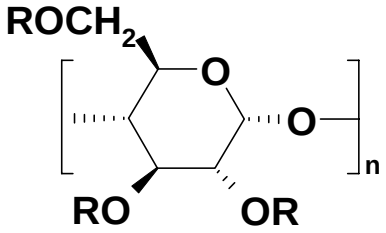

Figure 3.5: Cyclodextrin structure **[65]**. The number of saccharides (n) in the ring may be 6, 7, or 8, and are designated in nomenclature by α, β, or γ, respectively. R = H for natural cyclodextrin, though a number of derivatives are available.

Ionic strength principles for stacking in micellar CE or in CE with cyclodextrins are the inverse of conventional CE stacking, and are shown in Figure 3.6.

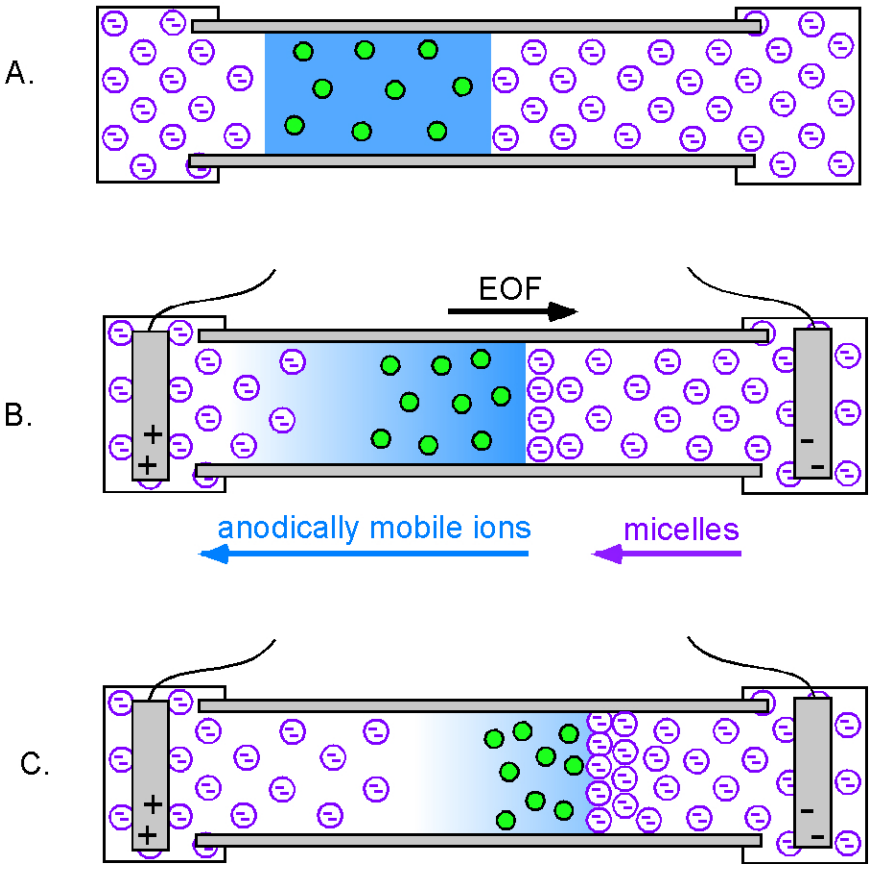

Figure 3.6: Neutral stacking in micellar CE **[64]**. A. A sample matrix containing neutrals (green) in high-concentration, high-anodic mobility background ions (blue) is injected onto a column containing micelles (purple), which are lower in both concentration and anodic mobility. B. When voltage is applied, the micelles are slowed by and accumulate against the sample buffer zone, while diffusion of the high-conductivity ions occurs towards the injection (anodic) side of the sample zone. Electroosmotic flow (EOF) sweeps neutrals towards the detector. C. Until the background sample ion (blue) completely diffuses, an interface continues to build between sample matrix and the micelles, thus stacking the analytes.

3.1.2 Multiphoton Excitation of Fluorescence

Common detection strategies for CE include electrochemical, ultraviolet or visible absorption, and laser-induced fluorescence methods; our lab was among the first to use multiphoton excitation (MPE) of fluorescence **[66]**. The equivalent of a shorter-

wavelength one-photon molecular transition can also be achieved by multiple longer-wavelength photons via an intermediate "virtual state," as in Figure 3.7.

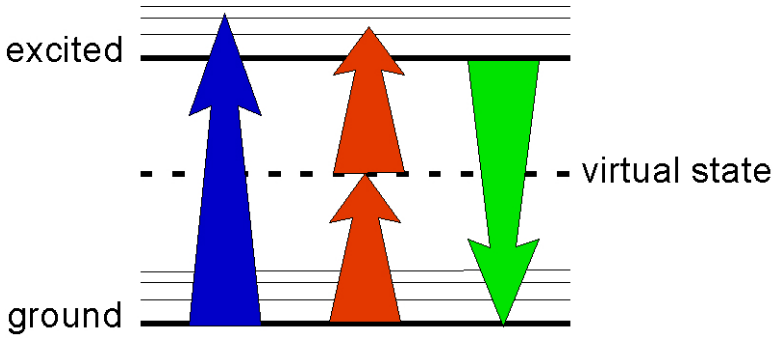

Figure 3.7: Single- vs. two-photon excitation. The near-simultaneous absorption of two photons (red) with half the energy of a single-photon excitation (blue) produces an excited state that can emit fluorescence (green). Arrow colors are also suggestive of the wavelength of light for each process.

Though the virtual state is represented as one intermediate, this is an order-of-magnitude approximation; virtual states are superpositions of energy levels, and the strength of two-photon transitions depend on contributions from all eigenstates as possible intermediates **[67]**. The lifetime (τ) of these virtual states must be short enough to avoid violating the uncertainty principle:

$$\Delta\nu \cdot \tau \geq 1 \qquad [3.9]$$

where Δυ is the energy (frequency) of the transition from ground to virtual state **[61, 67]**. For transitions in the visible frequency range, the lifetime of the virtual state is on the order of femtoseconds.

Since two photons (or more, for multiphoton processes) must interact with the molecule on these extremely short timescales, very high excitation intensity (*I*) is required. The dependence of molecular excitation on laser intensity can be modeled by considering a multiphoton process as a standard chemical reaction **[68]**, with *n* photons as reactants to excite a molecule (M) to its excited state (M*):

$$\mathrm{M} + n(\mathrm{h}\nu) \overset{k}{\longleftrightarrow} \mathrm{M}^* \qquad [3.10]$$

where k is the forward rate constant and hυ represents a photon. The rate of this "reaction" is given as:

$$\frac{\mathrm{d}[\mathrm{M}^*]}{\mathrm{dt}} = k[\mathrm{h}\nu]^n[\mathrm{M}] \qquad [3.11].$$

From Equation 3.11, it is evident that the rate of the reaction has an n-order dependence on the "concentration" of light—its intensity. Therefore, for example, doubling the excitation intensity for a two-photon process should produce four times the fluorescence. The benefit of high-intensity excitation does not increase without bound, of course; these calculations assume that there is no depletion of the ground state (M), and that no photochemistry or photobleaching is occurring.

Nevertheless, a need for high excitation intensity is clear. Lasers are already relatively high in intensity, but can be made more so through focusing, as shown in Figure 3.8.

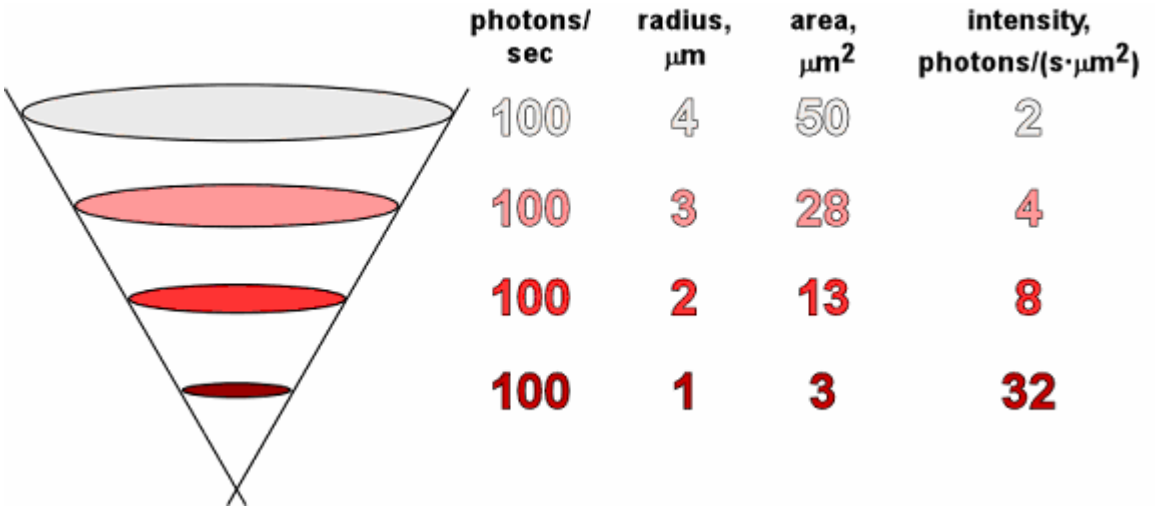

Figure 3.8: Increased intensity via focusing. Though each plane along the focusing axis gets the same total photon flux (photons/sec, here arbitrarily set to 100), the planes closest to the focal point experience the greatest intensity. A radius of 1 μm approaches real diffraction-limited focusing by high numerical aperture optics; an unfocused laser beam can easily be millimeters in diameter.

Focusing not only increases intensity, it also spatially confines excitation, which can greatly reduce background signal. However, focusing alone is usually insufficient to achieve the intensities needed for multiphoton excitation; to obtain greater (instantaneous) intensities, pulsed lasers are typically used. With a titanium:sapphire laser, for example, the interval between pulses is 10^5-fold longer than the pulses themselves, so the peak power is approximately 10^5-fold greater than the average power **[69]**. By the uncertainty principle, shorter pulses must have broader bandwidth; a 10-fs pulse, for example, has an associated spectrum spanning roughly 100 nm **[69]**. The titanium:sapphire laser used in the current experiments generally produces pulses that are ~100 fs in duration, yielding bandwidths of ~10 nm at 750 nm. By comparison, a continuous-wave laser typically has a bandwidth of only 0.01 nm or less **[61]**. It required the development of modern broadband crystals, which can emit and amplify multiple

wavelengths, to make pulsed lasers into practical and user-friendly instruments. The most popular such material, titanium-doped sapphire, can amplify from 700 nm – 1100 nm **[69]**, and is used in this work.

It is frequently necessary to perform a power study, comparing the fluorescence of an analyte to the input power of the laser, to determine optimum excitation wavelength and power under any given experimental conditions. Proper wavelength and power selection, however, allow excitation of spectrally diverse chromophores, which would not otherwise be possible without multiple sources. These disparate transitions, requiring substantially different energies, can be excited through absorption of different numbers of photons **[66]**. For example, the excitation spectra of serotonin, NADH, and flavin adenine dinucleotide (another redox cofactor) do not overlap adequately in any one spectral region to allow efficient excitation of all species (Figure 3.9), but CE-MPE has been used to fractionate and sensitively detect all three components in a single sample **[66]**.

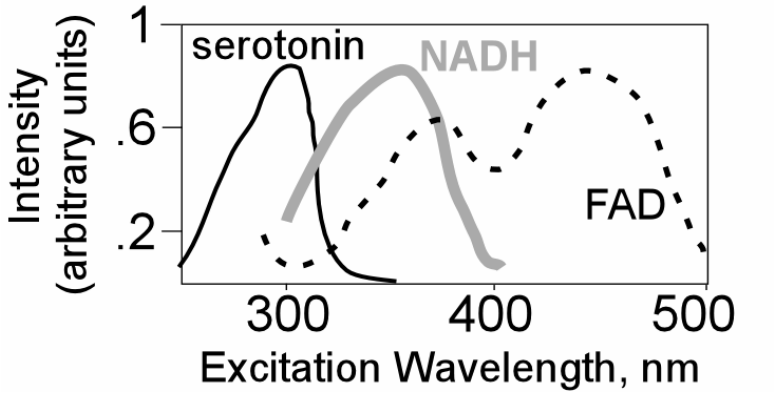

Figure 3.9: One-photon excitation spectra of serotonin, NADH, and FAD **[66]**.

MPE also allows access to deep-ultraviolet chromophores without the need for specialized optics, and allows easy spectral filtration of emission from excitation (per Figure 3.5; it is easier to filter green emission from red excitation than from blue

excitation). Furthermore, even red laser scatter that does strike the detector is poorly detected, since typical photomultipliers have low sensitivity to such low-energy photons.

In the special case of serotonin and related molecules, multiphoton excitation allows not only detection of native fluorescence, but also a photoderivatization process that has been exploited to improve CE-MPE detectability several-fold **[70]**. Serotonin undergoes a four-photon-excited phototransformation, forming a product that can be excited to fluoresce ($\lambda_{max,em}$ = 500 nm) upon absorption of two additional photons, as shown in Figure 3.10.

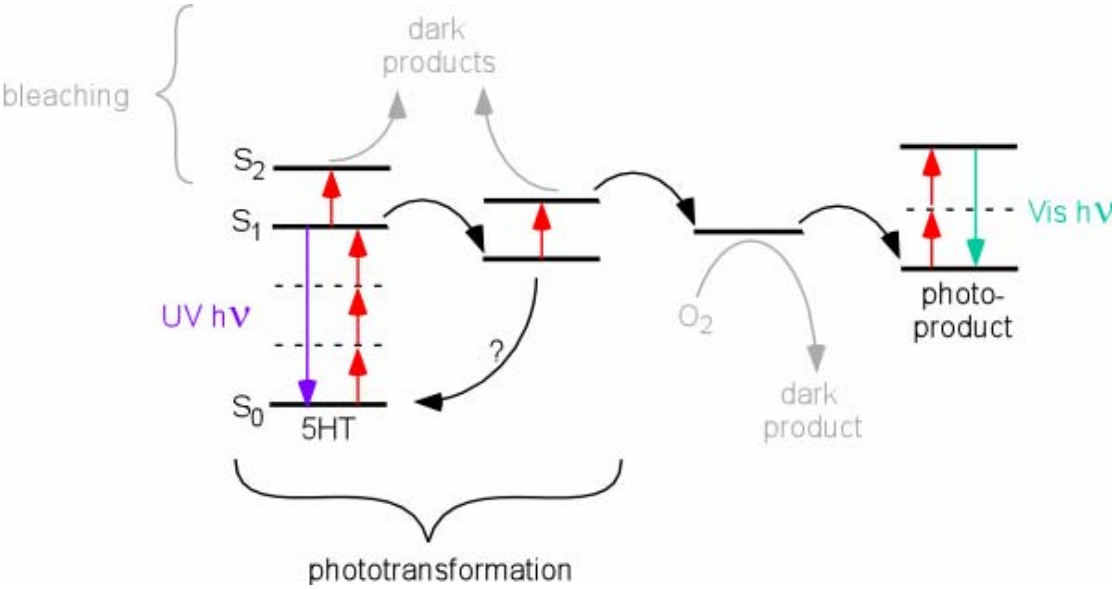

Figure 3.10: A proposed pathway for the generation of fluorescent serotonin photoproduct **[70]**. Visible emission requires first a multistep four-photon conversion, followed by a two-photon excitation.

Whether fluorescence is of a native or photoconverted molecule, detection at the photomultiplier can be further optimized by allowing fluorescence photons to accumulate in sampling intervals ("bins") that are as long as possible, since counting statistics dictate that N photons have a standard deviation of $\sqrt{N}$ (under shot noise limited detection conditions). Therefore, the relative standard deviation for counting 100 photons is 10%,

but is only 1% for 10,000 photons. Longer bins also ensure that a smaller fraction of signal photons are discarded during the dwell time between bins, during which the photomultiplier tube resets itself. The minimum dwell time for the system used in this work is 0.002 s. A peak with a full width of 2 seconds, for example, could be defined by 10 bins of 0.2 s and 10 dwell periods (so 1% of photons are lost), or by two bins of 1 s and two dwell periods (only 0.2% of photons are lost). However, bins must be short enough to give adequate peak shape information.

Previously, our lab has exploited the low injection volumes of CE and the low-background fluorescence from MPE to achieve the best mass detection limits yet published for some biological chromophores; such work is continued here. Though good concentration detection limits are often achieved, the distinction between mass and concentration detection limits is important. Multiphoton excitation volumes are necessarily small when using standard mode-locked laser sources. Because of limited MPE probe volume size, much of an analyte band migrating out of a capillary never intersects the probe site and is wasted. For example, when using a 5-μm inner-diameter capillary, the size mismatch between laser spot and capillary outlet allows >95% of analyte to diffuse into the outlet reservoir bulk solution without intersecting the MPE probe volume **[66]**. The MPE probe volume size could be increased somewhat by using lower numerical-aperture focusing optics; however, substantial increases in focal volume size decrease the rate of MPE, so fluorophores are inadequately excited during their residence in the beam focus. Alternatively, very high laser intensities can produce larger excitation profiles. The small focal volume is not always a liability: it can also be exploited to advantage. The analysis of subpicoliter biological samples—such as individual cells or organelles—puts extreme demands on detection capabilities. By

confining these samples to a small capillary and a small excitation volume, less signal is lost to dilution by diffusion.

3.2 EXPERIMENTAL METHODS

A 1.3-numerical aperture objective (Zeiss Fluar oil-immersion) was used to focus a Coherent Mira 900 titanium:sapphire laser beam at the outlet of a 15- or 25-μm inner diameter separation capillary (Polymicro Technology, Phoenix, AZ). Fluorescence from analytes migrating from the channel into a grounded outlet buffer reservoir was collected by the objective in an epi-geometry, and was directed via a dichroic through 2 cm of 1 M $CuSO_4$ solution and a colored glass filter (BG18, Schott Glass, Yonkers, NY) to a photomultiplier tube operated in photon-counting mode. Data was transferred to a LabView acquisition program via a GPIB interface. A modified LabView data acquisition driver was used to apply voltages of precisely specified duration and magnitude via a PCI-6024E digital-to-analog converter card (National Instruments, Austin, TX) communicating to a CZE1000R DC power supply (Spellman High Voltage Electronics, Hauppage, NY). Peaks were integrated using the Manual Peak Integrator program written for LabView by Professor Timothy K. Starn (West Chester University, PA). Other instrumental parameters that varied with experiment are given in their proper chapters, but a summary of the instrument is provided in Figure 3.11.

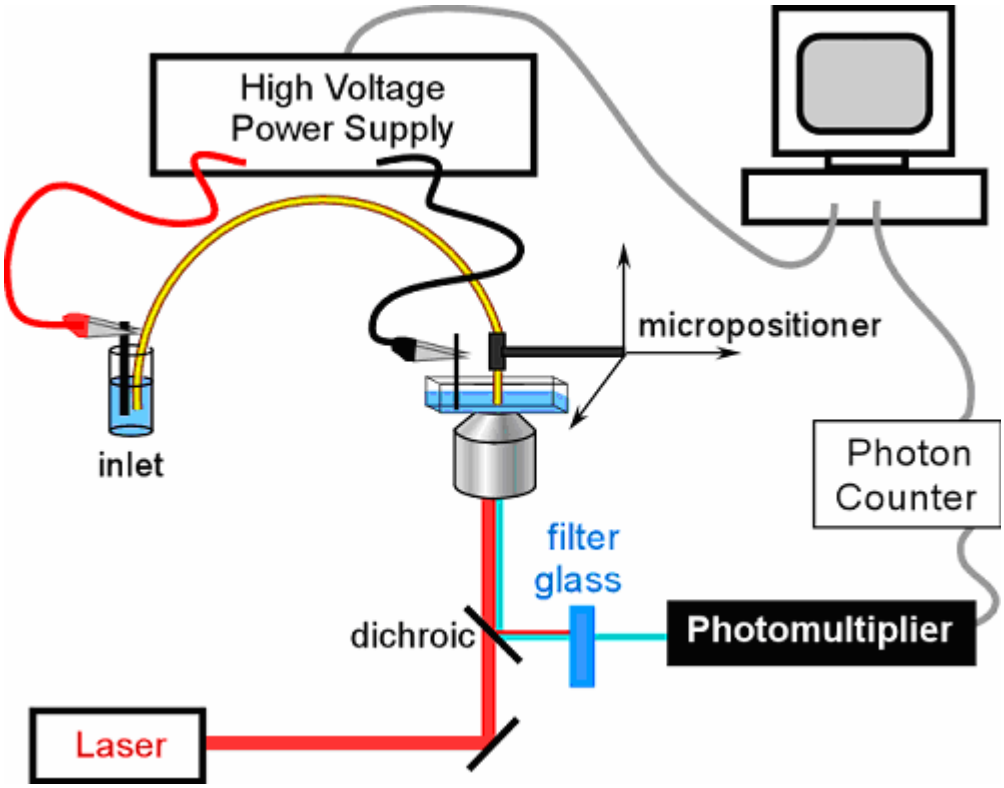

Figure 3.11: Instrumentation for CE-MPE.

Chapter 4: Tracking NAD(P)(H) Levels in Cultured SCN Cells

4.1 INTRODUCTION

As discussed in the first chapter, quantitation of NAD(P)(H) for extended periods in cultured cells is of clear interest. Besides the usual analytical parameters, this goal puts a premium on the need for a rapid, sustainable, and simple harvesting procedure. Further, some experiments require the samples to be stable for days or weeks, since day-long experiments yield dozens of samples in rapid succession, necessitating delayed analyses. Harvesting and extraction difficulties can be avoided by using fluorescence microscopy to quantify NAD(P)H in intact cells **[12, 24, 71]**, but this method cannot distinguish NADH from NADPH, cannot detect NAD(P), and must make assumptions and corrections for quantum-yield differences between free NAD(P)H and their protein-bound counterparts, which are as much as tenfold more fluorescent **[12]**. Moreover, as is shown here, even the most suitable method for analysis of all four NAD(P)(H) species in cultured cells **[72]** has serious shortcomings.

Quantitation can be nearly as challenging as extraction, since NAD(P)H are only weakly fluorescent; both species have an extinction coefficient of 6,200 mol^{-1} cm^{-1} and ~3% quantum yield **[12]**. Moreover, cellular samples are low in concentration and limited in practical quantity. In the past, our lab has exploited the low injection volumes of capillary electrophoresis and the low-background fluorescence from multiphoton excitation to achieve the best mass detection limits of NADH yet published **[66]**. However, because NAD(P) are not natively fluorescent, detection of these species requires chemical or enzymatic treatment. Further, quantitation methods based on calibration curves are rendered impractical by variation of instrumental parameters over many hours or days of analysis. Standard additions or internal standards would make

independent analysis of each sample possible, and would avoid complications of trying to matrix-match calibration standards to cellular samples.

To achieve these ends, we have adapted existing procedures **[72, 73]**, and have developed and systematically characterized a method for extraction of NAD(P)(H) from cultured cells, enzymatic reduction of NAD(P) to their fluorescent counterparts, separation of analytes by capillary electrophoresis, detection by multiphoton excitation of fluorescence, and quantitation by comparison to spiked samples. Millions of cells are required for each sample, but induced synchronization can ensure that these cells are locked together in circadian phase, and that each flask or dish removed for sampling can be treated as part of a pool of still-cycling cells.

4.2 EXPERIMENTAL METHODS

Unless otherwise noted, all chemicals and supplies were obtained from Fisher Scientific (Pittsburgh, PA) or Sigma Chemical Co. (St. Louis, MO) and were used as received.

4.2.1 Cell Harvesting

Because confluent cultures are not easily dissociated into a suspension of isolated cells amenable to counting and equal distribution among vials, a dispersion method more vigorous than the recommended scraping **[72]** was required. Cells were rinsed in calcium/magnesium free phosphate-buffered saline containing 20 mM glucose, then incubated for 4 min at 37 °C in 6 ml Hank's Balanced Salt Solution containing 2.5 g/l trypsin and EDTA. Trypsinization was quenched by trituration with 0.5 ml fetal bovine serum; the solution then was transferred to a 15 ml centrifuge tube, and clumps of cells were pelleted by setting the centrifuge to reach a maximum of 250 *g* at the end of a 7 s spin. The upper volume of supernatant (5.5 ml), which contained a suspension of

isolated cells, was transferred to a new centrifuge tube and pelleted at 250 *g* for 1 min. Supernatant then was removed and cells were resuspended in sufficient medium (~ 10 ml) to give final concentrations of ~ 3 x 10^6 cells/ml, as determined by hemacytometer count.

The cell suspension then was aliquotted into six microcentrifuge vials (1.5 ml each), yielding triplicate samples of both NAD(P)H and NAD(P); this redundancy allowed for human error so that at least duplicates would still remain at the time of analysis. Cells were sedimented (2 min, 500 *g*) and medium was removed by pipette. Vials then were centrifuged an additional 5 s at 500 *g* and remaining medium was touched off with a pointed cotton swab before the extraction buffer was added and sonication performed.

As a control for this harvesting method, extraction also was performed on still-adherent cells. Confluent cells on tissue-culture treated Petri dishes were rinsed in calcium/magnesium free phosphate-buffered saline containing 20 mM glucose and the rim of the dish was swabbed dry. The appropriate amount of extraction buffer then was added, and sonication carried out directly in the dish.

4.2.2 Extraction buffer

Some parameters of a previously reported procedure **[72]** were already at or near optimum. The suggested extraction buffer of 120 mM tris(hydroxymethyl)aminomethane (Tris) and 10 mM EDTA is suitable for solubilization both of various biomolecules and inorganic ions. Further, the buffer range of Tris (pK_a = 8.1) is ideal for cofactor storage **[74]** and enzymatic reduction of oxidized cofactors **[73]**, and Tris can inhibit degradation of oxidized cofactors under some alkaline conditions **[75]**. We initially speculated that it would be desirable to reduce the ionic strength of the extraction buffer, so that samples would better match CE run buffers. However, preliminary studies showed that lower

ionic strengths were neither sufficient for solubilization nor necessary for good separations.

To maximize analyte concentration in the final extract, cells should be homogenized into a minimal volume of buffer. However, large increases in the suggested ratio **[72]** of cells to buffer (10^6 cells per 75 µl) produced solutions too viscous for accurate transfer and CE analysis. Therefore, a ratio of 10^6 cells per 50 µl extraction buffer was used, which provides approximately one hundred volumes of extraction buffer for solubilization of each cell (200 – 300 µl of cell homogenate per vial).

The recommended extraction buffer **[72]** contained a nondenaturing, nonionic detergent (0.05% v/v Triton X-100) to support the activity of enzymes added to the extract. Extracts using this mild detergent were compared to extracts using anionic sodium dodecyl sulfate (SDS) and zwitterionic, cholesterol-based 3-[(3-cholamidopropyl)dimethylammonio]-1-propanesulfonate (CHAPS) in an extraction buffer optimized for pH (as below). The structures of these detergents are shown in Figure 4.1.

Figure 4.1: Detergents tested for cell extraction.

An acid-adjusted, detergent-free counterpart (AXB-D, pH 8.5) was prepared for these and every subsequent batch of extraction buffer, in order to prepare stock solutions of extract-matched ionic strength and composition without the complexities of foaming and poor surface tension that accompany the use of detergents.

Because reduced cofactors are unstable at low pH, and their oxidized forms are unstable at high pH, it generally has been necessary to prepare two extracts—an acid extract for the measurement of NAD(P), and an alkaline extract for the measurement of NAD(P)H **[73]**. To avoid the need for multiple extracts, earlier work **[72]** used an intermediate extraction buffer (pH 8). Because it was unclear whether such a solution could extract cellular cofactors as well as buffers having more extreme pH values, we evaluated a range of more basic conditions. Acidic conditions were not investigated, since alkaline conditions were required both for enzymatic activity and reduced cofactor storage.

4.2.3 Sonication

The sonication procedure for single samples **[72]** was altered in an attempt to homogenize six replicate vials contemporaneously and to minimize heating due to sonication. Samples were placed on ice and sonicated using a Sonic Dismembrator 60 (Fisher Scientific) at level 10. However, rather than 2 min of sonication per vial with a 30 s interval **[72]**, homogenization was made nearly simultaneous by using 15 rounds of 2 s followed by 3 rounds of 25 s, so that each vial received a total of ~ 2 min sonication. Sonication also was tested for a range of total durations, from 30 s to 3.5 min, by varying the total number of sonication rounds per vial. Following sonication, samples were immediately adjusted to pH ~ 8.5 by addition of 1.2 M HCl at a volume ratio of 2:25, mixed briefly by sonication at level 2, then centrifuged at 16,000 *g* to reduce foam in the emulsion.

4.2.4 Filtration

When unfiltered homogenate was injected into a capillary, analyte migration times slowed from run-to-run, indicating a steadily decreasing electroosmotic flow

velocity. To minimize changes to the capillary surface caused by adsorption of cellular macromolecules, a range of centrifugal filters was tested. Nylon and polyethersulfone membranes were found to bind NAD(P)H and to add undesirable interferents to the filtrate, so the more polar cellulose acetate membranes (Millipore, Billerica, MA) were chosen and subjected to a prewash cycle of water / 0.1 M NaOH / water (10 min each at 7,000 *g*). Washed filters were stored in water at 4 °C and dried by centrifugation (30 min at 7,000 *g*) immediately before use. A molecular weight cutoff of 30 kD was selected as a compromise between protein elimination and speed of filtration (smaller pores require longer centrifugation times). Filters prepared in this manner were used to remove large proteins from samples by filtration for 10 min at 7,000 *g*.

4.2.5 Enzymatic Conversion

Three of the six vials of extract from each flask of cells were treated enzymatically to convert the nonfluorescent oxidized cofactors to their fluorescent reduced forms. Glucose-6-phosphate dehydrogenase (G6PDH, EC 1.1.1.49) can catalyze the reduction of both NAD and NADP (Figure 4.2), although the K_M for NAD is somewhat lower than for NADP **[76]**.

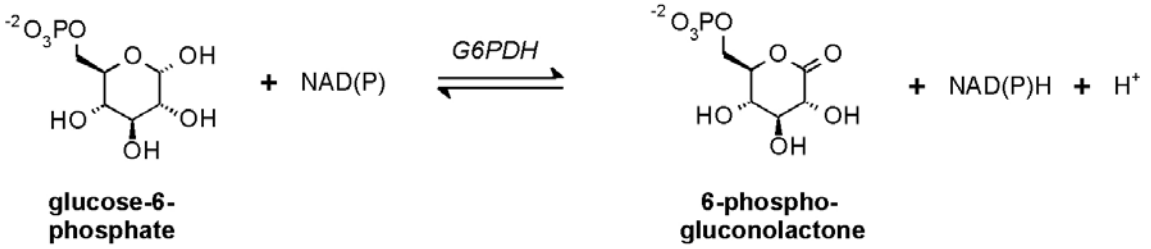

Figure 4.2: The reaction catalyzed by G6PDH.

Because products are not strongly favored (K = 6 at pH 7) **[73]**, a large excess of glucose-6-phosphate is required to drive the reaction to completion. Under our conditions, calculations show that 9 mM glucose-6-phosphate is sufficient to

quantitatively convert NAD(P) concentrations as high as 100 μM , which is more than tenfold greater than the levels observed in cell extracts.

Enzyme was supplied in 3.2 M $(NH_4)_2SO_4$ containing 50 mM Tris and 1 mM MgCl (pH 7.5); this solution was diluted 1:3 in AXB-D to yield stocks of 1 mg protein/ml. Stocks of both enzyme and substrate (0.2 M glucose-6-phosphate in AXB-D) were active after weeks of storage at 4 ºC and produced no measurable blank response (that is, the enzyme had no detectable NAD(P)(H) contamination) when cell-free, matched reactions were run in AXB-D. Stocks were added to cell extracts at a ratio of 1:20, yielding final concentrations of 45 μg G6PDH/ml and 9 mM glucose-6-phosphate. Conversions were carried out at 37 ºC for 30 min without mixing or agitation.

4.2.6 Instrumentation

As a compromise between the efficiency of two-photon NAD(P)H excitation **[77]** and laser stability, the laser was operated at 735 nm (full width at half maximum ≈ 4 nm); the beam was attenuated to ~225 mW before the long-pass dichroic mirror using a half-wave-plate/polarizer pair. Fluorescence was reflected from the laser beam path using a long-pass dichroic mirror (Chroma Technology, Rockingham, VT; part #500DCRB), which optimally reflects light in the approximate wavelength range 420 – 520 nm, a good match for the nicotinamide cofactors ($\lambda_{max,em} \approx 465$ nm) **[71]**. Data was acquired in 0.2-s bins with a 0.002-s interval.

The separation capillary was cut to a length of 30 – 35 cm and conditioned at least 10 min in 0.1 M NaOH before use. A relatively high-pH separation buffer was desirable to maintain the surface state of the capillary and to be compatible with cell extract samples, which were in pH ~8.6 buffer to protect reduced nicotinamide cofactors against degradation. Borate offers an appropriate pK_a (9.2) and the further advantage that it complexes with carbohydrates, such as the ribose rings in nicotinamide cofactors, which

increases their electrophoretic resolution **[78]**. A separation buffer of 100 mM sodium borate (pH 9.3) maintained reasonably fast electroosmotic flow, while retaining the capacity to baseline-resolve even the α- and β-anomers of NAD(P)H in preliminary tests of a standard mixture. The ability to differentiate between anomers was useful, to see that β-NADH in samples did not anomerize to α-NADH during storage. That process is slow (especially at high pH) **[79]**, and the equilibrium favors β-NADH about tenfold even at pH 7.5 **[80]**; however, it could have affected quantitation, since the spectral properties of α- and β- NAD(P)H are different **[79]**.

Samples were injected using a 2 kV potential for 10 s (non-enzymatic samples) or using 1 – 2 kV for 5 –10 s (converted samples), and separations were performed using potentials of 20 – 27 kV (~ 600 – 800 V/cm). Injection volumes (as calculated from electrophoretic mobilities of analytes) vary with these parameters and with the inner diameter of the capillary. As an example, an unconverted sample injected into a 15 μm inner diameter capillary 10 s at 2 kV corresponds to ~ 120 pL of NADPH. Larger injections tended to clog capillaries of this size inner diameter.

4.2.7 Standard Additions

The standard addition method of quantitation was adopted, which avoids the difficulty of producing standards matched to the composition of cell extracts and places less stringent demands on the stability of the CE-MPE fluorescence system. In the time required to collect data for a calibration curve, significant drift in instrumental parameters (laser intensity, pulse character, focal-point alignment, and condition of the capillary inlet) can occur. Therefore, solutions were analyzed in a pattern alternating the sample with its conjugate spike, until four consecutive electropherograms were obtained with ≤ 5% RSD between both sets of duplicates; these data were then used to calculate cofactor concentrations, as shown in Figure 4.3.

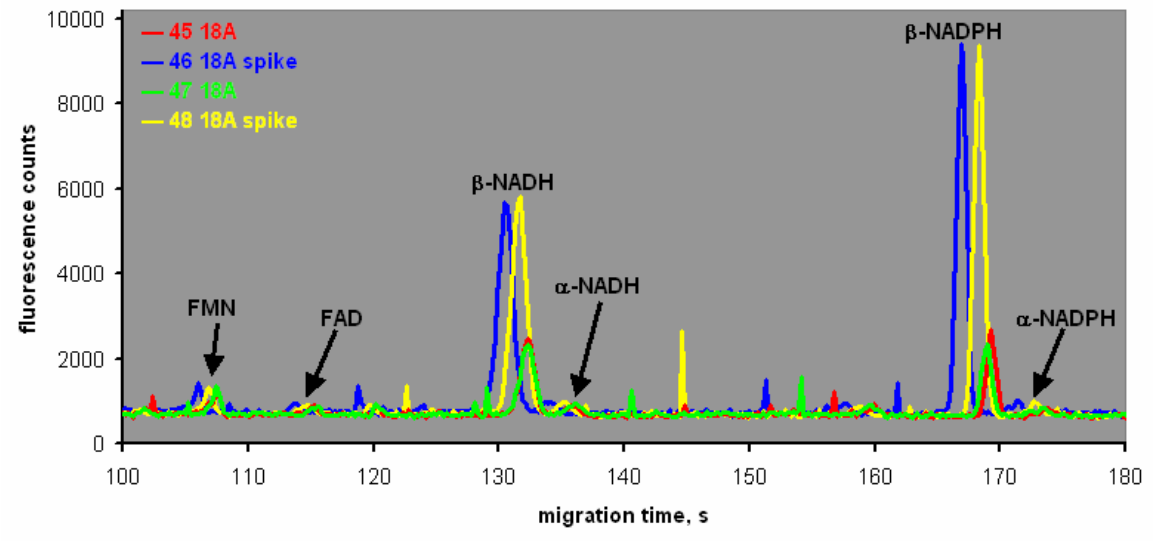

Figure 4.3: Overlay of four consecutive electropherograms of SCN2.2 cell extract and its conjugate spike. Samples were spiked 1:15 with a 15 µM mixture of NAD(P)H in AXB-D. The alpha anomers and the vitamin B_2 derivatives, flavin mononucleotide (FMN) and flavin adenine dinucleotide (FAD), were also detected in the sample; these peaks were identified by spiking (data not shown). In the legend key, the first number refers to the run (*i.e.*, these were the 45^{th} – 48^{th} samples injected for the day of analysis). The second legend number refers to the sample number (the 18^{th} sample taken in Clockwork XIV, 48.5 hours after the synchronizing pulse). The sample letter (A) indicates that this is the first of duplicate samples. From these four electropherograms, the sample was quantified at 0.53 ± 0.01 µM NADH and 0.27 ± 0.01 µM NADPH.

Samples were spiked at a volume ratio of 1:10 or 1:15 with standard solutions of NADPH and NADH in AXB-D. These volume ratios are as small as possible for practical use of pipettes. Spike stocks were 15 – 30 µM each in NADH and NADPH for non-enzymatic samples, and 75 – 150 µM NADH, 15 – 30 µM NADPH for enzymatically-converted samples. The concentration of the spikes was chosen to increase the signal of cellular samples to between 2 and 5 times of their original values. Samples were spiked immediately after filtration and stored at 4 ºC, though synchronized cells often required storage at –80 ºC to avoid significant degradation.

4.2.8 Results and Discussion of Methods Development

4.2.8.1 Sample Preparation

Trypsinization did not change NADP(H) or total NAD(H) content (> 90% confidence), but was found to cause a dramatic increase (~ 4-fold) in NADH. When changes to NADH levels are unacceptable, it is preferable to directly extract adherent cells. In-plate sonication requires two different plates for quantitation of NAD(P) and of NAD(P)H and a matched plate for counting of cells. Careful media changes are required so as not to dislodge cells. Because sonication of a thin layer of fluid may cause vaporization, it is helpful to add up to 5-fold more extraction buffer than dictated by the number of cells. This requires an appropriate dilution of standard solutions for spiking and larger injections for analysis; these more dilute solutions do not clog a capillary even when injected using 6 kV for 10 s.

Extraction efficiency was strongly dependent on buffer alkalinity: buffers having pH values between ~ 8 and 12 extracted significantly less NAD(P)H than those in the range, pH 12.4 – 12.8, while destruction of cofactors was evident at extremely high pH (Figure 4.4). Similar trends were not seen for total NAD(P)(H) content, as oxidized cofactors are readily extracted across the entire pH range examined (data not shown), though dramatic destruction is also seen at pH 13.3 for these species. The optimal pH range for extraction of reduced cofactors unfortunately is not ideal for the extraction of oxidized cofactors, due to instability of NAD(P) in strongly basic solutions. However, because alkali-promoted cofactor destruction is temperature-dependent, it can be minimized by using iced extraction buffer and limiting exposure time. For example, calculations based on literature kinetic constants **[74]** show that 15 min exposure to a pH 12.6 solution at 0 ºC should degrade only ~ 1% of oxidized cofactor. This prediction was experimentally examined.

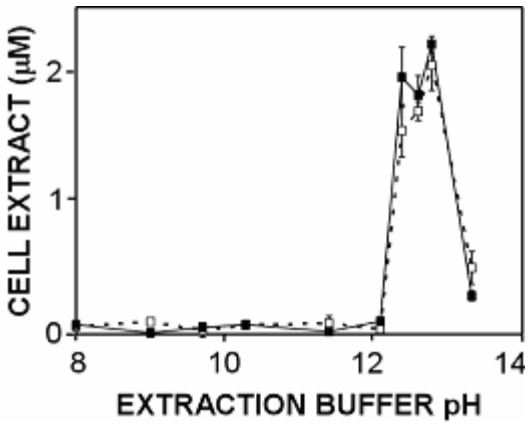

Figure 4.4: Extraction of reduced cofactors (NADH, - -□- -, and NADPH, —■—) from SCN 2.2 cells using CHAPS buffers of various pH values. After sonication, extracts were immediately adjusted to pH ~ 8.5; values are corrected for this dilution. Data points are single vials with error bars representing standard deviations (error analysis of duplicate CE runs and pipette tolerances).

Cellular NADH was extracted at similar efficiency by all three detergents, but both CHAPS and SDS extracted tenfold more NADPH than did Triton X-100, as shown in Figure 4.5. Consequently, SDS was used for initial experiments, but ultimately was discarded in favor of CHAPS for several reasons. Unlike SDS, CHAPS is suitable for enzymatic assays, soluble at high pH, and produces solutions with surface tensions sufficient for accurate pipetting. Further, SDS-based cell extracts often clogged and broke the centrifugal filters (suggesting that SDS was unable to fully solubilize cellular components), while CHAPS extracts passed through easily and yielded larger filtrate volumes. Therefore, CHAPS was added to the extraction buffer at 7 mM; this concentration is low enough to support enzyme activity, but above the critical micellar concentration **[81]**, a condition which may be necessary for cell lysis **[82]**.

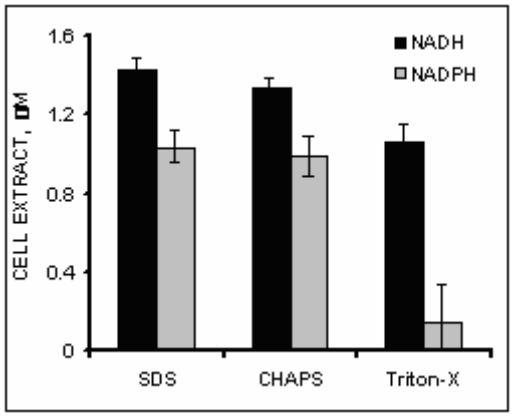

Figure 4.5: Quantitation of NAD(P)H in SCN2.2 cell extracts prepared with various detergents (2.5 mM each, designed to be above the effective critical micellar concentrations of SDS and Triton X-100. Even though this concentration is below the CHAPS critical micellar concentration, CHAPS extracts just as well as SDS).

A total sonication time of ~2 min per vial, recommended by earlier protocols **[72]**, was indeed found to be both necessary and sufficient for extraction of cofactors. However, the division of this time among the vials was crucial to the resulting NADH levels, although NAD(P)(H) and total NAD(H) levels were affected only to minor degrees. The longer cells were chilled before sonication, the lower NADH levels fell; thus, the third vial had much less NADH than the first, and the fifth vial had even less. However, it was possible to minimize this decay by keeping the cells warm and reducing the delay to sonication of later vials, as shown in Table 4.1.

Table 4.1: NADH remaining in delayed-sonication vials (normalized to Vial 1)

Sonication	Buffer temp.	Vial 3	Vial 5
6 x 5 s[a]	0 ºC	70%[b]	60%[b]
	37 ºC	90%[b]	80%[b]
20 x 2 s[a]	37 ºC	100%[c]	90%[c]

[a]Followed by 2 x 30 s
[b]One sample each: standard deviation ~10%
[c]Eight samples: standard deviation ~10%

Filtering a standard solution (300 µl, 30 µM each NAD(P)H) until the filtrate and retentate were equal in volume did not change cofactor concentrations in either fraction, indicating that the filter membrane itself does not adsorb or degrade analyte. Further, when ~300 µl cell homogenate was centrifuged through the filters in ~100 µl fractions, the second fraction contained the same amount of NAD(P)(H) as the first (within measurement error for N = 6 vials). Finally, when a cell pellet in 325 µl extraction buffer was spiked with 10 µl of standard solution (~15 µM each NAD(P)(H)), the spike was fully recovered (NAD(H), 110 ± 10%; NADP(H), 103 ± 8%) after sonication, pH adjustment, filtration, and enzymatic conversion.

An underlying goal in our procedure was to minimize both the number of pipettes and the changes in their settings; it is possible to produce final samples from cell suspensions using only five pipettes (two 1-ml pipettes, one set at 0.75 ml for cell suspensions and one with variable setting for extract buffer; two 20-µl pipettes, one variable for addition of acid, and one set at 5 µl for spike, substrate, and enzyme solutions; and a 100-µl pipette set at 50 µl for cell filtrates). The in-plate sonication experiment (for 8 cm^2 plates) requires only three pipettes (1 ml for extraction buffer, 75 µl for acid or filtrate, and 5 µl for stocks). Some pipettes must be dispensed twice to

deliver appropriate volumes, but this minimization of equipment greatly facilitates long-term and late-night experiments.

4.2.8.2 Quantitation

Separation and detection quality varied daily according to laser and capillary characteristics. However, a typical separation of an unconverted cell extract yielded ~10^5 theoretical plates and NAD(P)H limits of detection of ~100 nM (~50 amol). These concentration detection limits are comparable to previously published results from this laboratory **[66]**, as well as those achieved using other CE detection strategies **[83-85]**. The combination of filtration and a high-pH separation buffer made migration times extremely reproducible (*e.g.*, peak times could vary as little as 1% for 15 consecutive injections of cell extract).

Spiking confirmation curves were prepared from NAD(P)H standards in AXB-D to confirm the accuracy of quantitation by spiking, the appropriateness of the spike ratio and concentration, and the method of using samples as test solutions to evaluate instrumental stability. Confirmation curves prepared from NAD(P) standards subjected to the preparative process (2 min total sonication—2 x 15 s followed by 3 x 30 s—in iced pH 12.6 extraction buffer, pH adjustment with 1.2 M HCl, and conversion by addition of enzyme and substrate) show that no degradation of NAD(P) is detectable and that conversion is essentially complete. Table 4.2 summarizes these confirmation curves, for which each data point represented a 2 – 50 fold increase in unspiked signal, as shown in Figure 4.6. While a 50-fold increase at low sample concentrations is higher than desirable, more modest ratios are found in the usual working range of the confirmation curve.

Table 4.2: Confirmation curves for standard solutions

	Spike, µM	Slope[a]	Intercept[a]	N[b]	Range, µM
NADH	30	1.10 ± 0.05	0.0 ± 0.1	5	0.15 – 2.1
NADPH		1.08 ± 0.09	0.0 ± 0.2		
NADH[c]	150	1.04 ± 0.04	-0.1 ± 0.2	11	0.3 – 12
NADPH		1.02 ± 0.05	0.0 ± 0.3		
NAD	150	1.08 ± 0.03	0.0 ± 0.2	7	0.5 – 12
NADP		0.96 ± 0.09	0.02 ± 0.2		

[a]All R^2 values > 0.99
[b]N = Number of samples to generate confirmation curve
[c]Data plotted in Figure 4.6

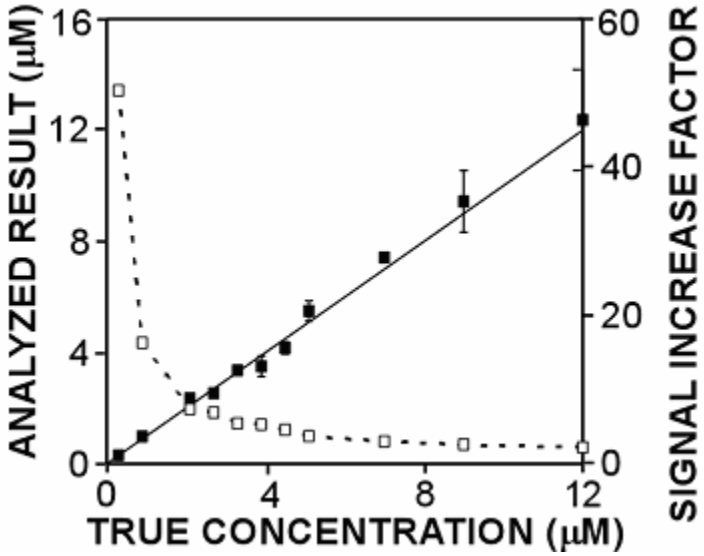

Figure 4.6: Confirmation data (■) for NADH standards ranging 0.3 – 12 µM, spiked 1:10 with 150 µM stock. The solid line represents the ideal response, (i.e., when analyzed concentration equals true concentration). Also shown is the factor by which the spike increased the raw signal for each data point (-□-).

Standard deviations for concentrations of unknown samples (c_u) were calculated for each sample by propagation of error from the equation for standard additions:

$$c_u = \frac{S_u \cdot c_s \cdot V_s}{(S_s - S_u) \cdot V_u} \qquad [4.1]$$

where S_s and S_u are the signal from the spiked and unspiked samples, respectively (error from standard deviation of duplicate peak areas), c_s is the concentration of the added spike (not propagated with error since it was constant throughout an experiment), and V_s and V_u are the volumes of the added spike and sample, respectively (error from pipette tolerances given by their manufacturers) **[61]**.

When the same vials of cell extract and its conjugate spike were analyzed five times over two consecutive days, no two results differed significantly (confidence > 90%). Further, analysis at two days and two weeks after collection yielded results that were not statistically different (confidence > 90%, N = 2). Together, these results support both quantitation reproducibility and long-term solution stability; any degradation of sample was normalized by matched degradation of its conjugate spike.

Published values for content of NADP(H) in cultured bovine aortic endothelial cells based on spectrophotometric measurements of homogenates **[72]** are much higher than values determined in the current studies. However, direct spectrophotometry neither separates out nor corrects for binding proteins and interfering chromophores, increasing the likelihood of overestimation. Fluorescence microscopy studies have demonstrated the need for such corrections **[12, 24]**: the observed fluorescence of NAD(P)H typically increases ~ 8- to 12-fold when it is bound as a coenzyme, and most NAD(P)H is bound in normal cells. Moreover, fluorescence from cellular components (such as collagen, elastin, FAD, or lipopigments) also contribute to a background signal **[12]**. Our method avoids these problems by dissociating cofactors from proteins and separating analytes to allow unambiguous determination of unbound NAD(P)H.

Some of the possible interferents, FAD and FMN, can be seen in Figure 4.3. These species were not unexpected; peaks from standard solutions were detected in this lab's early work with CE-MPE **[66]**. FMN and FAD have two-photon action cross

sections (at λ_{ex} = 735 nm) that are approximately a hundredfold and tenfold (respectively) better than the reduced nicotinamides **[77]**, and their emission is appropriate for collection by the dichroic mirror in use for these experiments. The identities of the peaks in Figure 4.3 were assigned by spiking. The structures of the flavins are shown in Figure 4.7.

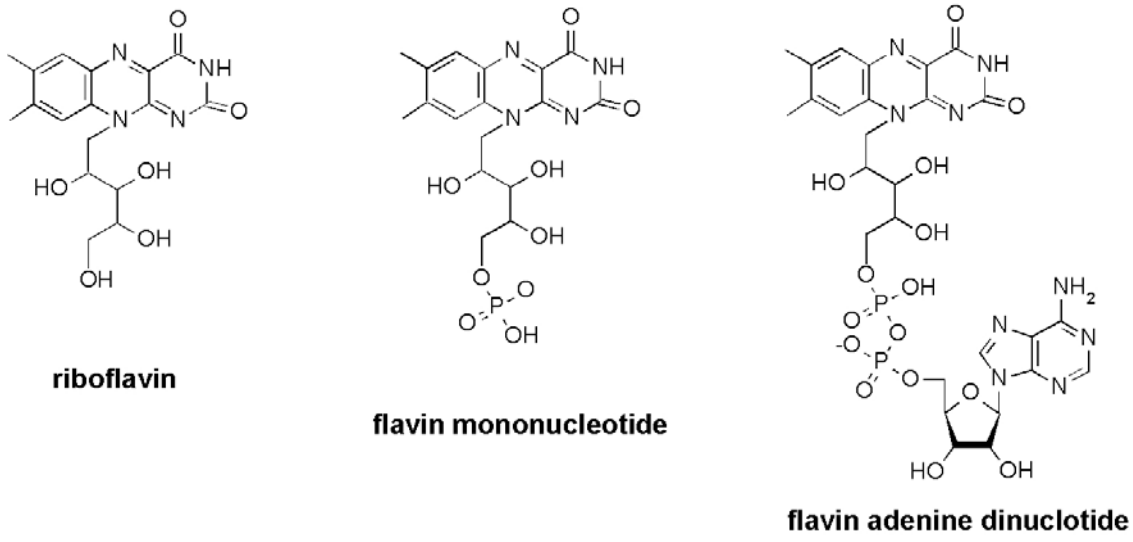

Figure 4.7: Structures of riboflavin (vitamin B_2), flavin mononucleotide, and flavin adenine dinucleotide. Approximate charge states (shown) are for pH 9.3; the pK_a of the second pyrophosphate hydrogen ion is 9.4 **[3]**. Riboflavin was not investigated in these cells, but is detected in cell extract studies presented in Chapter 5.

Though detected in nearly all samples, flavins were not quantified, and percent recoveries and stabilities were not investigated. However, this work is the first application in this lab of CE-MPE to cellular extracts containing flavins; ease of detection demonstrated here shows future work with these cellular analytes would be straightforward.

4.2.9 Conclusions on Methods Development

The method (shown in Figure 4.8) is necessarily more complex than its predecessors and alternatives **[71, 72]**, but is still suitable for one researcher to take

extractions at 2 – 3 hour intervals over a day or more, or as frequently as every half-hour for shorter durations.

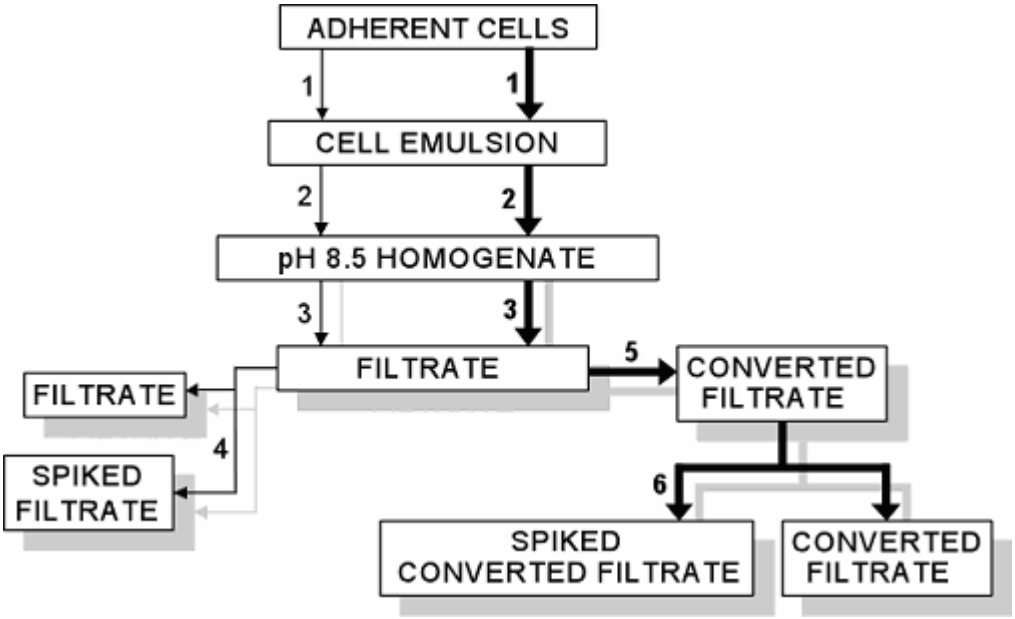

Figure 4.8: Flow chart for optimized procedures used in circadian experiments. Bold lines indicate pathway for samples intended for enzymatic analysis, and shadowed steps indicate duplicates.

1. Petri dishes (8 cm^2) of cells are rinsed by pipette in calcium/magnesium free phosphate-buffered saline containing 20 mM glucose (which is approximately equimolar with culture medium), and residual solution is removed from the rim of the dish with a pointed cotton swab. Extraction buffer is added (1 ml of 120 mM Tris, 10 mM EDTA, and 5 mM CHAPS, pH 12.6) at ~ 0 ºC for enzymatic samples or 37 ºC for nonenzymatic samples (performed 30 min after enzymatic samples). Petri dishes then are placed on ice and cells sonicated 3 min at level 10.
2. HCl (75 µl, 1.2 M) is added and mixed by brief sonication at level 2.
3. Homogenate is divided between two centrifuge vials with prewashed and dried 30 kD cellulose acetate filters. Filtration (15 min, 14000 *g*, 20 ºC) yields > 150 ml of filtrate in each of the duplicate vials.
4. Aliquots (75 µl) of non-enzymatic filtrates are spiked with 5 µl of stock solution containing 15 µM each NAD(P)H in AXB-D.
5. Enzyme (1 mg/ml) and substrate (0.2 M) solutions (5 µl each) are added to 150 µl of filtrate and incubated 30 min at 37 ºC.
6. Aliquots (75 µl) of converted filtrates are spiked with stock solution containing 75 µM NADH and 15 µM NADPH in AXB-D.

Samples are then stored at –80 ºC until analysis by CE-MPE.

Unfortunately, this method cannot provide subcellular information on reduced cofactor levels, and subcompartments may be significantly different in their contents. However, molecular shuttles and transport make it unlikely that robust rhythms could occur within cellular subcompartments without being communicated rapidly throughout the cell. It is especially unlikely that multiple subcellular rhythms for the same compound would coexist antiphase to one another. Although it is possible that arrhythmic character of one cell type could mask cycles in another, differentiation of SCN2.2 cultures in N2-containing medium or on laminin can produce up to 80% neuronal character **[39]**, and glucose uptake rhythms have been clearly observed in these mixed cultures **[47]**. By using a cell line from an isolated brain nucleus, appropriately synchronized and differentiated, this method offers unambiguous and time-defined NAD(P)(H) values, yielding the most appropriate information yet produced about the relevance of NAD(P)(H) in the master biological clock of the brain.

4.3 Results of Circadian Tracking Experiments

In the first day following serum shock, cellular NADH levels increased approximately threefold, and NAD(H) levels increased ~ 1.5-fold (Figure 4.9A). The overall effect was an approximately twofold increase in the NAD redox state (i.e., a greater percentage of the total pool is reduced). When the experiment was repeated with matched control cells (which received medium changes instead of a serum shock; data not shown), no NADH or NAD(H) increase was seen in control cells. Serum-induced changes in NADP(H) and NADPH were not obvious (Figure 4.9B) until the experiment was repeated with matched controls (Figure 4.9C). There was no statistical difference between control and pulsed NADP(H) levels, and both remained constant over the initial 24 h, so the concentration ratio is plotted for visual clarity. Figure 4.9C demonstrates a small but significant decrease in the NADP(H) redox state in the initial 24 h after a serum

pulse. Because our data show arrhythmic changes which plateau or recover after approximately one day, and previously reported protein cycles are more dramatic after this period **[46]**, subsequent investigations began at least 24 hours after the end of the FBS pulse.

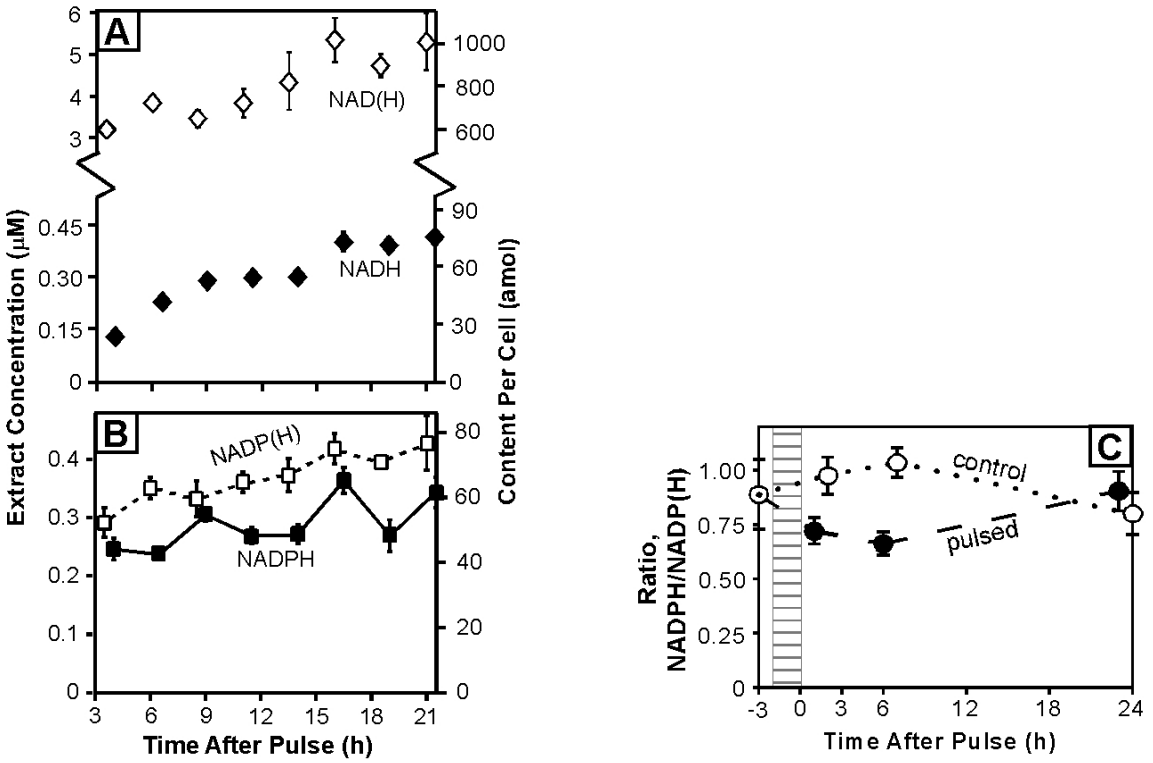

Figure 4.9: Tracking NAD(P)(H) in SCN2.2 cells the first day after an FBS pulse. A. NAD(H) (◊) and NADH (♦). Note break in y-axis. B. NADP(H) (- □ -) and NADPH (—■—). For A and B, each data point represents two vials from one Petri dish of cells; each vial was analyzed in duplicate as described in Section 4.2.7. Standard deviations and pooled standard deviations were calculated for each data point; error bars represent the larger value, and apply to the concentration axis only (standard deviation in content per cell is greater due to error in cell counting). C. Tracking the NADPH/NADP(H) concentration ratio in SCN2.2 cells before (⊙) and the first day after media changes (hatched area) or an FBS pulse (●) or control medium (○). Standard deviations were calculated for both NADPH and NADP(H) as in Figure 4.9B and were propagated together to yield error bars.

Three separate experiments were performed, sampling at 3-h intervals: the first ("Clockwork XIII") ranged 30 – 54.5 h postpulse, the second ("Clockwork XIV") from 24 – 75.5 h postpulse, and the third ("Clockwork XV") from 36 – 84.5 h using cells raised on laminin-coated plastic. Results are plotted in Figure 4.10: no cyclic behavior was observed in any of these experiments. Moreover, little variation of any kind was observed: the NADPH/NADP(H) ratio varied less than 15% (0.8 ± 0.1 for N = 44 measurements) and the NADH/NAD(H) ratio varied less than 20% (0.13 ± 0.03, N = 44). These ratios are comparable to RN33B cell ratios (data not shown): their NADPH/NADP(H) ratio was 0.9 ± 0.2 (N = 14) and the NADH/NAD(H) ratio was 0.08 ± 0.02 (N = 14).

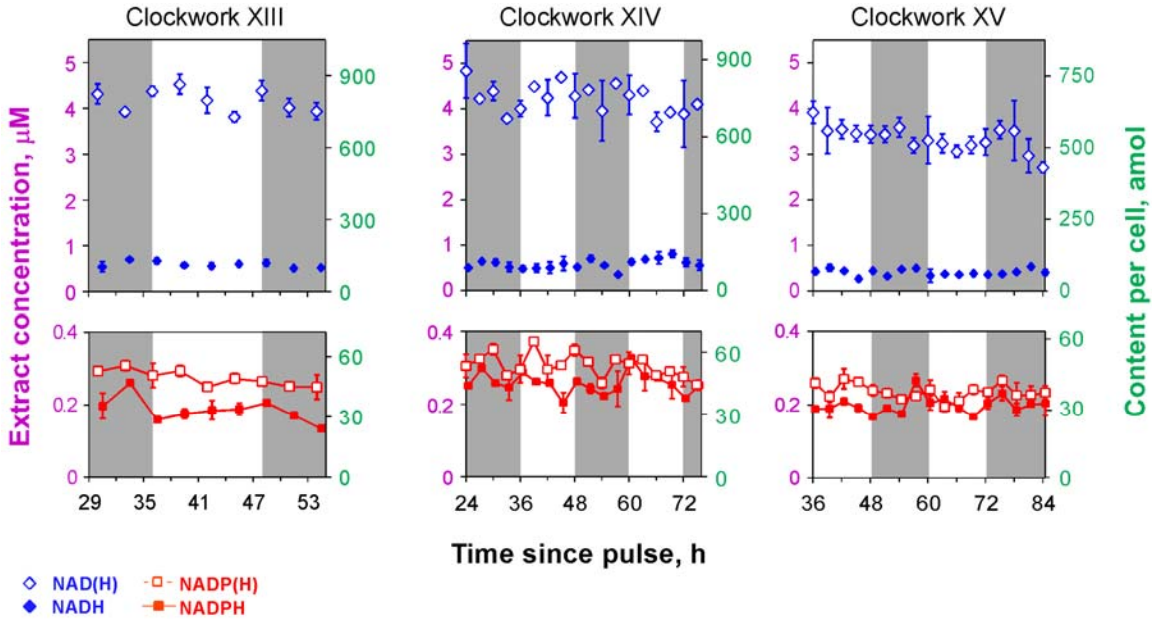

Figure 4.10: Tracking NAD(P)(H) in SCN2.2 cells 1 – 3 days after an FBS pulse; error bars as in Figures 4.6, 4.9A, and 4.9B. Shaded areas represent subjective night as determined by the FBS pulse.

Cofactor content per cell for these experiments, and comparisons to RN33B cells, are listed in Table 4.3. Because "Clockwork XV" was performed using cells cultured

under distinct conditions (laminin-coated plastic and fungizone), values for that study are given separately. Also given in Table 4.3 are approximate concentrations of cofactors per cell, calculated by assuming a cell can be modeled as a hemisphere, and using the smallest reasonable cell diameter (sizes range 6 – 12 μm for SCN2.2 cells **[39]**, and ~ 10 μm appears minimum for RN33B cells from published images **[37, 40]**.

Table 4.3: Cofactor content per cell.

Experiment	N[a]	NADH	NADPH	NAD(H)	NADP(H)
		amol per cell[b]			
SCN2.2, XIII & XIV	27	100 ± 20	39 ± 7	760 ± 60	53 ± 5
SCN2.2, XV	17	70 ± 10	29 ± 4	530 ± 40	37 ± 3
RN33B	14	34 ± 8	45 ± 3	440 ± 80	52 ± 8
		maximum concentration per cell, mM			
SCN2.2, XIII & XIV	27	0.9 ± 0.2	0.35 ± 0.07	6.7 ± 0.6	0.47 ± 0.05
RN33B	14	0.13 ± 0.03	0.17 ± 0.01	1.7 ± 0.3	0.20 ± 0.03

[a]N = Number of Petri dishes sampled.
[b]Standard deviations as in Figures 4.9A, 4.9B, and 4.10 were propagated together with error from hemacytometer counting to yield final standard deviations.

4.4 DISCUSSION

The most dramatic change observed in NAD(P)(H) levels in SCN2.2 cells was an approximate threefold NADH increase during the first day after an FBS pulse. Because FBS contains numerous components, it is difficult to assign this cellular response to a single stimulant. Nevertheless, a likely cause may be the removal and replacement of insulin that accompanies the serum shock; the concentration of insulin is ~ 250-fold greater in neuronal medium than in 50% serum mixture (see Table 2.2). Insulin promotes cellular glucose uptake, and has been shown to increase the NADH/NAD(H) redox state in smooth muscle **[86]**. The concurrent but smaller percentage increase in NAD(H) concentration, which may represent cellular compensation for NADH upregulation, is an interesting and previously unnoted finding that merits further investigation. Whatever the

cause, NADH upregulation also suggests a possible explanation for the FBS-induced decrease in NADPH redox state shown in Figure 4.9C; cellular excitation and increased metabolism produce reactive oxygen species, which are scavenged by a glutathione/NADPH pathway **[1]**. While these results are not relevant to circadian rhythms, and so were not further investigated, these data demonstrate the utility of our analysis methods for tracking changes in cellular cofactor content.

Despite the sensitivity of these methods to small changes in NAD(P)(H) levels in SCN2.2 cells over the appropriate time periods, no circadian NAD(P)(H) rhythms were observed. A possible explanation for this tight regulation of NAD(P)(H) levels may lie in the kinetics, equilibria, and regulation of cellular metabolism and oxidative phosphorylation. SCN cells exhibit circadian rhythms at both the metabolic entry point (glucose uptake) and at its end result (ATP content **[87]**). However, neuronal metabolism from glucose to ATP is sufficiently fast that no associated buildup or rhythm need necessarily be observed in intermediates, such as NADH. If an artificial bottleneck could be applied to halt the processes that deplete NADH in the ATP pathway—analogous to using 2-deoxyglucose in glucose uptake studies—a rhythm in NADH production might be observed. It is also possible, despite extensive published characterizations of the SCN2.2 line that show its utility as an SCN model **[39, 45, 47]**, that the observations in SCN2.2 cells do not reflect cellular behavior *in vivo*. Moreover, since SCN cells express Clock:BMAL1 as a clock-like transcription factor, it would be interesting to compare results from cells expressing the NPAS2:BMAL1 analogue.

The NADH/NAD(H) concentration ratio in SCN2.2 cells never rose high enough in these experiments to support the *in vitro* findings for clock-like transcription factor activity. A ratio of ~ 0.6 – 0.8 NADH/NAD(H) appears necessary to induce DNA binding of NPAS2:BMAL1 **[19]**, but we found the ratio to be no greater than 0.13 ± 0.03.

The ratio demonstrated here is even lower than that observed in other rat brain regions, reported to be 0.20 ± 0.04 in striatum and 0.3 ± 0.1 in cortex **[14]**. The ratio for SCN2.2 cells is also comparable to that found in RN33B cells (0.08 ± 0.02). The NADPH/NADP(H) concentration ratio in SCN2.2 cells was found to be 0.8 ± 0.1; this value is more appropriate to clock-like transcription factor activity and is comparable to, or higher than, values previously reported for other rat brain regions (0.4 ± 0.3 for hippocampus, 0.6 ± 0.1 for striatum and midbrain, and 0.6 ± 0.3 for cortex **[14]**). The ratio is SCN2.2 cells is also comparable to that found in RN33B cells (0.9 ± 0.2). However, the measured ratio is a whole-cell average, and the ratio in the nucleus should be much lower. Reduced cofactors are concentrated in mitochondria, lower in cytoplasm, and lowest in the nucleus; no comparable cellular differential should exist for oxidized cofactors, since they are less tightly bound to proteins **[10]**. Thus, total NAD(P)H/NAD(P)(H) concentration ratios determined for whole cells is less than that found mitochondria and greater than that in the cytosol and nucleus. Moreover, the redox state of unbound cofactors is expected to be far lower than that for the total cofactor content of a cell. For instance, it has been reported that the cytosolic NADH/NAD(H) concentration ratio in liver cells is 0.1 total, but only 0.001 for free cofactors; in mitochondria, that ratio is 0.3 total and 0.1 free **[10]**.

More revealing, however, are the absolute cellular concentrations determined in this work. Even when calculations were given favorable allowances (i.e., using the minimum cell diameter, to yield an upper bound for cellular concentration), the approximate intracellular NADPH concentration in SCN2.2 cells was found to be < 0.7 mM. Though greater than in RN33B cells (0.17 ± 0.01), this value is still much lower than the reported EC_{50} of 4.1 mM NADPH **[19]**, and the aforementioned intracellular compartmentalization and protein-binding of reduced cofactors should render the free

concentration of NADPH in the nucleus much lower than 0.7 mM. Consequently, the physiologic relevance of in vitro activation of clock-like transcription factors is not supported by this study.

4.5 Extensions and Future Work

It would be interesting to quantify NAD(P)(H) in cells expressing the forebrain analogue of the SCN Clock:BMAL1 complex, since the forebrain analogue (NPAS2:BMAL1) was emphasized by the authors of the seed paper for this work **[19]**. An appropriate neuroblastoma cell line was established in the same lab **[88]**, which would suit our experiments and would be make any results particularly relevant and noteworthy.

Our method could not reveal differences between mitochondrial, cytosolic, and nuclear changes. Preliminary attempts (data not shown) were made to isolate mitochondrial fractions from SCN2.2 cells by following a general protocol **[89]**. It was possible to extract and quantify mitochondrial NADPH and NADP(H)—with dubious certainty—but mitochondria clearly lost NAD(H) content, likely to diffusion and to cold-induced NADH consumption (as demonstrated in Table 4.1). Therefore, extraction of fractionated subcellular compartments would not yield useful information. It would be more interesting to perform intact quantitative multiphoton microscopy of the SCN2.2 line, toward which our lab has already demonstrated capabilities **[90]**. This would also help to distinguish content between neuronal and glial subtypes. Single-cell or single-subtype extractions could also be interesting.

Similarly, enzymatic screenings to reflect free-to-total ratios of NAD(P)(H) **[10]** in SCN2.2 cells would be more relevant than our literature comparisons to other cell types.

Chapter 5: Assays of Indoles and Poly-ADP-ribose Formation in Serotonergic Neurons

5.1 INTRODUCTION

Serotonin is a neurotransmitter of longstanding interest to our lab. In the brain, serotonin is perhaps best known for its role in depression, and serotonergic neurons arising from the pontine and midbrain raphe nuclei are targets of many popular antidepressant drugs. The serotonergic neurons from the medullary raphe nuclei, which are examined in this work, innervate the spinal cord more than the brain. Treatment of the medullary raphe with morphine or endorphins can produce analgesia, and the raphe can prevent the passage of nociceptive signals from the spinal cord into higher levels of the brain, where the perception of pain is generated **[91]**. Therefore, the medullary raphe nuclei are of interest for the pharmacology of pain management and related drugs of abuse.

Serotonin is synthesized *in vivo* from tryptophan, as shown in Figure 5.1. Several loci along its synthetic and catabolic pathways are targets of drug therapy. Tryptophan hydroxylase catalyzes the rate-limiting biosynthetic step, and evidence suggests that activation of this enzyme, and the consequent rate of serotonin synthesis, are governed by the level of firing in serotonergic neurons **[33]**. Depolarization-induced activation appears to involve phosphorylation of the enzyme **[33]**. Dietary supplements of 5-hydroxytryptophan are available over-the-counter, and increase basal levels of serotonin by skipping over this rate-limiting step **[92]**. Monoamine oxidase inhibitors, widely used to treat depression, seek to elevate levels of serotonin (and other neurotransmitters) by inhibiting catabolism. It is thus often useful to analyze levels of

serotonergic precursors and catabolites along with serotonin itself when assessing blood, tissue, or cerebrospinal fluid.

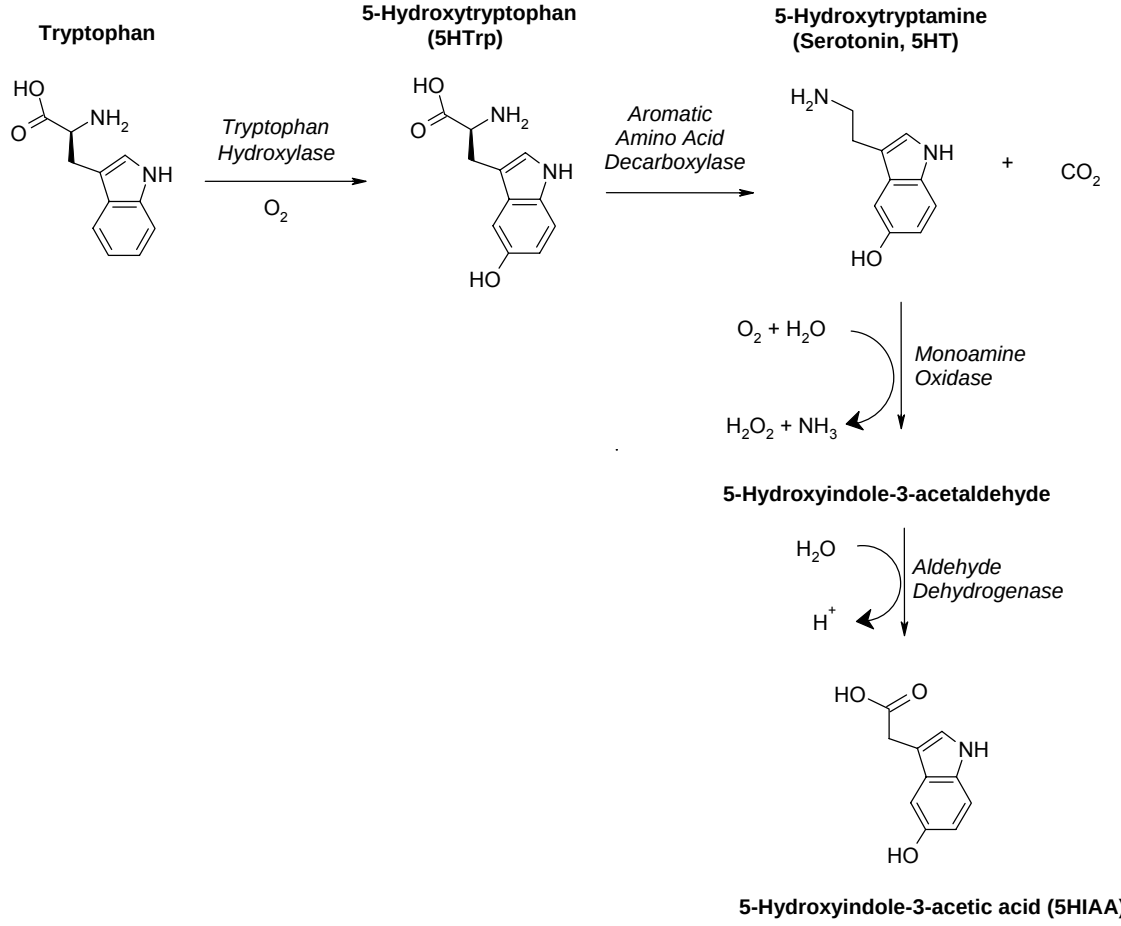

Figure 5.1: The major synthetic and catabolic pathways of serotonin **[33]**; enzyme cofactors not shown. The structure of the catabolic intermediate, 5-hydroxyindole-3-acetaldehyde, is omitted because conversion to 5-hydroxyindole-3-acetic acid is rapid *in vivo*.

Changes in 5HTrp, 5HT, and 5HIAA levels can be induced by electrical depolarization of the raphe nuclei *in vivo* **[93]**, and upregulation in serotonergic phenotype can be induced by chemical depolarization *in vitro* **[94]**. The differentiation of raphe-derived RN46A cells is a complex process; undifferentiated cells contain only small quantities of tryptophan hydroxylase or serotonin; treatment with BDNF causes an

upregulation in both tryptophan hydroxylase and aromatic amino acid decarboxylase **[32]**. However, cells still do not synthesize large amounts of serotonin until depolarized (*e.g.* with 40 mM KCl), which can cause a 3-fold increase in serotonin levels within four days **[32]**.

The membrane potential (V_m, in millivolts) caused by altering salt levels in the extracellular medium ($[K^+]_o$ or $[Na^+]_o$) can be estimated using the Goldman equation, which is based on the Nernst equation:

$$V_m = 61.5 \cdot \log \frac{P_K \cdot [K^+]_o + P_{Na} \cdot [Na^+]_o}{P_K \cdot [K^+]_i + P_{Na} \cdot [Na^+]_i} \qquad [5.1]$$

where P_K and P_{Na} are the relative permeabilities of the membrane to potassium and sodium (approximately 40 and 1, respectively), and $[K^+]_i$ and $[Na^+]_i$ are their intracellular concentrations (about 100 mM and 15 mM, respectively) **[91]**. From media components listed in Table 2.2, then, resting potential of a cell in Neurobasal™ medium is –70 mV, and increasing extracellular K^+ to 40 mM raises the potential to –20 mV.

The exact mechanism of serotonergic activation by depolarization is not known, though it appears to be calcium-dependent **[33]**. A mechanism with many shared characteristics has been well elucidated in cortical neurons, which involves a pathway from depolarization to activation of phospholipase C, inositol-triphosphate mobilization of calcium, and activation of poly-ADP-ribose polymerase **[31]**. In those cortical cells, depolarization with 60 mM KCl (to –10 mV by the Goldman equation) caused dramatic poly-ADP-ribosylation of nuclear proteins within 10 minutes **[31]**. Therefore, we hypothesized that depolarization-induced changes in 5HTrp, 5HT, and 5HIAA levels in immortalized raphe cells might be accompanied by a decrease in NAD levels, and we sought to track such changes using capillary electrophoresis with MPE fluorescence

detection, a system previously shown to simultaneously provide high sensitivity detection for these spectrally diverse compounds.

5.2 EXPERIMENTAL METHODS

The same methods for NAD(H) assays in Chapter 4 were used, with some few alterations to include analysis of hydroxyindole species.

5.2.1 Instrumentation

A dichroic mirror better able to collect both hydroxyindole and nicotinamide fluorescence was used (Chroma Technology #585DCXR). Bin length was increased from 0.2 s to 1 s with a 0.002 s interval, a change that improved detection limits at the cost of peak definition.

It has been demonstrated in our lab that CE-MPE detection limits for hydroxyindole species can be substantially improved either by deoxygenation of buffers or by the use of Good's buffers, such as HEPES **[95]**. To be compatible with cell extracts, a high-conductivity run buffer was required, so buffers previously optimized for CE-MPE of standard indolic solutions **[95, 96]** could not be used. In preliminary experiments, borate-based run buffers containing various concentrations of HEPES yielded a high background noise and tended to clog the capillary outlet. Therefore, borate run buffer (175 mM, pH 9.0) was deoxygenated in the instrument by bubbling argon at the inlet during runs, and by blowing argon over the outlet to maintain an argon blanket. The surface area-to-volume ratio of the outlet was decreased (by using one section of an 8-chambered coverslip, 0.8 cm^2, rather than a 1-chamber coverslip, 9.4 cm^2) in efforts to avoid excessive evaporation. While there is substantial run-to-run variability in peak areas, the results shown in Figure 5.2 may be considered representative of the effect of deoxygenation.

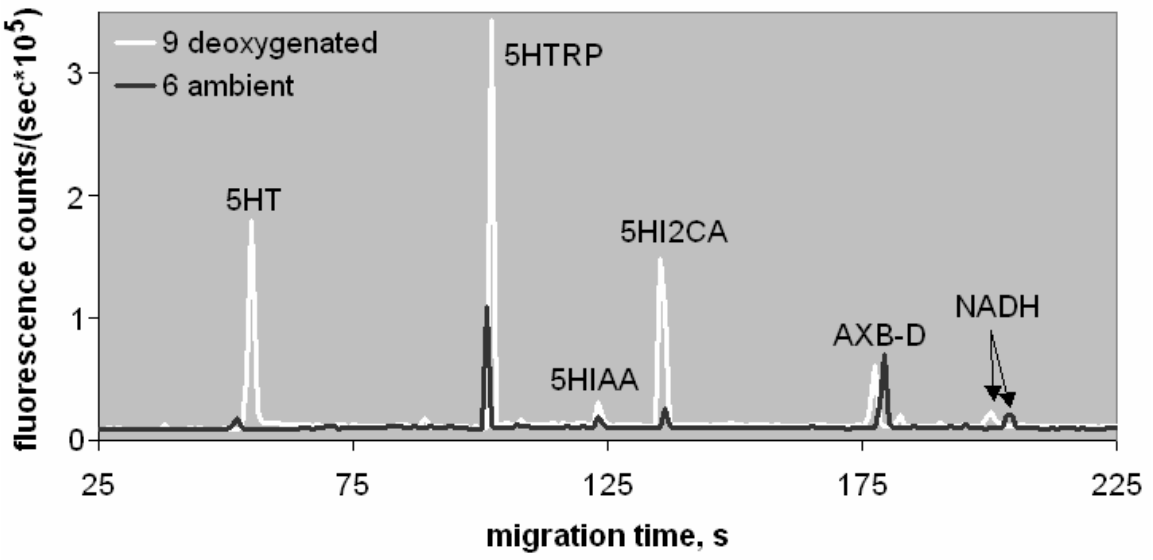

Figure 5.2: The effects of deoxygenation for CE-MPE of hydroxyindoles. Standards were dissolved AXB-D and are 5 μM for 5HT, 5HTrp, and 5HIAA; 0.3 μM for 5-hydroxyindole-2-carboxylic acid (5HI2CA); and 0.15 μM for NADH. The peak labeled "AXB-D" is a blank response peak. Laser parameters: 755 nm, 540 mW. Injection 6 kV 10 s, separation at 19.5 kV.

The relatively unchanged NADH peak areas in Figure 5.2 allows NADH to serve as an internal standard, since oxygen does not greatly affect NADH fluorescence. The multiphoton excitation of hydroxyindoles is a much more complicated process than that of NADH; oxygen can react with the hydroxyindoles to create nonfluorescent side products, as shown in Figure 3.10. The optimal wavelengths for the three-photon phototransformation step of indoles were observed at the short-wavelength limit of the titanium:sapphire laser (near 700 nm), and two-photon excitation of the photoproduct was maximal at ~780 nm **[70]**. Since NADH is maximally excited at the shortest wavelengths available, and since fluorescence characteristics may be altered by the pH and buffer type, a power study was performed to find a compromise for the best wavelength and excitation power of all species under investigation; results are given in Figure 5.3.

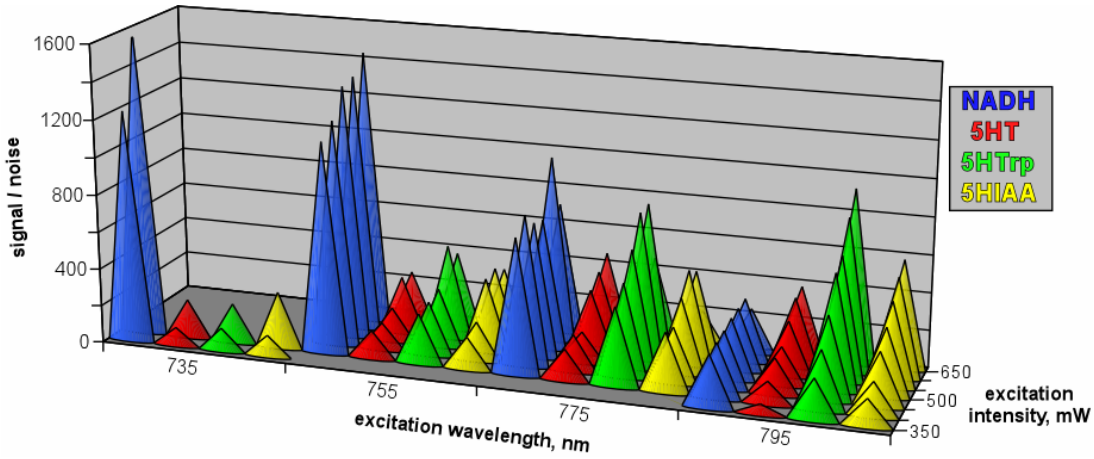

Figure 5.3: Power studies for indoles and NADH. Test solution was a standard mixture of 1 µM each analyte in AXB-D, with injection and separation conditions as in Figure 5.2. Each data point represents an average of duplicate runs; error bars, though not shown, are extremely large (~ 40%), so Figure 5.3 should be considered qualitative. Data at 735 nm cannot be obtained at higher excitation intensities because the laser cannot stably achieve more power than shown.

From these studies, 550 mW at 775 nm was chosen as the most appropriate.

5.2.2 Internal Standard Method

The MPE of hydroxyindoles is much more complex than NADH; the hydroxyindoles are susceptible to oxygen, require a multistep conversion, and have a 6-photon dependence (as compared to the 2-photon dependence of NADH), as shown in Figure 3.10. Therefore, analysis of these compounds was even less reproducible from run to run, and it was impractical to use the standard addition methods described in Chapter 4. Instead, a suitable internal standard was sought, which would allow quantitation within each electropherogram, rather than requiring four consecutive runs. Initial candidates for internal standards included melatonin, 5,7-dihydroxytryptamine, and 2-methylserotonin. However, since melatonin is uncharged, it was not resolvable from other neutrals in cell extracts. Similarly, 2-methylserotonin was not resolvable from

serotonin. Finally, 5,7-dihydroxytryptamine is reactive, and so was discarded in favor of a more stable molecule: 5-hydroxyindole-2-carboxylic acid (5HI2CA, Figure 5.4).

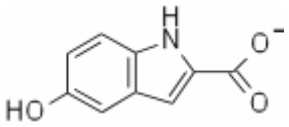

Figure 5.4: 5-hydroxyindole-2-carboxylic acid, shown in the charge state it would adopt under run buffer conditions (pH 9.0).

This molecule behaved almost ideally as an internal standard. Its peak eluted at a time in the electropherogram when no cellular interferents overlapped. Though the 5HI2CA photoproduct is much more fluorescent than those produced from the hydroxyindole analytes (this work and **[97]**), 5HI2CA displayed the same susceptibility to oxygen as did the hydroxyindole analytes. When a standard mixture of 10 μM hydroxyindole analytes and 1 μM 5HI2CA was subjected to CE-MPE as in Figure 5.2, deoxygenation enhanced photoproduct fluorescence for all four species by a factor of 5 ± 3 (N = 2 ambient and N = 2 deoxygenated). These enhancements are highly variable; more important is the constancy of response factors (*F*) under both oxygenated and deoxygenated conditions. Response factors are key for determining the suitability of an internal standard, and must remain constant across all concentrations examined. Response factors can be calculated from the equation:

$$\frac{\text{area of analyte signal}}{\text{concentration of analyte}} = F \cdot \left(\frac{\text{area of internal standard signal}}{\text{concentration of internal standard}} \right) \qquad [5.2].$$

Because the photoproducts of hydroxyindole analytes are less fluorescent than that produced from 5HI2CA, their *F* values are less than 1. Under ambient and deoxygenated conditions, the response factors for each analyte were not statistically different (95% confidence level for N = 2 ambient and N = 2 deoxygenated). So long as the peak areas of analytes were on the same order as the peak area of the internal standard (ratio of

analyte area to 5HI2CA allowed to range 0.2 – 2), the response factor remained constant across all concentrations examined (up to 12 µM, data not shown). The most useful concentration region, working near the limit of quantitation and tailored towards the low concentrations expected in cell extracts, is shown in Figure 5.5.

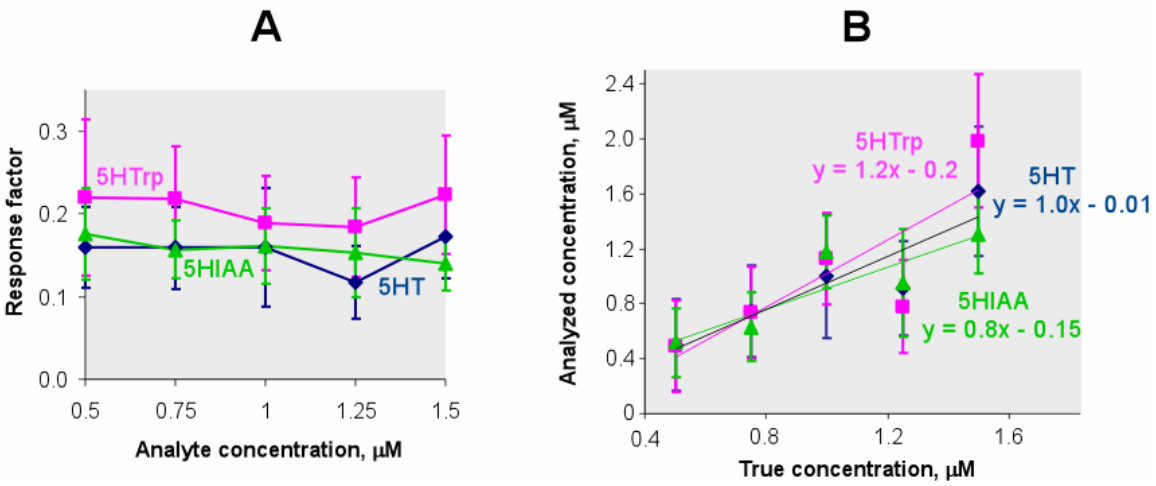

Figure 5.5: Characterization of 5HI2CA as an internal standard. Samples (75 µl each) of concentration 0.5 – 1.5 µM were spiked with 5 µl of 5HI2CA solution (4 µM; final concentration was 0.25 µM) and subjected to CE-MPE with parameters as in Figure 5.2, except laser excitation was 600 mW, 775 nm. At least seven electropherograms were integrated for each concentration, and were collected over a series of three days and two different capillaries, with no difference observed between days or capillaries. A. Response factors. B. Confirmation curve. All $R^2 > 0.7$.

Response factors, as shown in Figure 5.5A, had much larger RSD than was desirable—approximately 30% in all cases, which would lead to quantitation errors at least three times larger than for quantitation of NAD(P)H. This variability is largely due to changes in laser parameters and oxygenation levels during the time an electropherogram is collected, as well as variability in relative injection sizes between analytes and internal standard. Detection limits were also much poorer for hydroxyindoles than for nicotinamides. Peak areas were extremely irreproducible,

making the limit of detection different for every run; electropherograms with detection limits as low as 50 nM for 5HT and 5HIAA were observed, but a more practical limit of quantitation was usually ~ 500 nM. Because the AXB-D blank yielded a small peak that co-migrated with 5-hydroxytryptophan (Figure 5.6) limits of detection and quantitation for 5HTrp were somewhat higher.

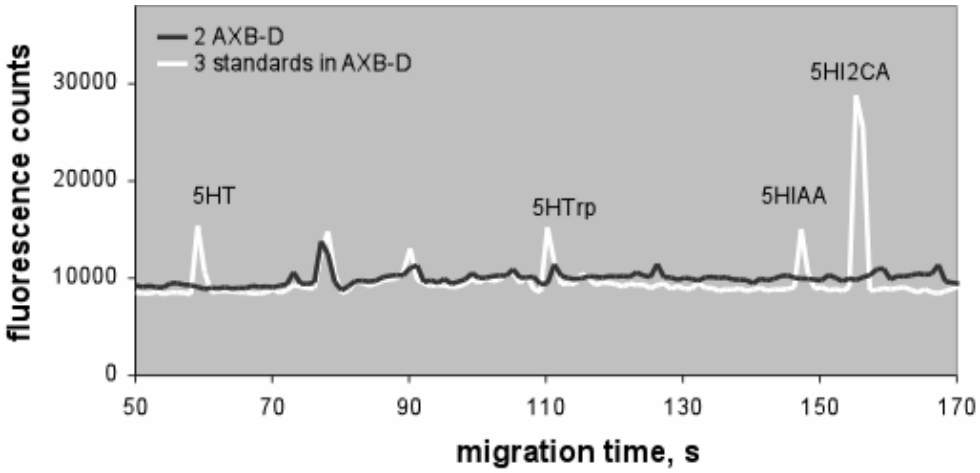

Figure 5.6: Electropherogram showing blank response for 5-hydroxytryptophan. Electrophoresis conditions as in Figure 5.2; laser parameters, 550 mW 775 nm. Hydroxyindole analytes were 0.5 μM and 5HI2CA was 0.25 μM.

The average blank response (for N = 4 injections of AXB-D) corresponded to 80 ± 20 nM 5HTrp, yielding a limit of detection of 200 nM and a limit of quantitation of 800 nM.

These quantitation parameters for CE-MPE of hydroxyindoles compare unfavorably with previous work in this lab **[95, 96]**, mostly due to necessary practical adaptations of those idealized conditions, such as changes in separation and sample buffers. This CE-MPE method also compares poorly with other methods used to assay serotonin content in RN46A or RN46A-B14 cells. High-performance liquid chromatography (HPLC) with electrochemical detection has detection limits substantially lower (0.8 nM for 5HT), and a working range of 20 – 500 nM with $R^2 > 0.99$ **[98]**.

Similarly, enzyme-linked immunosorbent assays (ELISA) for serotonin are described by their manufacturers as having a standard curve ranging 0.3 nM to 60 nM (Immuno Biological Laboratories, Hamburg, Germany). Though both of these methods require much more sample (100 µl for ELISA and 50 µl for HPLC) and more time for analysis (4 h for ELISA and 25 min per run in HPLC) than does CE-MPE, these parameters were not limiting to this work. Neither HPLC nor ELISA, however, offers concomitant quantitation of NAD(H). Moreover, ELISA does not discriminate well between indoles.

5.2.3 Sample Preparation

When frozen at –60 ºC, samples containing serotonin are known to be stable at pH 7.8 for up to 28 days **[99]**, and preliminary experiments with samples containing hydroxyindole standards and 5HI2CA indeed showed stability over several days when frozen at –80 ºC in pH 8.0 AXB-D. However, it was not initially certain that analytes would withstand the extraction procedure. Therefore, 5 µl of a solution containing 100 µM each hydroxyindole analyte was added to an 8 cm^2 Petri dish, diluted in 750 µl extraction buffer (pH 12.6), and treated to sonication, filtration, enzymatic conversion, and quantitation as described. Results were statistically equal to controls (samples diluted in AXB-D) and were quantified within experimental error of the expected result (0.6 µM final concentration).

5.3 RESULTS

Although it was possible to identify a number of components in RN46A and RN45A-B14 cell extracts, as shown in Figure 5.7, and although a number of differentiation conditions were tried, no serotonin or 5HIAA could reproducibly be identified under any conditions. In contrast, a compound tentatively identified as 5HTrp

was frequently present in cell extracts at concentrations near (and sometimes above) the limit of quantitation, as shown in Figure 5.8.

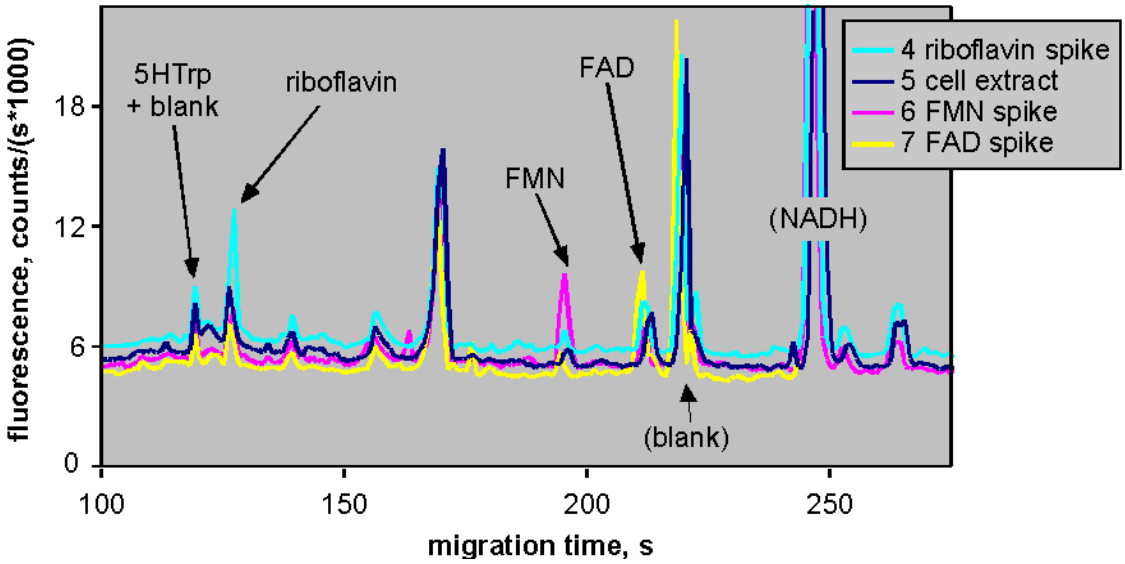

Figure 5.7: Electropherograms showing identification of various species in RN46A-B14 cells. Legend numbers indicate injection order (*i.e.*, the cell extract was the 5th injection that day). Final added concentrations in spiked samples: riboflavin 120 nM, FMN 50 nM, FAD 90 nM. Injections 10 s at 5 kV; separations at 17 kV; laser at 550 mW, 775 nm. The NADH peaks extend off-scale to better display low-intensity peaks.

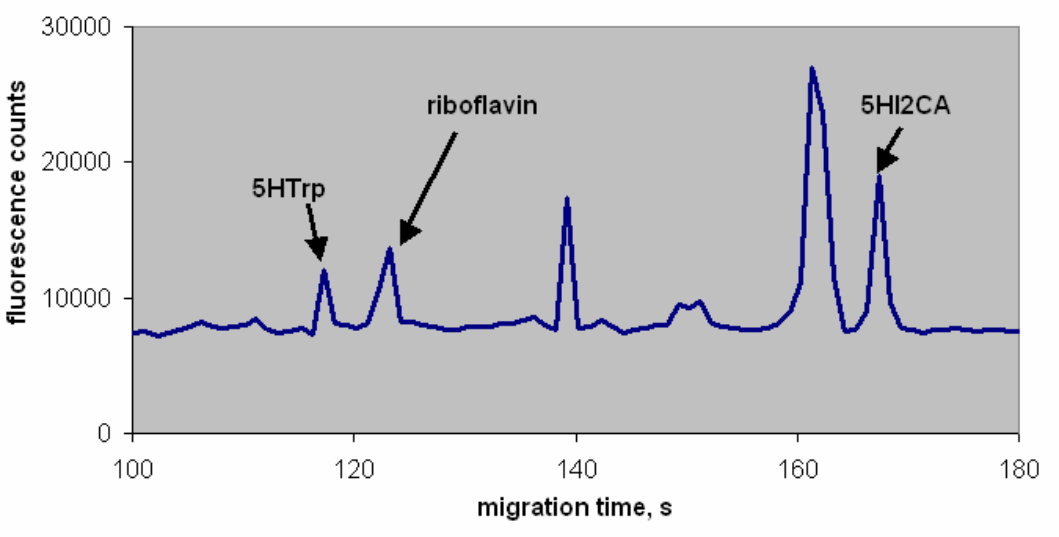

Figure 5.8: Electropherogram of quantifiable amounts of putative endogenous 5HTrp in RN46A-B14 cells. By comparison with the internal standard peak, which was present at 0.9 µM, this sample was quantified at 1.5 ± 0.5 µM 5HTrp. Separation and detection conditions were as in Figure 5.8.

The limit of quantitation was surpassed in this case by allowing cells to reach high density (8.5 ± 0.4 million per plate). The result indicates a cellular content of 160 ± 60 amol 5HTrp, as shown in Figure 5.9.

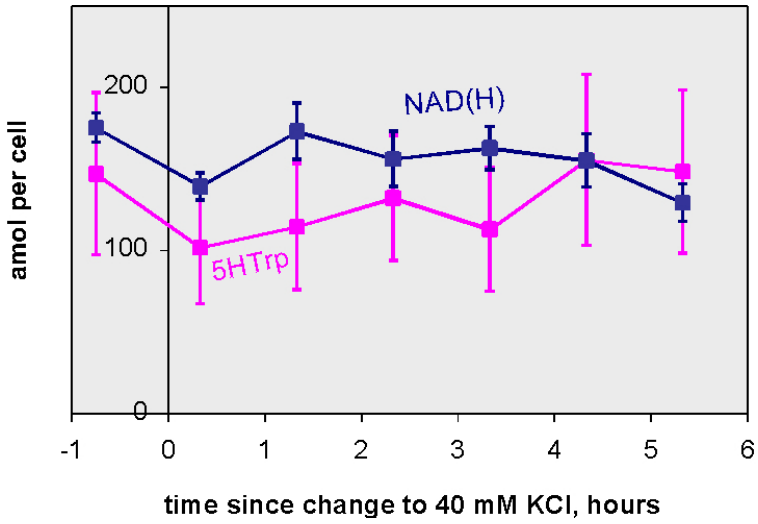

Figure 5.9: Tracking NAD(H) and 5HTrp levels in RN46A-B14 cells subjected to depolarizing conditions.

The experiment shown in Figure 5.9 used cells differentiated on Matrigel™-coated plates for four days in Neurobasal™ medium at 37 ºC, the only culturing conditions that allowed large numbers of cells to survive (warmer temperatures were lethal to cells within a few days, regardless of which medium was used). These results are representative of various experiments that were attempted; no consumption of NAD(H) was observed in two trials of cells exposed to 40 mM KCl and one of cells exposed to 60 mM KCl. Moreover, no change in any analyte level was seen in response to any change in culture conditions given in Figure 2.2 (temperature change or addition of BDNF to RN46A cells). No serotonin was detected and no change in 5HTrp levels was observed even after cells were cultured four days in elevated KCl.

As a positive control, Figure 5.10 is presented, which shows that it is indeed possible to observe changes in NAD(H) levels consistent with known PARP-activity experiments. The event observed in Figure 5.10 was irreproducible, but may be related to upregulation of glutamatergic phenotype and subsequent damage through known **[26]** reactive oxygen species pathways.

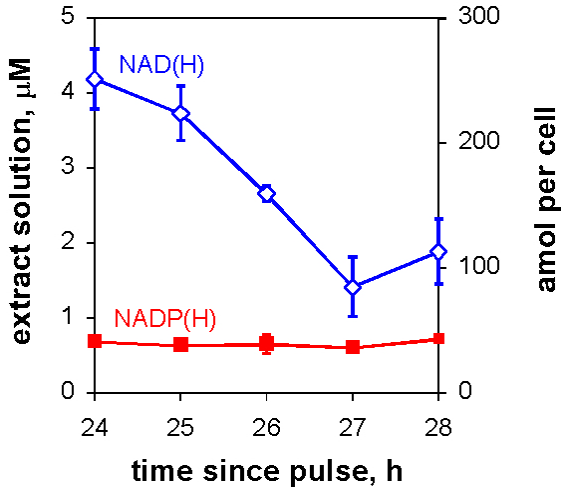

Figure 5.10: Tracking constant NADP(H) and dynamic NAD(H) levels in RN33B cells. Culture conditions described in Chapter 2.2.4, sampling and analysis as described in Chapter 3 for trypsinized cells.

Both the timescale and cellular content in Figure 5.10 are consistent with literature reports: when treated with low levels of a DNA-damaging agent, one cultured cell line fell from 430 amol/cell NAD to 20 amol/cell in three hours, without comparable changes in NADP levels **[28]**, as discussed in Chapter 1.3.

A second positive control is presented in Figure 5.11, which shows that it is possible to detect exogenous serotonin in RN46A-B14 cells. In this experiment, cells were cultured as in as in Figure 5.9, but after four days in KCl medium, they were incubated for one day in 40 μM serotonin and 10 μM clorgyline (a monoamine oxidase inhibitor) without added KCl. A matched plate was counted at 8.3 ± 0.4 million cells.

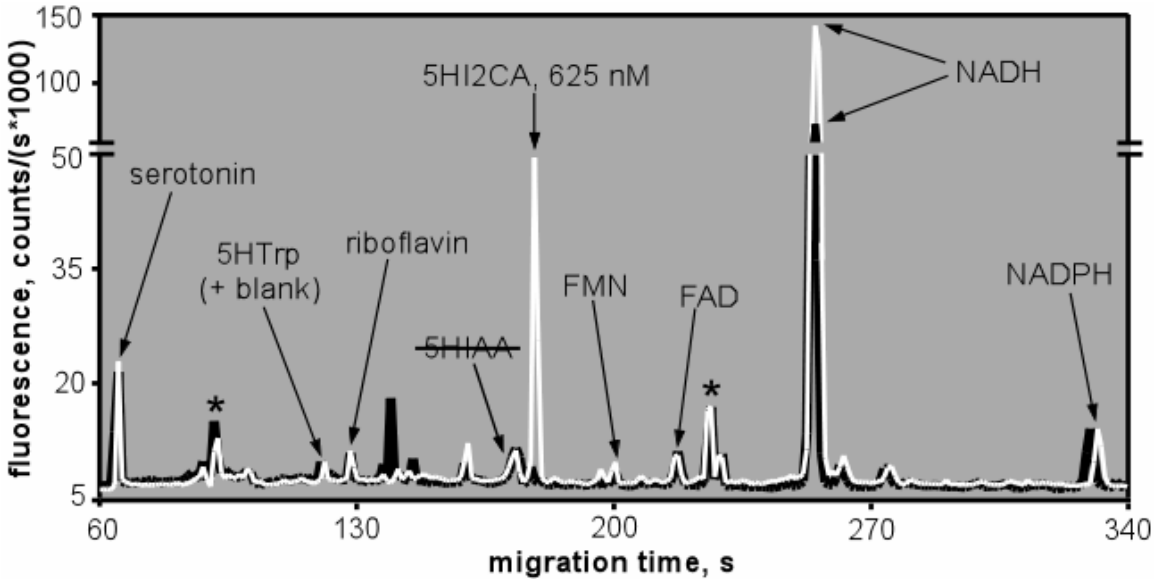

Figure 5.11: Overlaid electropherograms from two consecutive injections of extract (black) and spiked extract (white) showing exogenous serotonin uptaken by and then extracted from RN46A-B14 cells. Note break and change in scale in y-axis. Asterisks identify blank response peaks (also present in injections of AXB-D alone). 5HIAA was not detected in this or any other extract; its usual migration time is marked (as a shoulder on the peak at 173 s).

From comparison to the internal standard, serotonin was 0.8 ± 0.3 μM in this extract, or 80 ± 30 amol/cell. If one assumes hemispherical cells of 15 μm diameter, the

intracellular concentration was 90 ± 30 μM. Literature comparisons for serotonin content per cell are difficult to find; most analyses are expressed as concentrations per weight of protein or tissue. However, human medulla has been reported to contain 0.1 nmol serotonin/g wet weight **[98]**; calculations assuming the tissue has a density similar to water suggest a concentration of ~ 1 μm serotonin. Since this is an average of both serotonergic and nonserotonergic cells, as well as cellular and extracellular space, our value for incubated cells (90 ± 30 μm serotonin) seems reasonable.

5.4 DISCUSSION

This work demonstrates that it is possible to detect changing intracellular NAD(H) levels consistent with the activity of poly-ADP-ribose polymerase. However, no such NAD(H) changes were detected in response to subjecting RN46A-B14 or RN46A cells to depolarization or other differentiating culture conditions. Inability to reproduce published differentiation protocols—possibly because the cells were such high passage number (P27)—calls any subsequent results into question. Cellular extracts contained detectable endogenous 5HTrp, but not 5HT or 5HIAA, possibly because the cells were not synthesizing serotonin. In functional serotonergic cells, intracellular 5HT concentrations is much higher than 5HTrp concentration—as much as a hundredfold **[100]**—so, had RN46A or RN46A-B14 cells been synthesizing serotonin, it should have been easier to detect than 5HTrp. It would be helpful to assess the cells independently. For instance, immunohistochemistry against tryptophan hydroxylase and incubation of the cells with 5HTrp (to observe conversion to serotonin) might give an idea of functionality of these cells, per Figure 2.2.

Though much progress was made towards systematizing our lab's earlier proof-of-concept work, and in applying it to real biological samples, CE-MPE of hydroxyindoles seems to compare poorly to traditional analytical techniques. It is also

likely that any serotonin produced was below limits of detection. Nonetheless, it was demonstrated that it is possible to detect exogenous serotonin taken up by RN46A-B14 cells. This establishes an excellent model for future studies of serotonin uptake and metabolism.

5.5 EXTENSIONS AND FUTURE WORK

The most promising experiment in this work was the demonstration of all three classes of analytes (flavins, nicotinamides, and indoles) in cell extracts which had taken up exogenous serotonin. This is the first cellular demonstration in our lab of early *in vitro* proof-of-principle experiments **[66]**. It also is the most workable model for future studies, since exogenous indole is detectable without complicated culture protocols; these cells constitutively express the serotonin reuptake transporter, and uptake of 5HT is constitutive and independent of differentiation or BDNF supplementation **[37, 101]**. The serotonin uptake transporter is of intense interest to the research community as a target for antidepressant drugs, but blood platelets are traditionally used as a model for serotonergic neurons **[33]**. Our system could be a much more relevant model for the studies of selective serotonin reuptake inhibitors like fluoxetine (Prozac®, Eli Lilly & Co.), sertraline (Zoloft®, Pfizer Inc.), fluvoxamine (Luvox®, Solvay Pharmaceuticals Inc.) and clomipramine (Anafranil®, Novartis Pharmaceuticals Corp.).

This first cellular simultaneous demonstration of flavins, indoles, and nicotinamides also provides a model for screening and investigating an older class of psychoactive drugs, the monamine oxidase inhibitors. Popular monamine oxidase inhibitors include phenelzine (Nardil®, Pfizer Inc.), tranylcypromine (Parnate®, SmithKline Beecham Pharmaceuticals), and possibly even the herbal supplement, St. John's wort **[102]**. This class of drugs is particularly well suited to our system because of

the potential analytes in their target pathway, as shown in Figure 5.12 (and *cf*. Figure 5.1):

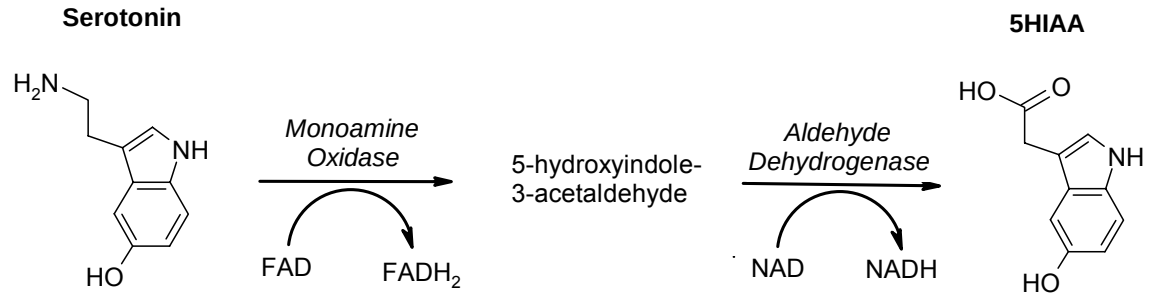

Figure 5.12: Serotonin catabolism pathway. $FADH_2$ = reduced (and nonfluorescent) form of FAD. Monoamine oxidase is covalently modified with flavin cofactor, while aldehyde dehydrogenase uses solution-phase cofactor.

Our multi-analyte CE-MPE offers a possibly unique insight into this pathway, since we can detect several of its components. Monamine oxidase comes in two isoforms (MAO_A and MAO_B), and there are dozens of monoamine oxidase inhibitors with varying levels of selectivity for these isoforms and with varying reversibility when bound, making possible numerous experiments.. These studies could even be extended to include more neurotransmitters than demonstrated here, since MAO_A preferentially deaminates serotonin and epinephrine, while MAO_B preferentially deaminates dopamine **[33]** under some conditions in the human brain. Both epinephrine and dopamine have been separated and detected by CE-MPE in this laboratory **[103]**.

Unfortunately, the FAD cofactor used to oxidize serotonin is covalently bound to monoamine oxidase, and thus not easily analyzed. Monoamine oxidase is a large protein; even its monomer form (~ 60 kD) would be excluded by the protein filter used in our cell extraction process. Intracellular free flavin concentration might reflect the protein-bound constituent (though this should be experimentally tested), which would allow our assay to be a straightforward reflection of monamine oxidase state. Alternately, flavoproteins

could be directly assessed by using larger-pore filters, though these more complicated extracts could clog capillaries. Surface modification of the capillary or trypsinization of the cell extract proteins to more manageable fragment sizes might reduce such complications.

Fortunately, the character of monoamine oxidase presents not only problems, but also more possibilities. *In vivo*, monoamine oxidase is bound to the outer mitochondrial membrane, and mitochondria are both morphologically and functionally diverse, with variety and individuality that is thought to have important biological consequences **[104]**. Our lab is equipped to prepare mitochondrial fractions from cultured cells by following a published protocol **[89]**, and characterization of individual mitochondria by CE with laser-induced fluorescence has already been described **[104]**. Therefore, it may be feasible to miniaturize monoamine oxidase experiments to the level of single mitochondrial incubations in a pre-column or on-column CE reactor, followed by separation and detection of reactants, products, and mitochondrion.

Chapter 6: Pinealocyte Extracts and CE-MPE of Neutral Analytes

6.1 Introduction

The rat pineal gland is known to contain and/or exhibit biorhythms in several compounds of interest to this lab. For instance, N-acetyl serotonin (NAS) and melatonin (MEL) levels are elevated nocturnally; serotonin and 5HIAA levels are elevated diurnally, and tryptophan (Trp) and 5-hydroxytryptophan levels are nearly constant **[105]**, as shown in Figure 6.1.

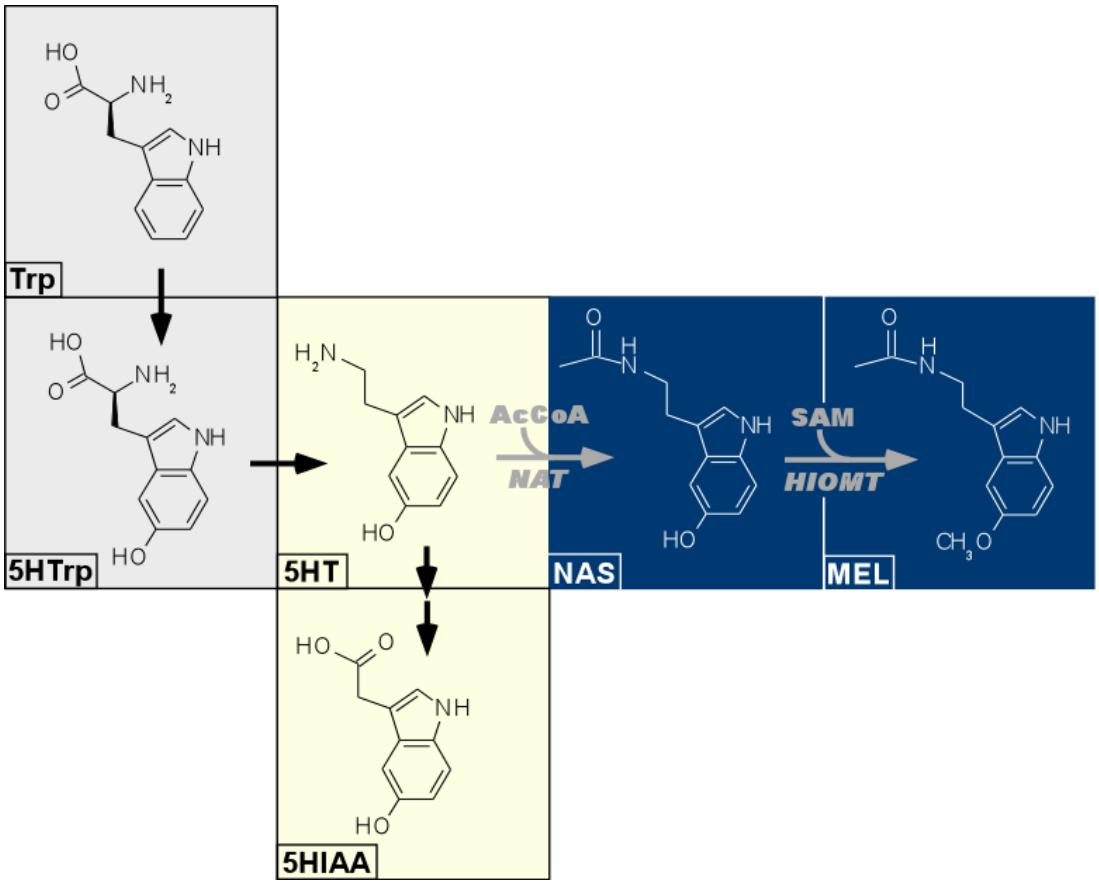

Figure 6.1: Indoles in the pineal gland. Yellow indicates diurnal elevation; blue indicates nocturnal elevation; and gray backing indicates constancy. HIOMT = hydroxyindole-O-methyltransferase; AcCoA = Acetyl CoA; SAM = S-adenosyl-methionine.

Other putative pineal indolic species are less well characterized. For instance, the presence of 5-methoxytryptophol (MTP) has been reported in rat pineal, with a peak nocturnal content (reviewed in **[106]**), though some researchers suggest proper sample preparation prevents MTP formation **[105, 106]**. The methylated metabolite 5-methoxyindole-3-acetic acid (MIAA), while quantified in the pineals of some animals, is of uncertain quantity in rat pineals **[105, 107]**. The possible pineal occurrence of O-methylserotonin (OMS) is also questionable **[105, 107]**. These disputed compounds are presented in Figure 6.2.

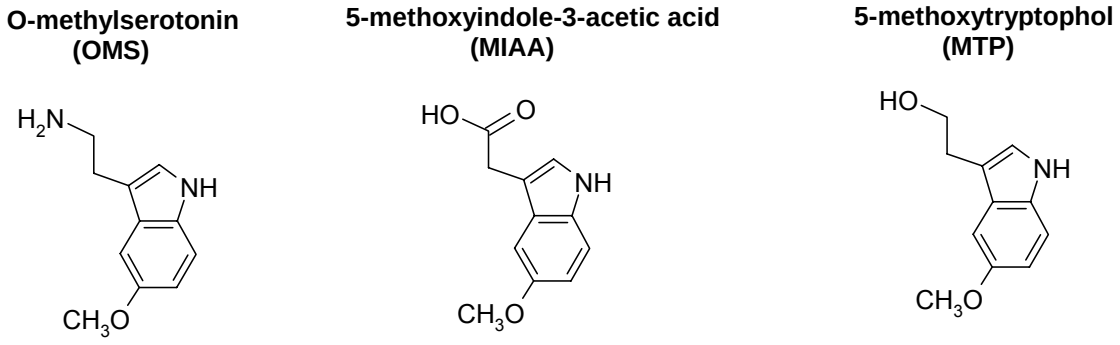

Figure 6.2: Some commercially-available methoxyindoles considered possible but not observed in rat pineal gland.

The absence of these compounds would indicate that HIOMT acts only on NAS in normal pinealocytes **[105]**. However, enzymes may not always be required to form possible pineal methoxyindoles, as the case of the cyclohydrogenation product of melatonin, 6-methoxyharmalan (6MH) **[107]**. Another structurally similar compound, pinoline, seems to have a circadian rhythm in avian pineal gland, perhaps regulated by HIOMT **[108]**. A number of such tricyclic indoles have been identified in human and animals tissues; those presented in Figure 6.3 are of particular interest for their relevance to the pineal gland and for their commercial availability.

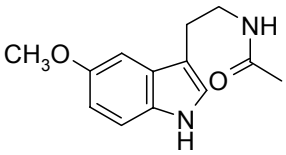

melatonin

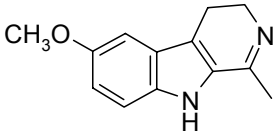

6-methoxyharmalan

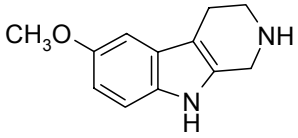

pinoline

Figure 6.3: Commercially available tricyclic indoles, and their structural similarity to melatonin.

Clearly, the indole content of pinealocytes is a complex and interesting problem to study, along with the nicotinamides already of interest to this work.

6.2 EXPERIMENTAL METHODS

6.2.1 Separation and Detection

Because a number of the indoles of interest are uncharged under accessible electrophoresis conditions, they cannot be separated by traditional CE; therefore, modified CE strategies are necessary. In these studies, we have optimized indole fractionation, using cyclodextrins as buffer additions (see Chapter 3). In addition to the advantages of cyclodextrins in effecting separation of unresolved components, inclusion complexes of cyclodextrins with indoles have fluorescence quantum yields better than that of the analytes alone **[109, 110]**. For example, depending on solution parameters (such as pH and addition alcoholic solvents), melatonin complexed with hydroxypropyl-β-cyclodextrin is twice as fluorescent, while melatonin complexed with cyclodextrin is ~ 1.5-fold more fluorescent **[110]**. The structures of these cyclodextrins are given in Figure 6.4.

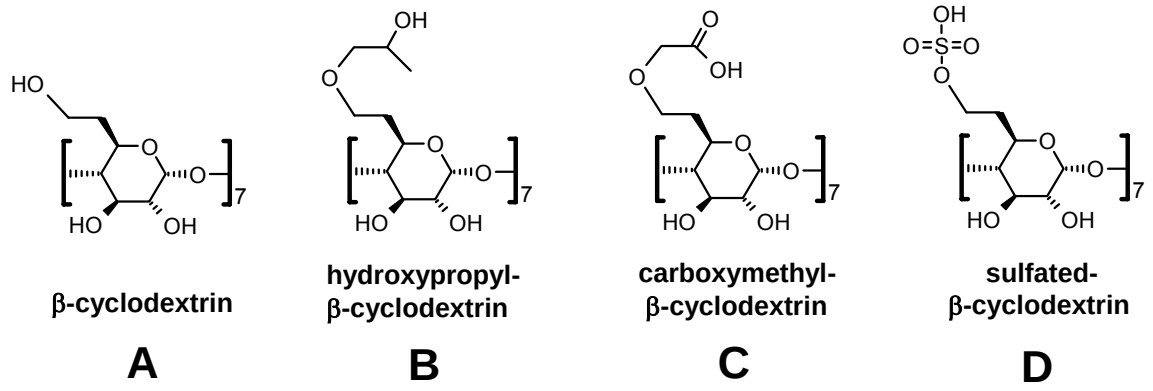

Figure 6.4: Cyclodextrins relevant to this work. Cyclodextrins are usually depicted with derivatization at the primary alcohol, though the secondary alcohols are also accessible. Degrees of substitution for hydroxypropyl, carboxymethyl, and sulfated derivatives average 5, 7, and 9, respectively.

The addition of methanol (up to 50% v/v) to melatonin:cyclodextrin solutions increases the fluorescence of both the complexes and of the free analytes; above 50% methanol, fluorescence of free melatonin approximately matches the complexed fluorescence **[110]**. However, addition of propanol to indole solutions increased the fluorescence of free indoles, but decreased the fluorescence of the complexes. This was thought due to the competition of propanol with indoles for the cyclodextrin cavity, while methanol stabilized the binary complexes **[109, 110]**.

The addition of alcohols to micellar CE separation buffers can increase peak efficiency (a measure of peak shape) **[64]** and can reduce conductivity, thus aiding in the generation of stacking conditions described in Chapter 3. Alcohols suppress electroosmotic flow, which initially can increase the analysis time for analytes, but as the hydrophobic character of the alcohol increases, neutral analytes have less affinity for the micellar or cyclodextrin phase. Moreover, the incorporation of alcohols in a separation buffer reduces its boiling point; at higher laser powers, these modified buffers can bubble at the detection site. Consequently, laser power was limited to 450 mW at 775 nm

throughout experiments in this chapter. Moreover, volatile solution modifiers tend to preferentially evaporate during a day's experiments, causing constantly changing experimental conditions. The type and percentage of alcohol used for cyclodextrin CE experiments, therefore, must be carefully considered. Methanol, ethanol, and ethylene glycol were evaluated at levels up to 20% content (v/v).

Because cyclodextrins produced a high visible background, detection of instrinsic indole fluorescence was accomplished by adding an ultraviolet channel, in which no significant cyclodextrin signal was observed. Ultraviolet fluorescence was collected with a dichroic mirror (Chroma Technology, Rockingham, VT; part #400DCLP) and filtered with two ultraviolet band-pass filters (Barr Associates Inc., Westford, MA; maximum transmittance at ~ 330 nm) and one UG11 Schott glass colored glass filter (Andover Corporation, part #011FG09-25, maximum transmittance at ~ 340 nm). The same visible dichroic mirror used in Chapter 5 and the same instrumentation discussed in Chapters 3 and 5 were used (Figure 6.5).

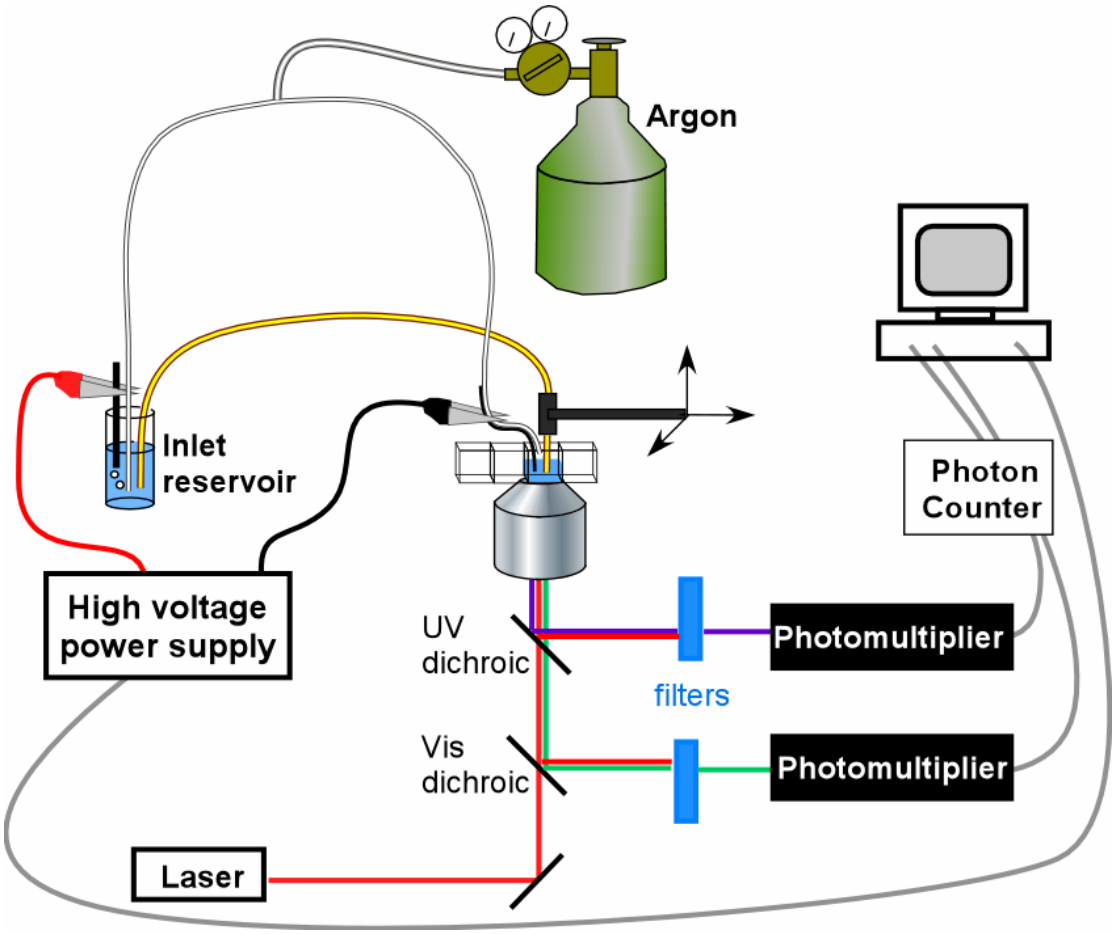

Figure 6.5: Dual-channel, deoxygenated instrumentation for CE-MPE.

Of the cyclodextrins investigated for separations (6.4C and 6.4D, which were chosen for their relatively low cost among commercially available derivatized cyclodextrins), no reproducible difference in background signal was observed. However, increasing pH did significantly raise the visible background of both types of cyclodextrins. Therefore, though higher pH often led to better separations, pH had to be compromised between separation and detection characteristics. As discussed in Chapter 4, borate offers an appropriately high pK_a and enhanced resolution of sugar-

containing analytes. The salt used to adjust final pH also affects the mobility and conductivity of the run buffer; both NaOH and KOH were evaluated.

Separations in cyclodextrin-modified CE are more dependent on capillary length and separation field than in traditional CE, since analytes must be allowed time to partition in and out of the cyclodextrins. Since a chromatographic separation mechanism has been added, flow rate must be neither too fast (which produces phase-transfer broadening) nor too slow (which produces too much diffusional broadening). Separations can be protracted with long capillaries and/or low separation voltages. Therefore, capillaries as long as 40 cm were used (*cf*. capillaries in Chapters 4 and 5 at 30 – 35 cm)

As discussed in Chapter 3, not only the run buffer, but also the sample buffer must be optimized. One easy manipulation of sample conductivity is to replace the primary buffering agent, Tris, with its derivative, N-[tris(hydroxymethyl)methyl]glycine (Tricine), as shown in Figure 6.6.

Tris
pK_a = 8.0

Tricine
pK_a = 8.15

Figure 6.6: Structures and acidity of sample buffers **[3]**.

At pH 8.5—a common post-extraction value in these studies—Tris is neutral, but Tricine carries a negative charge. This adjustment should allow an increase in conductivity (the desirability of which is discussed in Chapter 3.1.1.3) without compromising the benefits and characterizations of Tris discussed in Chapter 4. However, since high-conductivity

sample buffers generate such low electro-osmotic flow, they do complicate electrokinetic injections.

6.2.2 Pineal Cell Extracts

One sample was collected 30 min before switching plates to their chemical pulse or control medium (as discussed in Chapter 2.2.5). The first pulsed sample was collected 2.5 h thereafter, and was followed within 10 minutes by a control sample. These paired samples were collected at 3-h intervals for a full 24 hours, yielding 26.5 h of total data. A matched plate of cells, counted 30 min after the chemical pulse, was found to contain 12.1 ± 0.5 million cells. Extractions were performed in 0.75 ml of Tricine extraction buffer containing 7 mM CHAPS and adjusted to pH 12.6. Sonication was performed for 3 min at level 10 on ice, after which 50 µl of 1.2 M HCl was added and briefly mixed by sonication. A pH check on test strip paper indicated a post-neutralization pH of ~ 7 – 8. Extracts were filtered through prewashed 30 kD cellulose acetate centrifugal filters for 15 min at 10 ºC at 11,000 *g* and stored at –80 ºC until analysis.

6.3 Results and Discussion

6.3.1 Separation and Detection

For standard mixtures of the analytes in Figures 6.1, 6.2, or 6.3, dissolved in AXB-D (with a minimum of ethanol for stocks of hydrophobic analytes, totaling less than 1% in final sample solution), the best compromise of separations and detection parameters were achieved in separation buffers containing 10 – 15 mM cyclodextrin, 10 – 15 mM base (KOH or NaOH), 10 – 20 mM borate, and 10 – 15% alcohol. For injections of magnitude and duration comparable to those made in experiments described in Chapters 4 and 5, near-baseline resolution of all analytes was possible, as shown in Figure 6.7.

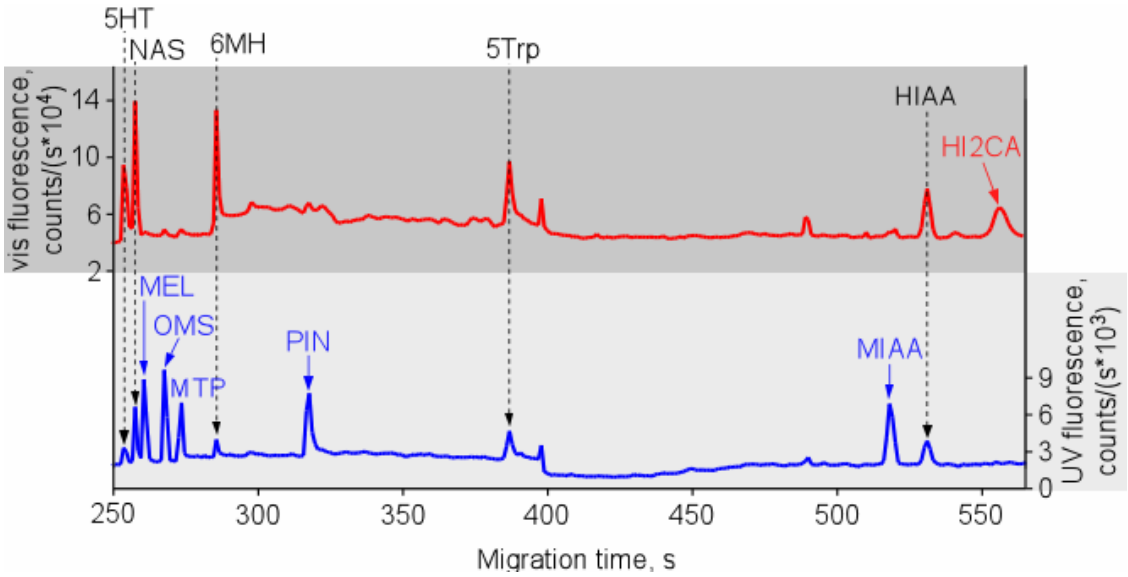

Figure 6.7: Separation of indole standards of possible interest in pineal extracts. Sample contained 10 µM each analyte in Tris AXB-D at pH 8.5 and was injected for 10 s at 3 kV. Separation buffer was 10% ethanol, 10 mM borate, 15 mM NaOH, and 15 mM carboxymethyl-β-cyclodextrin (CMβCD); separation voltage, 27 kV.

In order to make larger injections of less concentrated samples, however, it was necessary to generate a conductivity mismatch between sample and separation buffers. Simple substitution of Tricine for Tris in the extraction buffer was found to be sufficient, as shown in Figure 6.8.

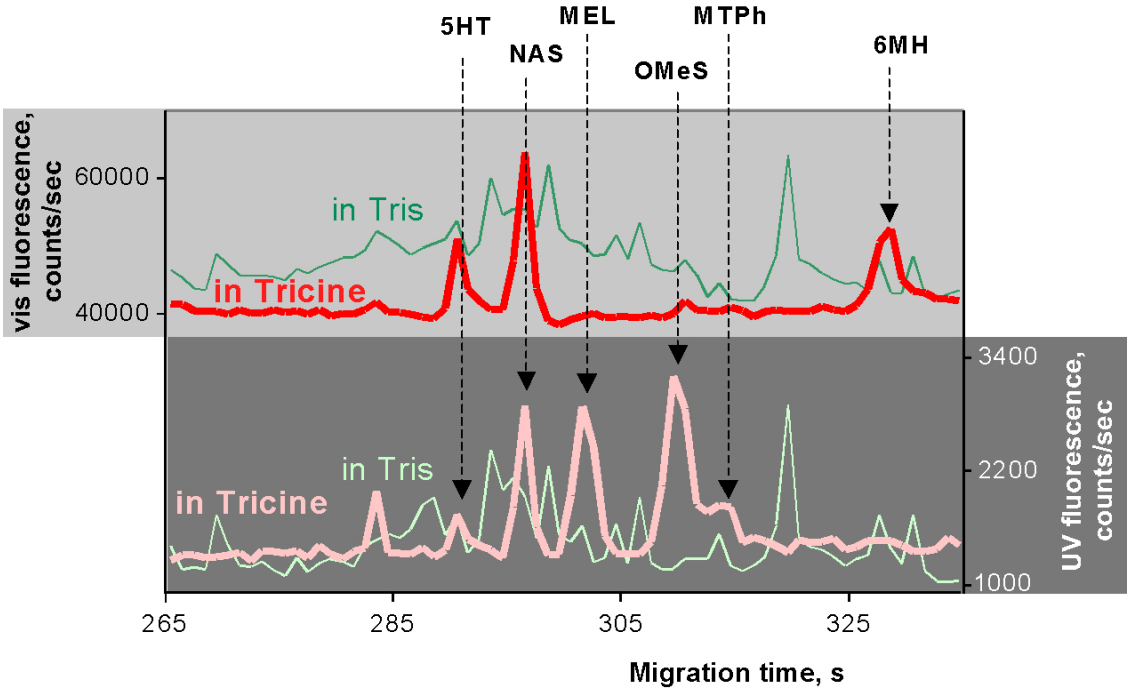

Figure 6.8: Detail of an electropherogram comparing samples (1 µM each analyte) dissolved in either Tris (green traces) or Tricine (red/pink traces), both injected for 10 s at 15 kV (an injection 5-fold larger than that shown in Figure 6.7). Separation buffer as in Figure 6.7; separation voltage, 24 kV.

Figure 6.8 shows that Tricine was sufficient to generate better stacking conditions than Tris, which generated no useful or reproducible peaks at all. This effect cannot be predicted by rough calculations of conductivity alone. Moreover, no extra benefit was gained by adding 100 mM Na_2SO_4 to Tricine AXB-D (data not shown), though preliminary calculations had suggested such would be necessary to surpass the conductivity of the separation buffer. It must therefore be concluded that the processes dictating buffer conductivities are too complex to be approximated by simple calculations; relative ion mobilities dramatically affect conductivity. Therefore, conductivity of solutions must be empirically measured; our lab is acquiring a conductivity meter for this purpose.

Though good separations were achieved in the systems described above, the inclusion of ethanol (boiling point 78 ºC) yielded constantly changing experimental conditions as ethanol evaporated over the course of a day. As an alternative, ethylene glycol (boiling point 197 ºC) was examined as a buffer additive; these solutions could generate stacking conditions sufficient to produce separations similar to that shown in Figure 6.7.

Extremely large injections were possible, though stacking and separation were not ideal and remain to be optimized. Injections as much as 30-fold larger than those demonstrated in Chapters 4 and 5 were readily feasible; a 24 kV 30 s injection is shown in Figure 6.9 and was not found to be different from a 3 kV 240 s injection (though the latter may have allowed more diffusion of analytes during the long injection time).

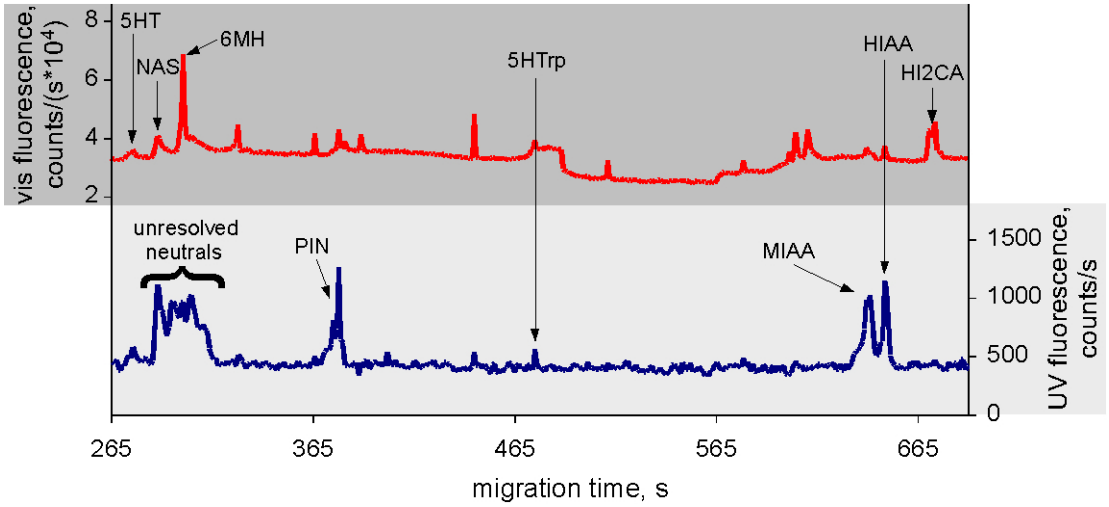

Figure 6.9: Electropherogram of an extremely large injection (24 kV 30 s) of analytes at low concentration (500 nM each) in Tricine AXB-D. Separation buffer was 15% ethylene glycol, 10 mM KOH, 10 mM borate, and 15 mM CMβCD; separation voltage 27 kV.

Preliminary attempts at manual pressure injections (with a syringe and septum) yielded separations even less satisfactory than that shown in Figure 6.9, so pressure injections

were not pursued. Depending on the analyte, literature optimizations of stacking conditions report the ability to fill 7 – 30% of the capillary length and still achieve sharp peaks **[64]**; the injection made for Figure 6.9 is in that regime, and filled about 10% of the capillary.

Unfortunately, under our conditions, cyclodextrins were not found to enhance the fluorescence of the analytes, as had been reported by others **[109, 110]**. Instead, though results shown here were preliminary and often irreproducible, it appears that CMβCD suppressed the fluorescence of melatonin. Solutions containing 10 mM borate, 10 mM KOH, and with or without both 15% ethylene glycol and/or 15 mM CMβCD (total volume 186 µl) were added to the outlet reservoir (without a capillary) and the UV background was allowed to stabilize for one minute and then measured as a blank 60 times in bins of 1 s each. Melatonin stocks (10 µl) then were added and mixed well (to a final concentration of 28 µM), and UV fluorescence was allowed to stabilize for two full minutes and then measured for 60 bins of 1 s each. Each experiment was corrected for its own blank; results are presented in Figure 6.10.

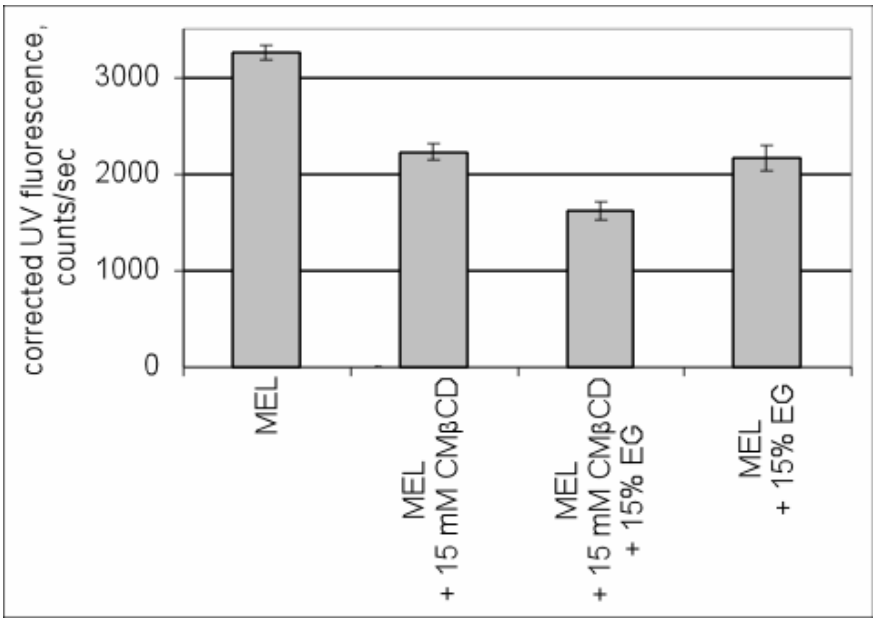

Figure 6.10: The effect of carboxymethyl-β-cyclodextrin and ethylene glycol (EG) on melatonin fluorescence. Error bars represent propagated error for standard deviation of 60 1-s blank signal measurements and 60 1-s melatonin signal measurements.

If this effect is indeed real, there are a number of explanations; the most obvious is the difference in excitation mode (literature one-photon excitation at ~ 275 nm, detection at ~ 355 nm, versus our use of multiphoton excitation). Moreover, a number of solution characteristics were different, including the form of cyclodextrin itself. Also, fluorescence quantum yield was not measured; these measurements are subject to possible differences in photobleaching rates. Future optimization could possibly resolve these issues.

6.3.2 Pineal Extracts

A prominent NADPH peak was seen in all samples, though no NADH was observed because samples were prepared in iced extraction buffer. No indole analytes were observed in either the control or pulsed samples at any timepoint, and no difference

was seen before or after pulsing. Representative electropherograms are shown in Figure 6.11.

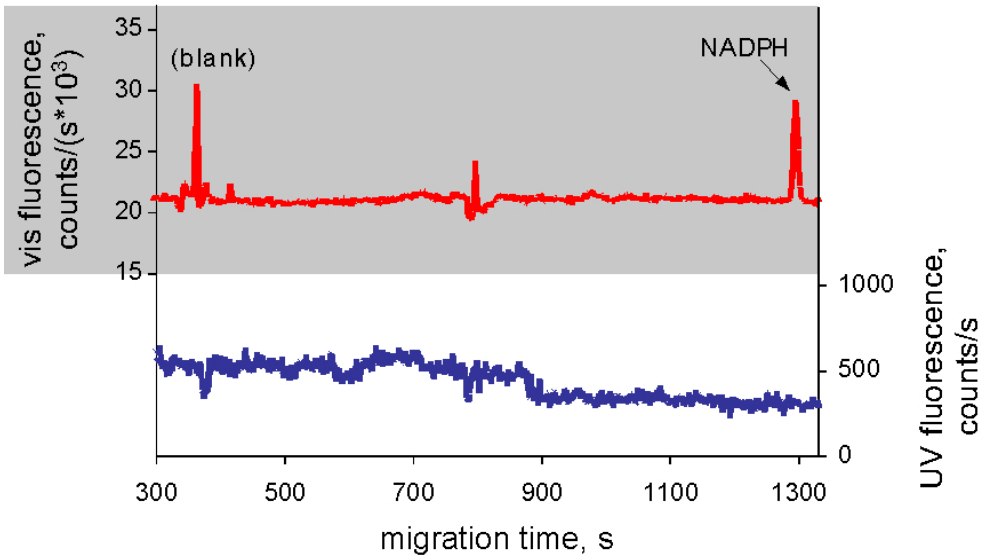

Figure 6.11: Electropherograms of a pineal extract. This extract was a taken 5 h after the pulse. Extract was injected at 6 kV for 10 s and separated at 21 kV in a buffer containing 15 mM sulfated-β-cyclodextrin, 15% ethylene glycol, 15 mM KOH, and 10 mM borate.

Many explanations are possible for failure to observe indoles in pineal cell extracts. Limits of detection may not have been low enough; though this parameter varied greatly from day to day, representative results during analysis of pinealocyte extracts are shown in Table 6.1.

Table 6.1: Representative figures of merit; conditions as in Figure 6.11. Results calculated from an injection of standards containing 2 µM each analyte in Tricine AXB-D. The cellular LOD is the minimum concentration required in cells to produce a detectable CE-MPE response after dilution to a cell extract.

	Methoxyindole (NAS)		Hydroxyindole (5HIAA)	
	UV	Vis	UV	Vis
LOD, solution	~ 350 nM	—	~ 300 nM	~ 4 nM
LOD, cellular	~ 260 µM		~ 230 µM	~ 3 µM

These detection limits compare unfavorably to some of the best methods for quantifying melatonin in rat pineal glands (13 nM melatonin by HPLC with fluorometric detection **[111]**, low enough to quantify melatonin in a single rat pineal gland). Approximate calculations can be made using reported pineal extract concentrations **[111]**, published volumes of rat pineal gland **[34]**, and the assumption that pineal tissue has a density similar to water; such calculations suggest pineals contain ~ 40 nM – 4 μM melatonin and ~ 4 – 400 μM serotonin. Clearly, then, if the concentration of the gland approximates the concentration of its cells, the melatonin detection limits for the method presented in this chapter are insufficient, though the serotonin parameters were more appropriate. It had been hoped that the cells might overexpress indoles up to detectable levels at their circadian peak, since they were immortalized with an oncogene fused to the tryptophan hydroxylase promoter (as discussed in Chapter 2). However, as previously discussed, PGT811 cells are less indolergic than both PGT-β cells and native pinealocytes. Optimization of cell culture parameters might increase indolergic character.

6.4 FUTURE WORK

The work presented here is only preliminary, and leaves much room for improvement or extension, much of which is discussed above. A number of techniques could be optimized to lower the CE-MPE detection limits; better stacking, preconcentration of samples (in a SpeedVac or by organic solvent extraction), and/or reducing background fluorescence from cyclodextrins. The latter could involve exploration of different varieties of cyclodextrins, different pHs (since visible background was seen to be pH-dependent), and/or spectral filtering (if cyclodextrin fluorescence is much different from the analyte fluorescence, filter glasses could minimize background).

Alternatively, if dilution of analyte (from cell to cell extract) could be avoided, our detection limits would be sufficient. The advantage of mass detection limits of CE-MPE, as discussed in Chapter 3.1.2, could be exploited here. Single cells could be injected into a capillary and then lysed in the inlet, immediately before separation.

Should indoles be detected in pinealocyte samples, the qualitative methods presented here should be developed into a quantitative protocol. If any of the putative pinealocyte indoles shown in Figures 6.2 or 6.3 were not detected in extracts, they could be investigated as an internal standards.

Finally, unlike the other projects presented in this manuscript, this project would lend itself well to animal studies. The pineal gland is easily the largest of brain structures discussed here—sufficient to easily prepare samples—and its anatomical location makes it easily accessible by surgery.

References

1. Stryer, L. *Biochemistry*. 1995, W. H. Freeman and Co.: New York. p. 483-579.
2. Rose, R.C. *Cerebral metabolism of oxidized ascorbate.* Brain Research, 1993. **628**(1-2): p. 49-55.
3. Harris, D.C. *Quantitative Chemical Analysis*. 5th ed. 1999: W. H. Freeman and Company.
4. Shibata, K., Hayakawa, T., and Iwai, K. *Tissue distribution of the enzymes concerned with the biosynthesis of NAD in rats.* Agricultural and Biological Chemistry, 1986. **50**(12): p. 3037-3041.
5. Sies, H. *Nicotinamide nucleotide compartmentation*, in *Metabolic Compartmentation*, H. Sies, Editor. 1982, Academic Press: London. p. 205-31.
6. Zhang, X.J., Kurnasov, O.V., Karthikeyan, S., Grishin, N.V., Osterman, A.L., and Zhang, H. *Structural characterization of a human cytosolic NMN/NaMN adenylyltransferase and implication in human NAD biosynthesis.* Journal of Biological Chemistry, 2003. **278**(15): p. 13503-13511.
7. Fernandes, M. *Properties of rat brain NAD-kinase.* Journal of Neurochemistry, 1970. **17**(4): p. 503-9.
8. Voet, D. and Voet, J.G. *Biochemistry*. 2nd ed. 1995, New York: John Wiley & Sons, Inc.
9. Steinbrecht, I. and Augustin, W. *Studies on NAD+ permeability in intact mitochondria from rabbit reticulocytes.* Acta Biologica Et Medica Germanica, 1977. **36**(3-4): p. 555-560.
10. Williamson, D.H., Lund, P., and Krebs, H.A. *Redox state of free nicotinamide adenine dinucleotide in the cytoplasm and mitochondria of rat liver.* Biochemical Journal, 1967. **103**: p. 514-27.
11. Erecinska, M., Nelson, D., and Silver, I.A. *Metabolic and energetic properties of isolated nerve ending particles (synaptosomes).* Biochimica Et Biophysica Acta-Bioenergetics, 1996. **1277**(1-2): p. 13-34.
12. Patterson, G.H., Knobel, S.M., Arkhammar, P., Thastrup, O., and Piston, D.W. *Separation of the glucose-stimulated cytoplasmic and mitochondrial NAD(P)H responses in pancreatic islet .beta. cells.* Proceedings of the National Academy of Sciences of the United States of America, 2000. **97**(10): p. 5203-5207.
13. Papa, S. *Control of the utilization of mitochondrial reducing equivalents*, in *The Energy Level and Metabolic Control in Mitochondria*, S. Papa, et al., Editors. 1969, Adriatica Editrice: Bari. p. 401-409.
14. Klaidman, L.K., Leung, A.C., and Adams, J.D., Jr. *High-performance liquid chromatography analysis of oxidized and reduced pyridine dinucleotides in specific brain regions.* Analytical biochemistry, 1995. **228**(2): p. 312-7.
15. Gillette, M.U. and Tischkau, S.A. *Suprachiasmatic nucleus: The brain's circadian clock.* Recent Progress in Hormone Research, 1999. **54**: p. 33-59.
16. Barinaga, M. *How the brain's clock gets daily enlightenment.* Science, 2002. **295**(5557): p. 955-957.

17. van Esseveldt, L.K.E., Lehman, M.N., and Boer, G.J. *The suprachiasmatic nucleus and the circadian time-keeping system revisited.* Brain Research Reviews, 2000. **33**(1): p. 34-77.
18. Namihira, M., Honma, S., Abe, H., Tanahashi, Y., Ikeda, M., and Honma, K. *Daily variation and light responsiveness of mammalian clock gene, Clock and BMAL1, transcripts in the pineal body and different areas of brain in rats.* Neuroscience Letters, 1999. **267**(1): p. 69-72.
19. Rutter, J., Reick, M., Wu, L.C., and McKnight, S.L. *Regulation of clock and NPAS2 DNA binding by the redox state of NAD cofactors.* Science, 2001. **293**(5529): p. 510-4.
20. Schibler, U., Ripperger, J.A., and Brown, S.A. *Chronobiology - reducing time.* Science, 2001. **293**(5529): p. 437-438.
21. Merrow, M. and Roenneberg, T. *Circadian clocks: running on redox.* Cell, 2001. **106**(2): p. 141-143.
22. Kann, O., Schuchmann, S., Buchheim, K., and Heinemann, U. *Coupling of neuronal activity and mitochondrial metabolism as revealed by NAD(P)H fluorescence signals in organotypic hippocampal slice cultures of the rat.* Neuroscience, 2003. **119**(1): p. 87-100.
23. Wagner, E., Deitzer, G.F., Fischer, S., Frosh, S., Kempf, O., and Stroebele, L. *Endogenous Oscillations in Pathways of Energy Transduction as Related to Circadian Rhythmicity and Photoperiodic Control.* Biosystems, 1975. **7**(1): p. 68-76.
24. Zhang, Q., Piston, D.W., and Goodman, R.H. *Regulation of corepressor function by nuclear NADH.* Science, 2002. **295**(5561): p. 1895-1897.
25. Ziegler, M. *New functions of a long-known molecule - Emerging roles of NAD in cellular signaling.* European Journal of Biochemistry, 2000. **267**(6): p. 1550-1564.
26. Ha, H.C. and Snyder, S.H. *Poly(ADP-ribose) polymerase-1 in the nervous system.* Neurobiology of Disease, 2000. **7**(4): p. 225-239.
27. Sevigny, M.B., Silva, J.M., Lan, W.C., Alano, C.C., and Swanson, R.A. *Expression and activity, of poly(ADP-ribose) glycohydrolase in cultured astrocytes, neurons, and C6 glioma cells.* Molecular Brain Research, 2003. **117**(2): p. 213-220.
28. Berger, S.J., Sudar, D.C., and Berger, N.A. *Metabolic consequences of DNA damage - DNA damage induced alterations in glucose metabolism by activation of poly(ADP-ribose) polymerase.* Biochemical and Biophysical Research Communications, 1986. **134**(1): p. 227-232.
29. Chabert, M.G., Niedergang, C.P., Hog, F., Partisani, M., and Mandel, P. *Poly(ADPR) polymerase expression and activity during proliferation and differentiation of rat astrocyte and neuronal cultures.* Biochimica Et Biophysica Acta, 1992. **1136**(2): p. 196-202.
30. Cohen-Armon, M., Visochek, L., Katzoff, A., Levitan, D., Susswein, A.J., Klein, R., Valbrun, M., and Schwartz, J.H. *Long-term memory requires polyADP-ribosylation.* Science, 2004. **304**(5678): p. 1820-1822.

31. Homburg, S., Visochek, L., Moran, N., Dantzer, F., Priel, E., Asculai, E., Schwartz, D., Rotter, V., Dekel, N., and Cohen-Armon, M. *A fast signal-induced activation of poly(ADP-ribose) polymerase: A novel downstream target of phospholipase C.* Journal of Cell Biology, 2000. **150**(2): p. 293-307.
32. White, L.A., Eaton, M.J., Castro, M.C., Klose, K.J., Globus, M.Y.T., Shaw, G., and Whittemore, S.R. *Distinct regulatory pathways control neurofilament expression and neurotransmitter synthesis in immortalized serotonergic neurons.* Journal of Neuroscience, 1994. **14**(11): p. 6744-6753.
33. Feldman, R.S., Meyer, J.S., and Quenzer, L.F. *Principles of Neuropsychopharmacology*. 1997, Sunderland: Sinauer Associates, Inc.
34. Binkley, S. *The Pineal: Endocrine and Nonendocrine Function*, ed. M.E. Hadley. 1988, Englewood Cliffs: Prentice Hall.
35. Zimmer, L., Pain, F., Mauger, G., Plenevaux, A., Le Bars, D., Mastrippolito, R., Pujol, J.F., Renaud, B., and Laniece, P. *The potential of the beta-microprobe, an intracerebral radiosensitive probe, to monitor the [F-18]MPPF binding in the rat dorsal raphe nucleus.* European Journal of Nuclear Medicine and Molecular Imaging, 2002. **29**(9): p. 1237-1247.
36. Vandenpol, A.N. *The hypothalamic suprachiasmatic nucleus of rat - Intrinsic anatomy.* Journal of Comparative Neurology, 1980. **191**(4): p. 661-702.
37. Whittemore, S.R., White, L.A., Shihabuddin, L.S., and Eaton, M.J. *Phenotypic diversity in neuronal cell lines derived from raphe nucleus by retroviral transduction.* Methods, 1995. **7**(3): p. 285-96.
38. White, L.A. and Whittemore, S.R. *Immortalization of raphe neurons - An approach to neuronal function in vitro and in vivo.* Journal of Chemical Neuroanatomy, 1992. **5**(4): p. 327-330.
39. Earnest, D.J., Liang, F.Q., DiGiorgio, S., Gallagher, M., Harvey, B., Earnest, B., and Seigel, G. *Establishment and characterization of adenoviral E1A immortalized cell lines derived from the rat suprachiasmatic nucleus.* Journal of neurobiology, 1999. **39**(1): p. 1-13.
40. Whittemore, S.R. and White, L.A. *Target regulation of neuronal differentiation in a temperature-sensitive cell line derived from medullary raphe.* Brain Research, 1993. **615**(1): p. 27-40.
41. Son, J.H., Chung, J.H., Huh, S.O., Park, D.H., Peng, C., Rosenblum, M.G., Chung, Y.I., and Joh, T.H. *Immortalization of neuroendocrine pinealocytes from transgenic mice by targeted tumorigenesis using the tryptophan hydroxylase promoter.* Molecular Brain Research, 1996. **37**(1-2): p. 32-40.
42. Damania, B. and Alwine, J.C. *TAF-like function of SV40 large T antigen.* Genes & Development, 1996. **10**(11): p. 1369-1381.
43. Ben-Israel, H. and Kleinberger, T. *Adenovirus and cell cycle control.* Frontiers in Bioscience, 2002. **7**: p. D1369-D1395.
44. Allen, G., Rappe, J., Earnest, D.J., and Cassone, V.M. *Oscillating on borrowed time: diffusible signals from immortalized suprachiasmatic nucleus cells regulate circadian rhythmicity in cultured fibroblasts.* Journal of Neuroscience, 2001. **21**(20): p. 7937-43.

45. Hurst, W.J., Earnest, D., and Gillette, M.U. *Immortalized suprachiasmatic nucleus cells express components of multiple circadian regulatory pathways.* Biochemical and Biophysical Research Communications, 2002. **292**(1): p. 20-30.
46. Hurst, W.J., Mitchell, J.W., and Gillette, M.U. *Synchronization and phase-resetting by glutamate of an immortalized SCN cell line.* Biochemical and Biophysical Research Communications, 2002. **298**(1): p. 133-43.
47. Earnest, D.J., Liang, F.Q., Ratcliff, M., and Cassone, V.M. *Immortal time: circadian clock properties of rat suprachiasmatic cell lines.* Science, 1999. **283**(5402): p. 693-5.
48. Newman, G.C. and Hospod, F.E. *Rhythm of suprachiasmatic nucleus 2-deoxyglucose uptake in vitro.* Brain Research, 1986. **381**(2): p. 345-50.
49. Balsalobre, A., Damiola, F., and Schibler, U. *A serum shock induces circadian gene expression in mammalian tissue culture cells.* Cell, 1998. **93**(6): p. 929-37.
50. Eaton, M. and Whittemore, S.R. *Autocrine BDNF secretion enhances the survival and serotonergic differentiation of raphe neuronal precursor cells grafted into the adult rat CNS.* Experimental Neurology, 1996. **140**(2): p. 105-114.
51. Lam, P.Y., Chen, K., and Shih, J.C. *The circadian rhythm of 5-HT biosynthetic and degradative enzymes in immortalized mouse neuroendocrine pineal cell line-a model for studying circadian rhythm.* Life Sciences, 2004. **75**(25): p. 3017-3026.
52. Sugden, D. *Comparison of circadian expression of tryptophan hydroxylase isoform mRNAs in the rat pineal gland using real-time PCR.* Journal of Neurochemistry, 2003. **86**(5): p. 1308-1311.
53. Roseboom, P.H., Coon, S.L., Baler, R., McCune, S.K., Weller, J.L., and Klein, D.C. *Melatonin synthesis: Analysis of the more than 150-fold nocturnal increase in serotonin N-acetyltransferase messenger ribonucleic acid in the rat pineal gland.* Endocrinology, 1996. **137**(7): p. 3033-3044.
54. Suh, B.C., Chae, H.D., Chung, J.H., and Kim, K.T. *Pharmacological characterization of beta(2)-adrenoceptor in PGT-beta mouse pineal gland tumour cells.* British Journal of Pharmacology, 1999. **126**(2): p. 399-406.
55. Yagita, K. and Okamura, H. *Forskolin induces circadian gene expression of rPer1, rPer2 and dbp in mammalian rat-1 fibroblasts.* Febs Letters, 2000. **465**(1): p. 79-82.
56. Whittemore, S.R., *Whittemore Lab Protocols*. 2001.
57. Walther, N., Einspanier, A., and Jansen, M. *Expression of granulosa cell-specific genes and induction of apoptosis in conditionally immortalized granulosa cell lines established from H-2K(b)-tsA58 transgenic mice.* Biology of Reproduction, 1999. **60**(5): p. 1078-1086.
58. Milovic, V., Ocklind, G., and Artursson, P. *Conditionally immortalized intestinal epithelial cells - A new model for studying intestinal epithelial cell turnover.* Intestinal Plasticity in Health and Disease, 1998. **859**: p. 201-203.
59. Brewer, G.J., Torricelli, J.R., Evege, E.K., and Price, P.J. *Optimized survival of hippocampal neurons in B27-supplemented Neurobasal(TM), a new serum-free medium combination.* Journal of Neuroscience Research, 1993. **35**(5): p. 567-576.

60. Brewer, G.J. and Cotman, C.W. *Survival and growth of hippocampal neurons in defined medium at low density - Advantages of a sandwich culture technique or low oxygen.* Brain Research, 1989. **494**(1): p. 65-74.
61. Skoog, D.A., Holler, F.J., and Nieman, T.A. *Principles of Instrumental Analysis*. 5th ed. 1998, Philadelphia: Harcourt Brace College Publishers.
62. Kuhn, R. and Hoffstetter-Kuhn, S. *Capillary Electrophoresis: Principles and Practice*. 1993, Berlin: Springer-Verlag.
63. Olechno, J.D., Tso, J.M.Y., Thayer, J., and Wainright, A. *Capillary electrophoresis - a multifaceted technique for analytical chemistry. 2. Separations and injection.* American Laboratory, 1990. **22**(18): p. 30-37.
64. Palmer, J., Munro, N.J., and Landers, J.P. *A universal concept for stacking neutral analytes in micellar capillary electrophoresis.* Analytical Chemistry, 1999. **71**(9): p. 1679-1687.
65. Mosinger, J., Tomankova, V., Nemcova, I., and Zyka, J. *Cyclodextrins in analytical chemistry.* Analytical Letters, 2001. **34**(12): p. 1979-2004.
66. Gostkowski, M.L., McDoniel, J.B., Wei, J., Curey, T.E., and Shear, J.B. *Characterizing spectrally diverse biological chromophores using capillary electrophoresis with multiphoton-excited fluorescence.* Journal of the American Chemical Society, 1998. **120**(1): p. 18-22.
67. Xu, C. and Webb, W.W. *Multiphoton excitation of molecular fluorophores and nonlinear laser microscopy*, in *Topics in Fluorescence Spectroscopy*, J.R. Lakowicz, Editor. 1997, Plenum Press: New York. p. 471-540.
68. Shear, J.B. *Multiphoton-excited fluorescence.* Analytical Chemistry, 1999. **71**(17): p. 598a-605a.
69. Hopkins, J.M. and Sibbett, W. *Ultrashort-pulse lasers: Big payoffs in a flash.* Scientific American, 2000. **283**(3): p. 72-79.
70. Gostkowski, M.L., Allen, R., Plenert, M.L., Okerberg, E., Gordon, M.J., and Shear, J.B. *Multiphoton-excited serotonin photochemistry.* Biophysical Journal, 2004. **86**(5): p. 3223-3229.
71. Bennett, B.D., Jetton, T.L., Ying, G., Magnuson, M.A., and Piston, D.W. *Quantitative subcellular imaging of glucose metabolism within intact pancreatic islets.* Journal of Biological Chemistry, 1996. **271**(7): p. 3647-51.
72. Zhang, Z., Yu, J., and Stanton, R.C. *A method for determination of pyridine nucleotides using a single extract.* Analytical Biochemistry, 2000. **285**(1): p. 163-167.
73. Klingenberg, M. *Nicotinamide adenine dinucleotides (NAD, NADP, NADH, NADPH); Spectrophotometric and fluorimetric methods*, in *Methods of Enzymatic Analysis*, H.U. Bergmeyer, Editor. 1974, Academic Press, Inc.: New York and London. p. 2045-2059.
74. Lowry, O.H., Passonneau, J.V., and Rock, M.K. *The stability of pyridine nucleotides.* Journal of Biological Chemistry, 1961. **236**(10): p. 2756-2759.
75. Colowick, S.P., Kaplan, N.O., and Ciotti, M.M. *The reaction of pyridine nucleotide with cyanide and its analytical use.* Journal of Biological Chemistry, 1951. **191**: p. 447-459.

76. Olive, C. and Levy, H.R. *Preparation and some properties of crystalline glucose-6-phosphate dehydrogenase from Leuconostoc mesenteroides.* Biochemistry, 1967. **6**(3): p. 730-6.
77. Xu, C., Zipfel, W., Shear, J.B., Williams, R.M., and Webb, W.W. *Multiphoton fluorescence excitation: new spectral windows for biological nonlinear microscopy.* Proceedings of the National Academy of Sciences of the United States of America, 1996. **93**(20): p. 10763-10768.
78. Stefansson, M. and Novotny, M. *Electrophoretic resolution of monosaccharide enantiomers in borate-oligosaccharide complexation media.* Journal of the American Chemical Society, 1993. **115**(24): p. 11573-80.
79. Klemm, A., Steiner, T., Cumme, G.A., and Horn, A. *Determination, Purification, and Characterization of Alpha-NADH.* Analytical Biochemistry, 1993. **212**(2): p. 375-380.
80. Oppenheimer, N.J. and Kaplan, N.O. *Alpha Beta Epimerization of Reduced Nicotinamide Adenine-Dinucleotide.* Archives of Biochemistry and Biophysics, 1975. **166**(2): p. 526-535.
81. Chattopadhyay, A. and Harikumar, K.G. *Dependence of critical micelle concentration of a zwitterionic detergent on ionic strength: Implications in receptor solubilization.* Febs Letters, 1996. **391**(1-2): p. 199-202.
82. Partearroyo, M.A., Ostolaza, H., Goñi, F.M., and Barberá-Guillem, E. *Surfactant-induced cell toxicity and cell lysis: A study using B16 melanoma cells.* Biochemical pharmacology, 1990. **40**(6): p. 1323-8.
83. Xu, D. and Chen, H. *Determination of reduced form of nicotinamide adenine dinucleotide by capillary zone electrophoresis with amperometric detection.* Fenxi Huaxue, 1997. **25**(4): p. 456-459.
84. Wang, Z. and Yeung, E.S. *Dual-enzyme assay of glutamate in single cells based on capillary electrophoresis.* Journal of Chromatography B: Biomedical Applications, 1997. **695**(1): p. 59-65.
85. Markuszewski, M.J., Britz-McKibbin, P., Terabe, S., Matsuda, K., and Nishioka, T. *Determination of pyridine and adenine nucleotide metabolites in Bacillus subtilis cell extract by sweeping borate complexation capillary electrophoresis.* Journal of Chromatography A, 2003. **989**(2): p. 293-301.
86. Kahn, A.M., Allen, J.C., and Zhang, S. *Insulin increases NADH/NAD+ redox state, which stimulates guanylate cyclase in vascular smooth muscle.* American Journal of Hypertension, 2002. **15**(3): p. 273-279.
87. Yamazaki, S., Ishida, Y., and Inouye, S.I.T. *Circadian rhythms of adenosine triphosphate contents in the suprachiasmatic nucleus, anterior hypothalamic area and caudate putamen of the rat - Negative correlation with electrical activity.* Brain Research, 1994. **664**(1-2): p. 237-240.
88. Reick, M., Garcia, J.A., Dudley, C., and McKnight, S.L. *NPAS2: An analog of clock operative in the mammalian forebrain.* Science, 2001. **293**(5529): p. 506-509.
89. Almeida, A. and Medina, J.M. *A rapid method for the isolation of metabolically active mitochondria from rat neurons and astrocytes in primary culture.* Brain Research Protocols, 1998. **2**(3): p. 209-214.

90. Wei, J. *Multiphoton detection strategies for analysis of biological microsamples with capillary electrophoresis.* Ph.D. thesis in Analytical Chemistry, The University of Texas at Austin. 2000.
91. Bear, M.F., Connors, B.W., and Paradiso, M.A. *Neuroscience: Exploring the brain*. 1996, Baltimore: Williams and Wilkins.
92. Lynn-Bullock, C.P., Welshhans, K., Pallas, S.L., and Katz, P.S. *The effect of oral 5-HTP administration on 5-HTP and 5-HT immunoreactivity in monoaminergic brain regions of rats.* Journal of Chemical Neuroanatomy, 2004. **27**(2): p. 129-138.
93. Boadle-Biber, M.C. *Activation of tryptophan hydroxylase from central serotonergic neurons by calcium and depolarization.* Biochemical Pharmacology, 1978. **27**(7): p. 1069-1079.
94. Eaton, M.J., Staley, J.K., Globus, M.Y.T., and Whittemore, S.R. *Developmental regulation of early serotonergic neuronal differentiation - the role of brain-derived neurotrophic factor and membrane depolarization.* Developmental Biology, 1995. **170**(1): p. 169-182.
95. Gostkowski, M.L., Curey, T.E., Okerberg, E., Kang, T.J., Bout, D.A.V., and Shear, J.B. *Effects of molecular oxygen on multiphoton-excited photochemical analysis of hydroxyindoles.* Analytical Chemistry, 2000. **72**(16): p. 3821-3825.
96. Gostkowski, M.L., Wei, J., and Shear, J.B. *Measurements of serotonin and related indoles using capillary electrophoresis with multiphoton-induced hyperluminescence.* Analytical Biochemistry, 1998. **260**(2): p. 244-250.
97. Gostkowski, M.L. *Detection approaches for the analysis of volume-limited biological samples.* Ph.D. thesis in Analytical Chemistry, The University of Texas at Austin. 2000.
98. Wester, P., Gottfries, J., and Winblad, B. *Simultaneous liquid-chromatographic determination of seventeen of the major monoamine neurotransmitters, precursors and metabolites. 2. Assessment of human-brain and cerebrospinal-fluid concentrations.* Journal of Chromatography-Biomedical Applications, 1987. **415**(2): p. 275-288.
99. Palazzolo, D.L. and Quadri, S.K. *Optimal conditions for long-term storage of biogenic amines for subsequent analysis by column chromatography with electrochemical detection.* Journal of Chromatography, 1990. **518**(1): p. 258-263.
100. Fickbohm, D.J., Lynn-Bullock, C.P., Spitzer, N., Caldwell, H.K., and Katz, P.S. *Localization and quantification of 5-hydroxytryptophan and serotonin in the central nervous systems of Tritonia and Aplysia.* Journal of Comparative Neurology, 2001. **437**(1): p. 91-105.
101. Bethea, C.L., Lu, N.Z., Reddy, A., Shlaes, T., Streicher, J.M., and Whittemore, S.R. *Characterization of reproductive steroid receptors and response to estrogen in a rat serotonergic cell line.* Journal of Neuroscience Methods, 2003. **127**(1): p. 31-41.
102. Butterweck, V. *Mechanism of action of St John's wort in depression - What is known?* CNS Drugs, 2003. **17**(8): p. 539-562.

103. Gostkowski, M.L. and Shear, J.B. *Subattomole fluorescence determination of catecholamines in capillary electrophoresis effluent streams.* Journal of the American Chemical Society, 1998. **120**(49): p. 12966-12967.
104. Fuller, K.M. and Arriaga, E.A. *Advances in the analysis of single mitochondria.* Current Opinion in Biotechnology, 2003. **14**(1): p. 35-41.
105. Mills, M. *The effect of stress on melatonin and monoamine metabolism in the rat pineal.* Advances in Pineal Research, 1991. **6**: p. 91-8.
106. Reiter, R.J., Richardson, B.A., and King, T.S. *The pineal gland and its indole products*, in *The Pineal Gland*, R. Relkin, Editor. 1983, Elsevier Biomedical: New York.
107. Quay, W.B. *Pineal Chemistry*. 1974, Springfield Illinois: Charles C. Thomas.
108. Kari, I. *6-Methoxy-1,2,3,4-Tetrahydro-Beta-Carboline in Pineal-Gland of Chicken and Cock.* Febs Letters, 1981. **127**(2): p. 277-280.
109. Galian, R.E., Veglia, A.V., and de Rossi, R.H. *Cyclodextrin enhanced fluorimetric method for the determination of tryptamine.* Analyst, 1998. **123**(7): p. 1587-1591.
110. Galian, R.E., Veglia, A.V., and de Rossi, R.H. *Hydroxypropyl-beta-cyclodextrin enhanced fluorimetric method for the determination of melatonin and 5-methoxytryptamine.* Analyst, 2000. **125**(8): p. 1465-1470.
111. Vitale, A.A., Ferrari, C.C., Aldana, H., and Affanni, J.M. *Highly sensitive method for the determination of melatonin by normal-phase high-performance liquid chromatography with fluorometric detection.* Journal of Chromatography B-Biomedical Applications, 1996. **681**(2): p. 381-384.

Vita

Dana Diane Wise was born in Ohio on 12 January 1978 to Marilyn and Michael Wise. She attended Rootstown public schools, followed by the University of Toledo (Ohio), where she earned an Honors Bachelor of Science in Chemistry (*summa cum laude*).

Publications:

"Analysis of Flavin, Nicotinamide, and Serotonin Derivatives in Neuronal Extracts Using Capillary Electrophoresis with Multiphoton Excitation." D.D. Wise and J.B. Shear. Submitted to *Journal of Chromatography A*, 2005.

"Circadian Tracking of Nicotinamide Cofactor Levels in an Immortalized Suprachiasmatic Nucleus Cell Line." D.D. Wise and J.B. Shear. *Neuroscience*. **128** (2004) 263-268.

"Tracking Variations in Nicotinamide Cofactors Extracted from Cultured Cells Using Capillary Electrophoresis with Multiphoton Excitation of Fluorescence," D.D. Wise and J.B. Shear. *Analytical Biochemistry*. **326** (2004) 225-233.

"An Internal Standard Method for the Measurement of Choline and Acetylcholine by Capillary Electrophoresis with Electrochemical Detection." D.D. Wise, T.V. Sorokina, P.-A. Brault, J.R. Kirchhoff, R.A. Hudson, W.S. Messer. *Journal of Chromatography B*. **775** (2002) 49-56.

Permanent address: 930 Elizabeth Court, Cuyahoga Falls, Ohio 44221.

This dissertation was typed by the author.